Design of Insole using Image Base Analysis

by
Vinicius Aguiar de Souza

A thesis submitted in partial fulfillment
of the requirements for the degree of
Master in Science

Thesis supervisor: Associate Professor Katsuyuki Suzuki

The University of Tokyo
Graduate School of Frontier Sciences
2007

Table of Contents

Index of Figures

Index of Tables

Acknowledgements

I would like to thank the Japanese Ministry of Education and Science (文部科学省) for supporting this kind of program, aimed to foreigners, which make possible this challenge of studying in Japan. Moreover I would like to express my gratitude to all people of Japan for allowing me inside their intriguing, at same time fascinating, universe of effervescent and ancestral culture.

An academic degree is never a work of a man alone. To reach the stage of completion the road was long, arduous and full of surprises lurking its way. To reach this point, three people were of ultimate importance: professor Alfredo Aires de Los Santos, professor Sergio Jun Ono Fonseca and professor Katsuyuki Suzuki.

The first one explained exhaustedly about the relevance of studying in Japan, especially at the University of Tokyo. Otherwise I would be digging holes in lawns or delivering pizzas in California. Professor Sergio Jun Ono Fonseca, who at first introduce me to the marvelous world of Finite Element Method, what itself is splendid. However he went beyond: he was responsible for the recommendation that brought me to the Tokyo University. Without his assistance and concern about my complicated case none of this would be possible. My gratitude cannot find words to express itself.

And finally at last, but never least, professor Katsuyuki Suzuki. I really appreciate from the bottom of my heart the chance that he gave in his laboratory. Make a blind bet on someone who was dismissed (really hard to find an appropriate word here) from other laboratory, involves a lot of courage and trust. Moreover, he was always open to discuss science, always full of ideas, and despite busy schedules, could always find time to elucidate my doubts. This work would not be possible without your kind help. Thank you so much for being a REAL advisor. Day after day, they are becoming endangered species…

I would like to express my gratitude also to Dr. Yokota Hideo and Dr. Himeno Ryutaro, from RIKEN (Alive Human Body Team), who kindly provided me the CT data and mask edition software. Without their data I could never start this project. Partnerships are the future of quality research.

Mr. Nakano Isao, and Mr. Fujihara Seiji were really important during the development of this research. The first one has years of experience on footwear design, the main target of this research, thus he was the source of many useful advices, including key ones during experiment design. Mr. Fujihara Seiji was working directly with me during this project: he was a tireless assistant and a hard-working colleague. Thank you so much.

To M.Eng. Levent Kirkayak, whose finite element analysis expertise helped me a

lot during the duration of this work. My most sincere thank to him. Moreover, he was my closest friend during master course, always supporting and encouraging me in so many ways. More than earn a degree, I earn a marvelous friend.

To my grandmother Norma de Aguiar who at early age gave me books instead of toys. Among them, I read stories about a fascinating country half across the globe, with warriors, princesses, castles, heroes and acts of nobility and honor. These stories made this country so real that living there became part of my most intimate dreams. Praise the Lord!!!! I could live long enough to fulfill my dream and learn from this adventure.

To all Graduate School of Frontier Sciences' employees. They were always supportive, helpful, and most important kind. Thank you so much. To my colleagues in professor Sukuki's laboratory. Thanks for the Japanese lessons and help. To Ana Paula Bortoleto, Rafael Takai, Marcos Fukase Maeda, Lirian Mina Nozawa, Marcia Sayuri Kondo and Pedro Ivo Macedo who were close friends sharing my agony during my worst period in Japan. Without your assistance I would have abandoned my dream in March of 2005. Muchas gracias hermanos!!!!!!Special thanks to Pedro Ivo Macedo for all Winning Eleven hours…They made many bad moments just disappear (Thanks to KONAMI for making such wonderful game. Love you guys). Special thanks also to Oscar Milewski and Min Park who kindly correct the English grammar presented here. Being a non-native speaker is hard.

Para minha esposa Cristina Moraes de Souza que abandonou tudo no Brasil: familiares, emprego e amigos para viver comigo esta aventura. Ela merece um agradecimento especial por ter me apoiado todo este tempo. Mais do que ser meu porto seguro, foi minha professora em uma parte de minha vida que achei estar irremediavelmente perdida a muito tempo. Peco perdao pelos momentos que hesitei e reafirmo meus votos. E pedindo emprestado a quem ja me emprestou o nome, te dedico algo que reflete o que cultivastes em meu peito. Com amor.

Soneto da Fidelidade

De tudo, ao meu amor serei atento
Antes, e com tal zelo, e sempre, e tanto
Que mesmo em face do maior encanto
Dele se encante mais meu pensamento.

Quero vivê-lo em cada vão momento
E em seu louvor hei de espalhar meu canto
E rir meu riso e derramar meu pranto
Ao seu pesar ou seu contentamento.

E assim, quando mais tarde me procure
Quem sabe a morte, angústia de quem vive
Quem sabe a solidão, fim de quem ama

Eu possa (me) dizer do amor (que tive):
Que não seja imortal, posto que é chama
Mas que seja infinito enquanto dure.

Vinicius de Moraes

Finally to myself for persevere despite all adversities.

"Vi Veri Universum Vivus Vici" Christopher Marlowe (1964-1593).

虎穴に入らずんば虎児を得ず。

Nothing Ventured, Nothing Gained.

1 Introduction

1.1 Modeling the foot: a Finite Element Method Approach

Looking at the very definition of the word *model* in a Merriam-Webster dictionary, one will read the following: "*to plan or form after a pattern*", , or "*a representation of something, either as a physical object which is usually smaller than the real object, or as a simple description of the object which might be used in calculations.*" Cambridge and Oxford Dictionaries defines it as: "*devise a mathematical model of*",

Probably Engineers, Mathematicians, Physicists and all sorts of researchers working with modeling, are more concerned about a narrower definition of the word, which involves only mathematical perspective. When researchers, like the ones mentioned above, use the word model, as a verb or a noun, they are referring to a mathematical tool that can be used to simulate and represent reality, based on data originated from an experiment or theory.

Thus, to model, or is an attempt to represent or simulate matters, which can be Nature Laws, or objects under certain Physical fields effects. The power of modeling is increasingly recognized in Biomechanical research, and when combined with experimental data, becomes a even more powerful scientific tool, making a proper approach to many situations possible. A model seems to be a powerful tool to increase the understanding of mechanisms, and has been applied, therefore, quite frequently in many daily and/or research situation (Nigg *et al.*, 1994).

Since few years ago, many researchers have been working in the development of mathematical models that simulate the complicated mechanics behind situations faced by the human body, e.g., sport activities, movements pertaining to daily life, or interaction between the body and any kind of apparatus. Among these, one apparatus can be mentioned as the most widely used one and which has been in use by humans for centuries: the shoes.

It is impossible to estimate exactly during which stage on earth history, man first thought about protecting his feet from the natural hazards of weather and climate, as well as from rough terrain over which they hunted and searched for refuge. However, in the history of human development shows that the importance of protecting the feet was recognized early. There is evidence, which shows that the history of the shoe starts around 10.000 BC, that is, at the end of the Paleolithic period. Paintings, making references to footwear, found in caves in Spain and in south of France are clues pointing to this date. Among the cavemen's rock utensils, there were several used to scrape skins, which indicates that the art of tanning is very old.

Shoes are important and reliable accessories wore by people in our modern society, offering protection, improving sportive performances, or, for esthetic reasons. The shoe has always had an important place in costume. Through all this development, comparatively little attention was devoted to fitting qualities or comfort. Research on footwear only became attractive to scientists when the fitness and running activities started to boom in the early 1970's (Nigg *et al.*, 1977; James *et al.*, 1978; Krissoff *et al.*, 1979; Light *et al.*, 1979; Cavanagh, 1980; Clement *et al.*, 1981; Hamill *et al.*, 1983). Consequently, many questions emerged regarding footwear biomechanics and most important: the effects of poor footwear on human health.

Human feet are repeatedly subject to substantial forces during daily activities, not the least of which is the transient force caused by heel-strike (Denoth, 1986; Nigg et al., 1995; Wakeling et al., 2003) apud (Chi *et al.*, 2005). This impact force, caused by inertial change of the lower extremity over approximately 20 ms, reaches two or three times the body weight (Whittle, 1999) and generates a shock wave that is transmitted along the body (Dickinson et al., 1985; Smeathers, 1989; Wakeling et al., 2003) apud (Chi *et al.*, 2005). Some researchers like Collins and Whittle (1989), Gill and O'Connor (2003) indicate the impact force and the shock wave as one of the primary etiological agents in many degenerative diseases and injuries of the musculoskeletal system, as plantar fasciitis, Achilles tendinitis, muscle tears and stress fractures.

The heel pad of the foot experiences high forces during locomotion that result in repetitive and elevated local stresses. As consequence heel pad is believed to attenuate foot-ground impact forces and protect the musculoskeletal system (Whittle, 1999). As a matter of fact, during impact phase the heel pad is the major source of energy absorption, because the geometry of the contact limb does not change and no muscle activity is detected during this period (10–20 ms after heel-strike) (Jefferson et al., 1990; Wakeling et al., 2003) apud (Chi *et al.*, 2005).

Thus, such high plantar pressures at the heel need to be relieved somehow to avoid certain pathological conditions. It is important to recognize the link between these transient forces and pathological conditions, since the magnitude of these forces — and by implication, the incidence of these conditions — can be reduced by the use of viscoelastic materials, either in shoe construction or as an insole (Whittle, 1999) (Figure 1-1).

Nowadays, support surface interfaces typically classified as protective devices, such as athletic shoes and mats composed of soft expanded polymer foam materials, are used to protect against these injuries. A variety of over-the-counter and custom insole products are frequently used to relieve plantar pressures (Goske *et al.*, 2006).

Currently there are many commercially available insole materials, but there is limited information on the effects of stress redistribution of insoles with different combinations of materials and thicknesses.

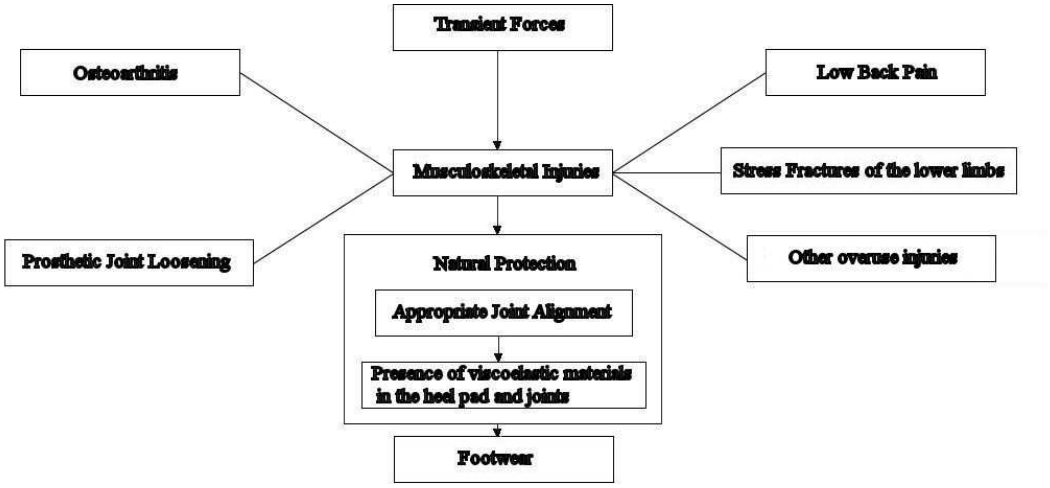

Figure 1-1: Schematic relation among transient forces, musculoskeletal diseases and prevention.

Moreover, the design of an insole is often intuitive and is not always based on scientific principles. Therefore, further investigation and utilization of more scientific principles is necessary. Currently, there are two feasible approaches to quantifying foot pressure. One approach employs the well-established in-shoe measuring techniques to obtain plantar pressure during gait with different insole combinations (Chen *et al.*, 2003) . However, this approach is time-consuming and a large number of measurements need to be performed on different subjects with different insole combinations in order to obtain statistically significant results.

The other approach is to use the finite element method to model the foot–insole structure and to analyze the effects of different insole variable combinations, like conformity, thickness and material, on the plantar stress distributions. This approach has the benefit of allowing modification of different insole combinations and performing parametric analysis with a relatively quick and easy procedure.

1.2 Objectives

Obviously, there is still a broad range of unanswered but fundamental questions regarding the biomechanics of the foot, especially regarding footwear biomechanics, however for the present study a more modest set of initial questions is going to be addressed.

The main question concerning this study is: what is the effect (s) of the footwear (insole) design variables on the plantar pressure distribution? In the universe of biomechanical variables we opt for peak plantar pressure.

This variable was chosen to evaluate the efficacy of designs variables because of the widespread clinical and experimental use (Cavanagh et al. 2000) of this quantity and its links to diseases (Veves *et al.* 1992 *apud* Erdemir *et al.*, 2006).

The design variables in question are conformity (Figure 1-2), and material. The word conformity, while used in this study, is referred to the degree of congruity between the plantar region and the insole surface in the unloaded state.

Thus the main question can be reformulated in two different ones:

1- Does conformity have effect on peak plantar pressure value?

2- Does material have effect on peak plantar pressure's value?

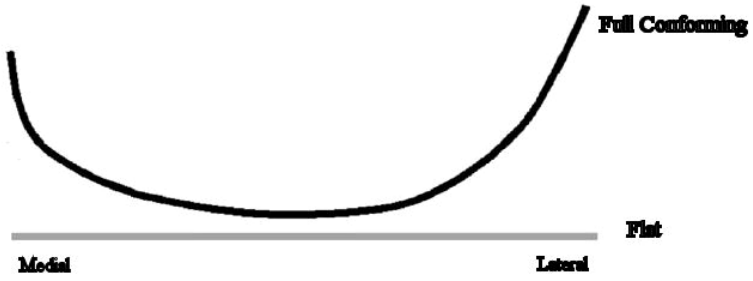

Figure 1-2: Conformity (Goske, 2006).

To answer these questions two approaches are going to be used: an experiment, which is explained in details in the section 4 and numerical simulation, which is explained in the section **Error! Reference source not found.**. The whole methodology, and the way that the study was segregated, is explained detailed in section **Error! Reference source not found.**.

Results of both: numerical simulation and experiment are going to be compared, to completely understand the influence of the proposed footwear variables on the plantar

pressure distribution. Thus, the first step of study is to model a three-dimensional, sufficiently anatomically detailed human foot and its structures based on computer tomography (CT) scans.

Using this model, the next step is to perform a Finite Element Analysis (FEA) to evaluate foot-insole interaction, under standardized loading conditions, i.e., test a variety of design criteria, as mentioned above, by systematically changing its geometric and constitutive properties.

The particular issue, which is going to be investigated, is plantar pressure, and as mentioned above the peak plantar pressure. This value is going to be compared with experimental data to validate the model, and better understand the nature of foot-insole (through the two variables mentioned above) interaction.

With that in hand, it is expected that the model will become a tool to optimize parameters (manufacture variables) in the development of performance footwear, and later on used to simulate more complex movements and loadings cases.

1.3 Significance

The understanding of biomechanical behavior of foot is important in numerous applications: medical (towards diagnosis and prognosis), biomechanics (concerning the design or performance enhancements) or safety areas. For example, locating points of highly elevated stresses in the foot during gait is of major clinical importance in understanding the development mechanisms of stress fractures, arthrosis, or diabetic ulcers.

Focusing in a specific area for example, humans who perform sports involving impulsive contact between the plantar aspect of the foot and a support surface, such as in running and gymnastics, are frequently injured (Robbins S. *et al.*, 1997). The injuries are thought to be caused by the cumulative effect of repeated trauma from excessive vertical impact (Robbins S. *et al.*, 1997).

Thus, the comprehension of the mechanical behavior of the foot under this kind of situations can enhance the design of shoes as a whole (insole, midsole, and walls) playing a major role in the prevention of injury, and, secondarily, improve comfort, which is important for the appropriate execution of sports activities.

In fact, the relative contributions of the available design variables such as geometry and material properties on pressure relief are not known, thus performing accurate computational simulations of the foot and footwear are promising alternatives to experimentation when designing insoles for plantar pressure relief since the design space, e.g. material properties, geometry, can be systematically evaluated to optimize the product. Furthermore, this computational approach reduces the cost and danger of other testing procedures, as well the burden of large volume of data.

1.4 Literature Review

1.4.1 Numerical Analysis of 3D models by Finite Element Method

The latest quantitative models that have analyzed the human foot as a mechanical structure used various simplifying assumptions concerning its geometry, mechanical properties of its tissues, and muscle loading. Nakamura et al. (1981) used a two-dimensional Finite Element (FE) model in an attempt to predict the stress states within the plantar soft tissue of the human foot for different shoe conditions. In his work, a single elastic body represented the complex bony structure of the foot with its articulated joints.

A major breakthrough was achieved by Simkin (1982), who developed a static model of the foot during standing, using matrix structural analysis. This model was both representative and quantitative in the three dimensions. However, as some joint geometric misrepresentation could not be avoided when using matrix structural analysis, the resulted reduced accuracy in the field of displacements did not allow a complete validation of the model.

More complex models of similar concept, consisting of hinge joints, springs, and dampers to represent viscoelastic behavior, were recently suggested by Gilchrist et al. (1996) and Chu et al. (1995) presented an asymmetric three-dimensional FE foot model for analysis of ankle-foot orthosis effects. Linear elastic ligaments and soft tissue were included in this model, yet, the complex articulated structure of the foot skeleton was treated as a single body.

Patyl and colleagues (1996) used a two-dimensional finite element (FE) model to study regions of high stress in normal and neuropathic feet during gait, was constructed according to the two-dimensional cross-sectional anatomy of the foot, obtained from a lateral X-ray image; although their work is an important step toward the ability to predict structural stress concentrations in normal and disordered feet, the two-dimensional approach limits the model validity. In the latest three-dimensional FE model of Patil's group (1996), bones of the medial and lateral arches in the medio-lateral directions are combined, forming, nonetheless, a simplified foot structure.

Geffen and colleagues (1998) achieved some enhancement in the simulation of foot behavior by using a five planar sections approach, in which each of the five foot rays is modeled as an individual two-dimensional structure. Nevertheless, this methodology cannot account for the three-dimensional interlinks among the foot skeletal components.

In the next year, Genda et al. (1999) constructed a model of 14 bones and 59

ligaments of the foot to study load transmission in the foot. They used Rigid Body Spring Modeling, in which bones were modeled as rigid bodies and ligaments were represented by springs. Contact surfaces were created between rigid bodies of the bones to transfer loads. For example, the results showed that the subtalar joint and talonavicular joints transmitted 62% and 38% of the load respectively.

In their next work, Geffen and colleagues (2000) presented for the first time in literature a complex three-dimensional finite element model of a normal foot structure, including cartilage and ligaments for simulation of realistic joint articulations, in discrete events during the stance phase of gait. In their model, the mechanical properties of bone and cartilage tissues of the foot were assumed to remain constant in time and to be homogenous, isotropic, and linear elastic. This assumption is generally adequate for analysis of bones subjected to dynamic loading but in the cartilage tissue, a quasi-linear viscoelastic assumption should be considered (Fung, 1994; Jacob *et al.*, 1996).

For their model, it is possible that introduction of a more realistic approach, not only for the cartilage but also for the plantar tissue pad, will decrease the foot-ground reaction forces, due to energy attenuation, and thereby, impose use of larger muscle forces to obtain successful validation with experimental data. Finally, imaging of the foot motion during gait was performed only in the sagittal, and not in the transverse plane. Therefore, the model still lacks input of the relative motion between bones in the transverse plane during the subphases of stance.

In the same year, Ledoux and colleagues created an anatomically accurate three-dimensional finite element model of the human foot and ankle, including ligaments and plantar aponeurosis, with origin from cadaveric dissection, description in the literature and photographic anatomy atlases. However, the model was simplified by grouping certain bones together to form single rigid bodies: the tibia and fibula, the first through fourth metatarsals and phalanges, the first metatarsal and phalanges, and the navicular and three cuneiform. Moreover, there were several limitations to the model, including the exclusion of muscle, which prevents accurate force application, and cartilage, which prevents accurate joint space descriptions. Additionally, all ligaments were assumed to be linear, which can potentially underestimate stiffness.

In the following work, Giddings et al. developed a FEM model of the foot that included some ligaments and the plantar fascia. The study aimed to create a model of the calcaneus without knowledge of the applied loads and joint pressures. The load was applied at the base of calcaneus and at the metatarsal heads based on ground reaction force experiments and the analysis was carried out in discrete increments of 20% of the stance phase of walking and running. In the calcaneus, they visually verified the

trajectories of principal stresses with orientation of trabeculae and found good correspondence. Even though there were variations in stress magnitudes for running and walking, the directions of principal stresses were unchanged. The predicted contact forces in the talocalceneal joint were 5.4 times body weight for walking and 7.9 times body weight for running.

The year of 2001 was a very prolific year: four significant works were published. Asai and colleagues performed a finite element analysis using a commercial foot skeletal model for computer graphics and anatomical data, with some simplifications. The hard tissue parts of their foot model consisted of 23 bone models, and the soft tissue parts that were modeled consisted of 15 joint models. The ligaments and retinacula were not geometrically represented. They solved this model for two cases: linear static analysis and dynamic transient analysis. As results, it seems that the stiffness of the soft tissue in their simulation model was slightly lower than that of a real human foot (cadaver). Moreover the vertical peak force, for the boundary condition set by them, was much higher than that reported for real human running.

Bandak and colleagues developed a three-dimensional finite element model of the human ankle joint to study the mechanisms of impact injury to the major bones of the foot. The model was based on anatomically realistic bone geometry obtained from medical imaging and included the major ligaments of the ankle. Careful consideration was given to model the soft tissues of the plantar surface of the foot. The model was used to simulate axial impulsive loading applied at the plantar surface of the foot. The stability of the ankle joint was achieved in the model strictly by the intrinsic anatomical geometry and the ligamenteous structure. The time history response of input/output accelerations and forces compared reasonably well with experimental data. Results indicate that the calcaneus experiences the highest stresses followed by the tibia and talus. The findings were in agreement with several experimental data on calcaneal fracture in axial dynamic loading. Also, the model gave stress localization in the lateral-collateral ligaments that agrees with injury observations for that region.

Amit Gefen presented a study to determine the effects of ankle dorsiflexor muscle weakness on the structural stability of the foot and, consequently, on the risk of falls during gait. The finite element model utilized in that study had been developed and published in the previous year. Weng-Pin Chen and colleagues developed a 3-D Finite Element model with several simplifications. Among these simplifications we can mention: bones in the five phalanges were modeled to be five integrated parts in the rest of the metatarsals and tarsal bones were modeled with to rigid columns (medial and lateral) without segmenting each of the individual bones in order to reduce the

complexity of the model. The medial column consisted of the first three metatarsals, three cuneiforms (medial, intermediate and lateral), navicular, talus and tibia. The lateral column consisted of the fourth and fifth metatarsal, cuboid, calcaneus, and fibula. The joint spaces between each of the five phalanges and its connective metatarsal bones were modeled with cartilage elements in an attempt to allow deformation and to simulate the metatarsalphalangeal joints. Also the joint space between the medial and the lateral columns representing the metatarsal and the tarsal bones was also modeled with cartilage elements. Despite the simplification on the model, including geometry and materials, the plantar pressure patterns were similar to measurement result from previous literature.

Their analysis was performed for loading condition simulating barefoot gait during mid-stance to push-off. The peak plantar pressure ranged from 374 to 1003 kPa and the peak von Mises stress in the bone ranged from 2.12 to 6.91 MPa at different instants. It is important to mention that their findings on plantar pressure patterns were similar to previous measurements results found in literature. However the magnitude of the measurements for plantar pressure differs significantly from previous works as Soames (1985) and Brown et al. (1996). In Soames' work, foot-mounted pad transducers were used to measure foot pressure during barefoot gait. The highest mean plantar pressure was found under the third metatarsal head and the values ranged from 550 to 590 kPa.

In the other hand, Brown and colleagues, used the FSCAN in-shoe pressure measuring system to determine the efficacy of pressure redistribution with Plastazote, Spenco, cork, and plastic foot orthoses as compared with that of the control (no orthosis). They concluded that Plastazote, cork, and plastic foot orthoses could be beneficial in relieving pressure in certain regions of the shoe–foot interface, but at the cost of increasing pressure in other areas of the plantar surface. There were no statistically significant changes in peak pressure between the orthotic and control conditions in the great toe, first metatarsal head, second through fifth toes, or total foot regions. Decreases in peak pressure were found in the forefoot, heel, and second through fifth metatarsal head regions when orthoses were worn. The average peak pressure ranges for the orthotic and control conditions at the three highest-pressure regions were: forefoot (1002–1126 kPa), heel (765–863 kPa), second through fifth metatarsal heads (383–453 kPa). These peak pressure values were higher than those reported in the previous studies by Lord and Hosein (1994) and Kato et al. (1996). These inconsistent results might be due to differences between measurements techniques and variations between subjects used in the experiments and subsequent

simulations.

In 2003, Chen et al. presented a new study, using the finite element model developed and described in their first study (2001). There, they used the model to investigate the effects of total contact insoles on the plantar stress redistribution. The result of their work is going to be presented in the section 5. In 2005 Cheung et al. presented two studies using the same finite element model. In the first study, they investigated the effect of material stiffness of flat and custom-molded insoles on plantar pressures and stress distribution in the bony and ligamentous structures of the foot during balanced standing. In order to do that, a three-dimensional finite element model of the human ankle-foot complex and a custom-molded insole were developed from 3-D reconstruction of magnetic resonance images and surface digitization. The distal tibia and fibula, together with 26 foot bones and 72 major ligaments and the plantar fascia, were embedded in a volume of soft tissues.

The main outcome measures were: Foot-support interfacial pressure, von Mises stress in bony structures, and strain of the plantar fascia. Their findings show that custom-molded, soft (Young modulus, E=0.3MPa) insole reduced the peak plantar pressure by 40.7% and 31.6% at the metatarsal and heel region, respectively, compared with those under a flat, hard (E=1000MPa) insole. Meanwhile, a 59.7% increase in the contact area of the plantar foot was predicted with a corresponding peak plantar pressure increase of 22.2% in the midfoot. The predicted plantar pressure distribution pattern was, in general, comparable to the F-scan measurement.

The predicted peak von Mises stress showed that the midshaft of the second and third metatarsals were the most vulnerable regions. The confined positions of these metatarsals, especially with tissue stiffening, are probably the cause of stress concentration. Apart from the midshaft of the metatarsals, the junctions of the subtalar and calcaneocuboid joints were also possible sites of fracture or lesion under weight bearing.

1.4.2 Footwear Related Research

Hitherto, there are only a limited number of studies in the literature that have investigated footwear using finite element method. The pioneer study on foot-insole interaction was published in 1997 by Lemon et al. (David Lemmon, 1997). They investigated alterations in pressure under the second metatarsal head as a function of insole thickness and tissue thickness using, both experimental and quasi-static plane strain, finite element analysis. As results, they found that the orthoses chosen reduced plantar pressure by a maximum of approximately 30% and were more effective (on a percentage basis) in the setting of reduced sub-metatarsal tissue thickness. Peak normal stresses predicted by the Finite Element models were, on average, within 5.9% of experimentally measured values for the normal tissue case and 8.1% for the reduced tissue case. It has been demonstrated that the finite element method can be a promising means for predicting the stress distributions in the foot–insole interface if the complex geometry and material conditions of the foot and insole are properly taken into account.

In 2003, Chen et al. (Chen *et al.*, 2003) presented a study about effects of total contact insoles on the plantar stress distribution. Results showed that the peak and the average normal stresses were reduced in most of the plantar regions except the midfoot and the hallux region when total contact insoles were worn compared with that of the flat insole condition. The reduction ratios of the peak normal stress ranged from 19.8% to 56.8%. Similar results were reported by Lord and Hosein (1994) who used pressure-measuring insole systems. In their study, custom-molded inserts used in the orthopedic shoes of diabetic patients at risk of plantar ulceration were compared with flat inserts. They found that the pressure was reduced significantly with the use of molded inserts (flat inserts: 305±79 kPa; molded inserts: 216±70 kPa; $n = 6$, $p < 0.005$). Kato et al. (1996) investigated the effects of foot orthoses on the distribution of plantar pressures using a pressure sensitive insole in seven diabetic patients (13 feet). They found that the pre-orthotic peak pressure was 130.6±41.9 kPa, while the post-orthotic peak pressure was reduced to 52.6±17.9 kPa. The mean reduction of pressure was 56.3%.

In an axisymmetric finite element model of the heel, Verdejo and Mills (2004) (Verdejo *et al.*, 2004) evaluated running-shoe midsoles and estimated a 65% decrease in vertical compressive stresses of the heel compared with barefoot loading. It is widely believed that conformity, or cupping the heel, is effective in reducing both heel plantar pressure and heel pain, and such products have proven to be effective for patients

suffering from plantar fasciitis (Pfeffer et al., 1999). None of these studies investigated insole design variables such as conformity, material, and thickness that potentially influence pressure distribution underneath the heel. In addition, midsoles or insoles were modeled as isolated components, ignoring other features of footwear such as sidewalls that might confine the heel and alter pressure distribution.

Edermir et al. (2005) published an investigation about multiple design variables such as conformity of the insole, insole thickness and material. They included on the model the major components of the footwear (midsole and sidewalls), which is up to now, the footwear model with more details and components. As main outcome of this research, they found that full-conforming insole designs provide the greatest reduction of heel pressures compared to the barefoot condition. Keeping insole material and thickness under the mid portion of the heel constant and changing the insole profile from flat to full conforming allowed reduced peak pressures by up to 26.3%. This finding is very similar to the relative decreases in peak pressures reported by Bus et al. (2004) of up to 23% by simply using a custom-made conforming insole instead of a flat one. Absolute reductions in heel peak pressures (when compared to barefoot) were up to 60% when using an insole that conformed to the heel (Lobmann et al., 2001; Bus et al., 2004).

In 2006, Goske and colleagues presented a two-dimensional plane strain finite element model to investigate 27 insole designs: combinations of three insole conformity levels (flat, half conforming and conforming), three insole thickness values (6.3, 9.5 and 12.7 mm) and three insole materials (Poron Cushioning, Microcel Puff Lite and Microcel Puff) during the early support phase of gait. As good points on this study we emphasize that plantar pressures predicted by the model were validated by experimental trials conducted in the same subject whose heel was modeled by loading the bare foot on a rigid surface and on foam mats. Another very important point is that at first time in literature, other footwear components (midsole and walls) were taken into account. The results showed that conformity of the insole was the most important design variable, whereas peak pressures were relatively insensitive to insole material selection. The model predicted a 24% relief in pressure compared to barefoot conditions when using flat insoles; the reduction increased up to 44% for full conforming insoles. The only disadvantage of this study was to confine the study to 2D, consequently consider only a section on the rearfoot region, neglecting other regions.

1.5 Thesis Scope

The attempt of this thesis is to find how two footwear design parameters (conformity and material) affect plantar pressure distribution. In order to find the proposed, we use numerical simulation and experiment, to generate the necessary data.

1.6 Chapter Overview

Chapter 1: It defines the main question of the study with its goals, significance and review of previous studies.

Chapter 2: It presents a detailed explanation about the structure subject of our study: the human foot and its components, anatomical terms, kinesiology terms, and biomechanical terms.

Chapter 3: It describes the methodology, i.e., a research design adopted to answer the main question and its nuances. Moreover shows, in detail, the model's construction.

Chapter 4: It dissertates about the experiments: pilot and final, clarifying about subjects, apparatus and experiment design.

Chapter 5: It debates about results and its interpretation. It is the rationale of this study.

Chapter 6: It presents limitation of the study and it draws conclusions and suggestions about the theme.

Chapter 7: It is about future direction of this study. In other words: what else can be done about the theme.

Chapter 8: It presents bibliography references.

Chapter 9: It contains extra information about the experiment and simulation data, which are going to be used in a following study.

2 Foot Anatomy

2.1 Human Foot: an overview

The human foot is a complex multi-articular mechanical structure consisting of bones, joints and soft tissues, playing an extremely important role in the biomechanical function of the lower extremity and is controlled by both intrinsic and extrinsic muscles. It is the only part of the body that acts on an external surface, providing support and balance during standing and stabilizing the body during gait(Abboud, 2002).

The foot has two important functions: weight bearing and propulsion. These functions require a high degree of stability. In addition, the foot must be flexible, so it can adapt to uneven surfaces. The multiple bones and joints of the foot give it flexibility, but these multiple bones must form an arch to support any weight.

The foot must also be relatively compliant to cope with uneven ground, both bare and shod, while maintaining its functional integrity. During ground contact, foot function reverses the convention that a muscle is fixed at its origin and moves from its insertion. The conventional anatomical insertion is often fixed against the ground, and the origin in the heel or leg moves in relation to that fixed point. This provides both flexibility and stability during walking. The important mechanical structures of the foot and ankle contain:

1. The bony skeleton containing 26 bones: seven tarsals, five metatarsals, and 14 phalanges. Working in synergy with the ligaments and arches, provides relative rigidity and the essential lever arm mechanism required to maintain balance during standing and facilitate propulsion,

2. The lower extremity joints have the following nomenclature: ankle, subtalar, midtarsal, tarsometatarsal, metatarsophalangeal (MTP) and interphalangeal (IP) joints, confer flexibility and resiliency to the foot structure,

3. More than 100 different soft tissues such muscles (20), tendons and ligaments, which control foot movement and stability,

4. A network of blood vessels, nerves and soft tissue as fat and skin.

The foot is the end part of the lower kinetic chain that opposes external resistance. Normal arthrokinematics and proprioception within the foot and ankle influence the ability of the lower limb to attenuate the forces of weight bearing (static and dynamic). The lower extremity should distribute and dissipate compressive, tensile, shearing, and rotatory forces during the stance phase of gait. Inadequate distribution of these forces can lead to abnormal movement, which in turn produces excessive stress, which can

result in the breakdown of soft tissue and muscle. The normal mechanics of the foot and ankle result in the most efficient force attenuation(Abboud, 2002). Structurally, the foot can be separated in four segments: the hindfoot, the midfoot, the forefoot and the phalanges.

2.2 Foot Structure Division

2.2.1 The Hindfoot

The hindfoot consists of three joints and two bones: the talus and calcaneus, linking the midfoot to the ankle through talus. Its top is connected to the long bones of the lower leg: tibia and fibula, forming a hinge that allows the foot to move up and down. Moreover, the three parts of the talus: body, neck, and head, are orientated to transmit reactive forces from the foot through the ankle joint to the leg. Lying between the calcaneus, and tibia, it communicates thrust from one to the other.

The calcaneus is the largest and most posterior tarsal bone in the foot and forms the heel. It provides a lever arm for the insertion of the Achilles tendon, which is the largest and one of the strongest tendons in the body through which gastrocnemius and soleus impart powerful plantar flexion forces to the foot. Its height, width and structure enable the calcaneus to withstand high tensile, bending and compressive forces on a regular basis without damage. It joins the talus to form the subtalar joint, which enables the foot to rotate at the ankle(Abboud, 2002).

The shape of calcaneus is complex. On its upper surface are three smooth facets, posterior, middle, and anterior, which articulate with corresponding facets on the lower surface of the talus to form the subtalar joint. Of these three talocalcaneal facets, the posterior is the largest, covering almost the entire width of the calcaneal body. The middle and anterior facets are located on the medial side of the upper calcaneal surface, and are usually continuous with each other. The middle and posterior facets are separated from each other by a deep groove, which together with a corresponding groove on the talus, forms a channel between the two bones called the sinus tarsi.

The lateral wall of calcaneus is nearly flat, except for a small ridge called the peroneal tubercle. The medial wall has a shelf-like projection, the sustentaculum tali. This shelf carries the middle talocalcaneal facet on its upper surface. The undersurface of the shelf has a groove for the flexor hallucis longus tendon.

The front or anterior process of calcaneus articulates with the cuboid bone to form the calcaneocuboid joint. The rear part of calcaneus consists of a large rounded projection, the calcaneal tuberosity, which forms the back of the heel and provides attachment for the Achilles tendon. The undersurface of the tuberosity forms the bottom of the heel; this surface comes into contact with the ground during weight bearing, cushioned by a fibroelastic fat pad.

The talus, which rests on top of calcaneus, also has a complex shape. The main part or body of the talus is roughly cubical. Its smooth, dome-shaped upper surface (the

talar dome) articulates with the distal ends of the tibia and fibula, the two bones of the lower leg, to form the ankle joint. The rear surface of the talar body protrudes backward to form a posterior process. In some individuals, the posterior process ossifies (develops into bone) independently, and may remain separate from the talar body as a small accessory bone called the os trigonum.

Projecting forward from the talar body is the head of the talus, which is separated from the body by a slight constriction called the neck. The talar head articulates with the navicular bone, forming the talonavicular joint. The lower surface of the talus contains three smooth facets, posterior, middle, and anterior, which articulate with the corresponding facets on the upper surface of calcaneus. The posterior facet (the largest of the three) covers the undersurface of the talar body; the anterior and middle facets are located on the undersurface of the talar head. Together, these three talocalcaneal articulations form the subtalar joint.

The subtalar joint is bound together by several talocalcaneal ligaments. In addition, it is supported by portions of the medial and lateral ligaments of the ankle, which span both the ankle and the subtalar joint. The calcaneocuboid and talonavicular joints, together referred to as the midtarsal joint, form the boundary between hindfoot and midfoot.

2.2.2 The Midfoot

The midfoot is composed of five of the seven tarsal bones, the navicular, cuboid, and three cuneiform bones. These can be thought of as being arranged in two irregular rows, with the cuboid occupying space in both rows. The proximal row contains the navicular (on the medial side of the foot) and the cuboid (on the lateral side). The navicular, medial to the cuboid, articulates with the head of the talus anteriorly and is the keystone at the top of the medial longitudinal arch.

The distal row contains the three cuneiforms (medial, intermediate, and lateral) and the cuboid (lateral to the lateral cuneiform). The cuboid articulates with the calcaneus proximally and the fourth and fifth metatarsals distally. The three cuneiforms, are convexly shaped on their broad dorsal aspect whilst the plantar surface is concave and wedge shaped so that the apex of each bone points inferiorly. The medial, intermediate, and lateral cuneiforms articulate, respectively, with the first, second and third metatarsals distally. This multi-segmental configuration in conjunction with connecting ligaments and muscles contributes greatly to the stability of the midfoot(Abboud, 2002).

The boundary between the midfoot and forefoot consists of five tarsometatarsal (TMT) joints, the joints between the distal row of the midfoot and the bases of the metatarsals. There are also multiple joints within the midfoot itself. The distal row of the midfoot has two intercuneiform joints (between adjacent cuneiforms) and a cuneocuboid joint (between the lateral cuneiform and the cuboid). Proximally, the three cuneiforms articulate with the navicular bone (the cuneonavicular joints). In some individuals, there is also a small articulation between the cuboid and navicular.

In addition to its articular surfaces, each tarsal bone has specific features adapted for function. For example, the medial surface of the navicular projects downward to form a tuberosity, which serves as an attachment for the tibialis posterior tendon. The lateral surface of the cuboid also has a tuberosity, which serves as a ligament attachment. The cuboid bone has no major tendon attachments; however, the peroneus longus tendon passes across the cuboid tuberosity, to run in a groove on the plantar surface of the bone. The peroneus longus tendon often contains a sesamoid bone, which articulates with a small facet (articular surface) on the tuberosity.

2.2.3 The Forefoot

There are five metatarsals in the forefoot, these all tapered distally and articulating with the proximal phalanges, the bones of the digits or toes. The first metatarsal is the shortest and widest. Its base articulates with the medial cuneiform and is somewhat cone shaped. Of the metatarsal bones, the first bears the most weight and plays the most important role in propulsion; it is therefore the shortest and thickest. It provides attachment for several tendons, including tibialis anterior and peroneus longus. The head of the first metatarsal additionally articulates with two sesamoids on its plantar articular surface.

The second, third, and fourth, called the internal metatarsals, are the most stable of the metatarsals, in part because of their protected position; but also because they have only minor tendon attachments, and therefore are not subjected to strong pulling forces. The second metatarsal extends beyond the first proximally, and articulates with the intermediate cuneiform as well as with the medial and lateral cuneiforms in a “key-like” configuration which promotes stability and renders the second ray the stiffest and most stable portion of the foot playing a key role in stabilizing foot posture after hallux surgery.

The third, fourth and fifth metatarsals are broad at the base, narrow in the diaphysis (shaft) and have dome-shaped heads. The fifth has a prominent styloid or tuberosity (protuberance), laterally and proximally at its base, on which the peroneus brevis tendon inserts. The tuberosity of the fifth metatarsal can be felt halfway along the lateral side of the foot.

The joints between the metatarsals and the proximal phalanges are called the metatarsophalangeal (MTP) joints. Each digit also has two interphalangeal (IP) joints, proximal (PIP) and distal (DIP), except for the big toe, which has only one IP joint. Each MTP and IP joint is bound together by several ligaments, one on each side of the joint (medial and lateral collateral ligaments), and one along the plantar (sole) surface (plantar ligament).

The first metatarsophalangeal (MTP) joint has an additional feature. Near the head of the first metatarsal, on the plantar surface of the foot, are two sesamoid bones. A sesamoid is a small, oval-shaped bone, which develops inside a tendon, where the tendon passes over a bony prominence. In this case, the tendon is that of flexor hallucis brevis, as it passes over the first metatarsal head. These sesamoid bones articulate with the head of the first metatarsal, and function as part of the first metatarsophalangeal (MTP) joint. They are held in place by their tendons, and are also supported by

ligaments. These include the sesamoid collateral ligaments (which bind the sesamoids to the metatarsal head) and the intersesamoidal ligament (which connects the sesamoids to each other).

2.3 The Phalanges

As the metatarsals, phalanges are long bones. Each has a diaphysis with slightly flaring ends. The proximal end or base of each bone has a smooth articular surface where it forms a joint with the adjacent bone. The distal end or head also has an articular surface, except for the distal phalanges, whose distal ends provide attachment for the soft tissue (pulp) of the digit tips.

Phalanges constitute digits. Each digit has three phalanges: proximal, middle, and distal, except for the big toe, which has two: proximal and distal. The digits and their metatarsal rays are numbered from one to five, starting with the big toe or hallux. The hallux consists of two phalanges, all other toes containing three. The heads of the proximal and middle phalanges tend to be trochlear shaped allowing for greater stability. Functionally, the toes contribute to weight bearing and load distribution and also effect propulsion during the push-off phase of gait.

2.4 Ossicles

The foot contains a variable number of ossicles or small bones. These are of two types, sesamoid bones and accessory bones. Sesamoids are small bones that develop inside a tendon, where the tendon passes over a bony prominence. The two sesamoid bones of the first metatarsophalangeal (MTP) joint have already been mentioned; these are a constant feature. The other metatarsophalangeal (MTP) joints only occasionally have sesamoid bones. The peroneus longus tendon frequently contains a sesamoid bone, at the point where it passes over the cuboid tuberosity. Sesamoids may also occur in other locations in the foot.

The foot may also contain ossicles that are not associated with a tendon, but result from developmental variations. In the fetus, the skeleton initially consists of cartilage, which gradually ossifies during fetal development and childhood. Each bone has a primary ossification center. The process of ossification progresses outward from this center, until the bone is completely ossified. In long bones, the primary center is located in the middle of the shaft; later, secondary ossification centers develop at the ends of the long bone.

Irregularly shaped bones such as the tarsal bones may also develop secondary centers. In some individuals, complete ossification does not occur; the secondary center remains separate from the rest of the bone, forming an accessory ossicle. An example is the os trigonum, which arises as a secondary ossification center in the posterior process

of the talus. About 50% of individuals have an os trigonum. Accessory ossicles may also occur in other locations in the foot.

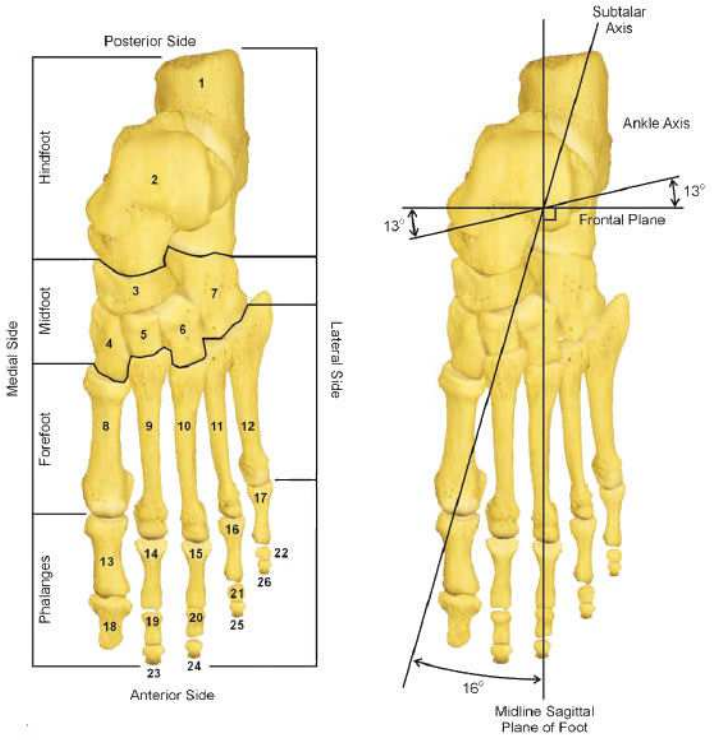

Figure 2-1: Foot structure: four segments: hindfoot (1, 2), midfoot (3-7), forefoot (8-12), phalanges (13-26). Foot Bones nomenclature: calcaneus (1), talus (2), navicular (3), medial cuneiform (4), intermediate cuneiform (5), lateral cuneiform (6), cuboid (7), first metatarsal (8), second metatarsal (9), third metatarsal (10), fourth metatarsal (11), fifth metatarsal (12), proximal phalanges (13-17), distal phalange (18), middle phalanges (19-22) and, distal phalanges (23-26).

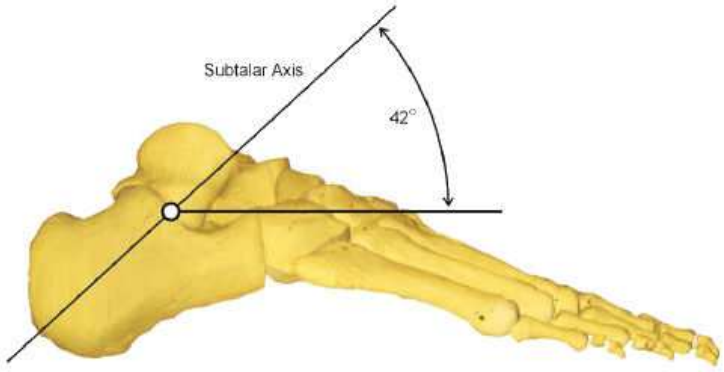

Figure 2-2: Lateral view: ankle and subtalar axis (Abboud, 2002).

2.5 Function

Joints of the foot are controlled by extrinsic and intrinsic muscles of the lower limb and provide for the major motion function, angulation and support of the foot. As with all joints, motion occurs by rotation about an axis in a plane of motion. The three planes of motion in the foot are defined as: sagittal plane (sp), frontal plane (fp) and transverse plane (tp)(Abboud, 2002). These movements are complex - mainly because they are described with respect to the anatomical axes, while the axis of joint movement lie at an angle to these axes.

The foot, or any part of the foot, is defined as being adducted when its distal aspect is angulated towards the midline of the body in the transverse plane and deviated from the sagittal plane passing through the proximal aspect of the foot, or other specified anatomical reference point. Abduction is when the distal aspect is angulated away from the midline (Figure 2-3(A)).

The foot is defined as being plantar flexed when the distal aspect is angulated downwards in the sagittal plane away from the tibia, and dorsiflexed when the distal aspect is angulated towards the tibia in the sagittal plane (Figure 2-3(B)). The foot is described as being inverted when it is tilted in the frontal plane, such that its plantar surface faces towards the midline of the body and away from the transverse plane, and everted when its plantar surface faces away from the midline of the body and away from the transverse plane (Figure 2-3(C)).

The foot is considered to be supinated when it is simultaneously adducted, inverted and plantar flexed, and pronated when it is abducted, everted and dorsiflexed (Figure 2-3(D)). With the exception of the midtarsal, metatarsophalangeal (MTP) and interphalangeal (IP) joints, the three remaining major joints move in only one plane, i.e. one degree of freedom. The former three joints have two degrees of freedom of motion occurring independently of one another (adduction-abduction/ dorsiflexion-plantar flexion). The ankle joint is the articulation between the distal part of the tibia and the body of the talus, permitting dorsiflexion and plantar flexion of the foot around its axis of motion, which passes obliquely in a lateral-plantar-posterior, to medial-dorsal-anterior direction (Figure 2-2).

The minimum range of ankle joint motion as necessary for normal locomotion is 10^{o} of dorsiflexion and 20^{o} of plantar flexion. The ankle joint also has slight movement in the transverse plane during plantar flexion, causing instability of the joint in this position.3 The subtalar joint includes both the talocalcaneal joint and the talocalcaneal part of the talocalcaneonavicular joint, i.e. it is a composite terminology for the two

joints beneath the talus. Its axis of motion passes through the subtalar joint obliquely at approximately 42^{o} from the transverse plane (Tp) and 16^{o} from the sagittal plane (Sp) and resultant motion in frontal plane (Fp) (Figure 2-2); these motions occur simultaneously. The normal motions exhibited by this joint are supination and pronation. The talonavicular and the calcaneocuboid joints together form the midtarsal joint. This joint has two axes of motion, an oblique axis and a longitudinal axis, which are confined to the talonavicular joint, and the calcaneo-cuboid joint, respectively. Each axis allows movement in one plane only, but because it forms angles to the three body planes, supination/pronation of the forefoot results.

The interfaces between the posterior aspect of the metatarsal bones and the lesser tarsus produce the tarsometatarsal joints, which have a very limited range of gliding action. The exception to this is the joint between the first metatarsal bone and the medial cuneiform where considerable movement is possible. At the metatarsophalangeal (MTP) joints, the rounded heads of the metatarsal bones are located in the shallow cavities of the phalanges. Up to 90^{o} of extension is possible at these joints, but only a few degrees of flexion. All of the interphalangeal (IP) joints allow extension, which is related to abduction, and flexion, which is related to adduction, of the foot.

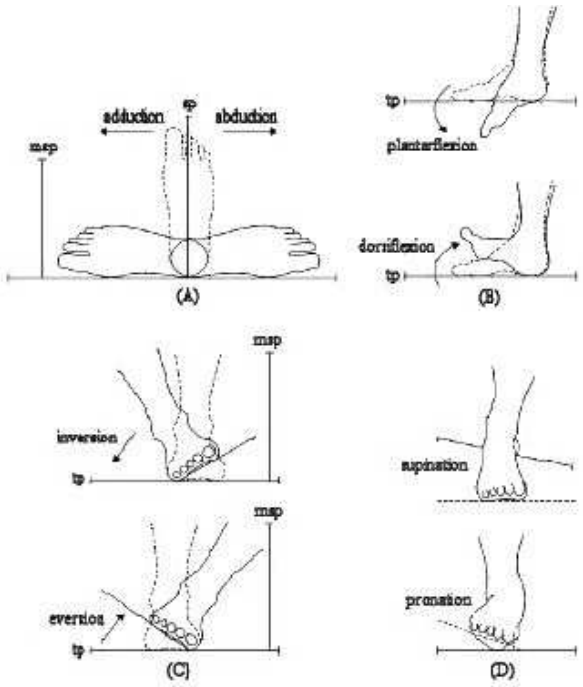

Figure 2-3: Movements of the Foot (Abboud, 2002).

2.6 Arches of the Foot

The foot has to both support body weight whilst standing and to act as a lever to propel the body during locomotion. These functions require a high degree of stability. In addition, the foot must be pliable, so it can adapt to standing and walking on uneven surfaces, forming a rigid platform that will not collapse under body weight, making good contact with almost any supporting surface. This is made possible by a series of multiple bones and joints forming longitudinal and transverse arches (TAs), maintained by ligaments and muscles.

Thee foot may be considered to have three arches: the medial longitudinal arch (MA), the lateral longitudinal arch (LA), and the transverse arch (TA). The medial longitudinal is the highest and most important of the three arches. It is composed of the calcaneus, talus, navicular, cuneiforms, and the first three metatarsals. The pillars of the arch are the tuberosity of the calcaneus posteriorly and the heads of the medial three metatarsal bones anteriorly. The talus occupies the highest point of the arch; with its head wedged between the calcaneus and navicular, it is the "keystone" that holds the arch together(Abboud, 2002).

The lateral longitudinal arch is lower and flatter than the medial longitudinal arch, consisting of the calcaneus, the cuboid and the fourth and fifth metatarsal bones, with cuboid as a keystone. The medial longitudinal arch and the lateral longitudinal arch are relatively rigid in standing but become more compliant during walking; where the medial longitudinal arch is the more flexible of the two.

The transverse arch, at right angles to the longitudinal arches, is formed by a series of transversal arches which exist around the metatarsophalangeal joints, forming a convex curve in the direction of the dorsum when looking at the plantar surface of a non-weight bearing foot. This series of transversal arches disappear and flatten to varying degrees, during weight bearing.

The integrity of the arches is supported by the ligaments, muscles and tendons, which provide the combined strength, flexibility and movement necessary for normal function. Their relative importance differs in the three arches; while muscles are indispensable to the maintenance of the medial longitudinal arch, ligaments are a relatively more important part in the lateral longitudinal arch (Abboud, 2002). The transverse arch is composed of the cuneiforms, the cuboid, and the five metatarsal bases. The wedge shapes of the cuneiforms help hold the transverse arch together.

The arches of the foot are maintained not only by the shape of the bones themselves, but also by the ligaments that bind the bones together. In addition, muscles

and tendons play an important role in supporting the arches.

2.7 Muscles and Tendons of the Foot

The muscles of the foot are essential to maintain the shape of the functional foot. They can be divided into extrinsic muscles arising from the lower leg, and intrinsic muscles arising within the foot itself. These can in turn be divided into dorsal and plantar groups. During locomotion, all of the muscles of the lower limb are actively providing stability and balance during standing, and a strong lever arm effect during propulsion(Abboud, 2002).

The intrinsic muscles are located within the foot and cause movement of the toes. These muscles are flexors (plantar flexors), extensors (dorsiflexors), abductors, and adductors of the toes. Flexor hallucis brevis, whose tendon contains the sesamoid bones of the first MTP joint, is an intrinsic plantar flexor of the big toe. Several intrinsic muscles also help support the arches of the foot.

The extrinsic muscles are so called because they are located outside the foot, in the lower leg. They have long tendons that cross the ankle, to insert on the bones of the foot and assist in movement. The exception is the talus, which has no tendon attachments. Altogether there are thirteen tendons that cross the ankle. They are responsible for movements of the ankle, foot, and toes; some of these tendons also help support the arches of the foot. The extrinsic muscles and their tendons are described below.

Gastrocnemius and soleus, located in the posterior part of the lower extremity also known as calf, are the main plantar flexors of the ankle. Gastrocnemius has its origins on medial head from posterior nonarticular surface of medial femoral condyle; lateral head from lateral surface of femoral lateral condyle. The two heads unite into a broad aponeurosis which eventually unites with the deep tendon of the soleus to form the Achilles tendon.

Figure 2-4: Grastrocnemius (Copyright 2003-2004 University of Washington).

Soleus has its origins on posterior aspect of fibular head, upper 1/4 - 1/3 of posterior surface of fibula, middle 1/3 of medial border of tibial shaft, and from posterior surface of a tendinous arch spanning the two sites of bone origin. Eventually unites with the gastrocnemius aponeurosis to form the Achilles tendon, inserting on the middle 1/3 of the posterior calcaneal surface.

Figure 2-5: Soleus (Copyright 2003-2004 University of Washington).

Tibialis posterior located, located deep inside the calf, is the main invertor of the foot; in addition, it assists gastrocnemius and soleus with plantar flexion of the ankle. It has its origins on posterior aspect of interosseous membrane, superior 2/3 of medial posterior surface of fibula, superior aspect of posterior surface of tibia, and from intermuscular septum between muscles of posterior compartment and deep transverse septum.

Its tendon descends on the medial side of the ankle, passes behind and beneath the medial malleolus, and continues onto the foot. It splits into two slips after passing inferior to plantar calcaneonavicular ligament; superficial slip inserts on the tuberosity of the navicular bone and sometimes medial cuneiform; deeper slip divides again into slips inserting on plantar sufraces of metatarsals 2 - 4 and second cuneiform. About its actions: principal invertor of foot; also adducts foot, plantar flexes ankle, and helps to supinate the foot.

Figure 2-6: Tibialis Posterior (Copyright 2003-2004 University of Washington).

Tibialis anterior, located in the front of the leg, is the main dorsiflexor of the ankle; in addition, it assists tibialis posterior with foot inversion. It has its origins on the lateral condyle of tibia, proximal 1/2 - 2/3 or lateral surface of tibial diaphysis, interosseous membrane, and the deep surface of the fascia cruris. Its tendon descends over the front of the ankle, passing underneath a band of fibrous tissue called the extensor retinaculum, which holds the tendon in place. The tendon continues over the dorsum onto the medial side of the foot, to insert on the medial and plantar surfaces of 1st cuneiform and on base of first metatarsal.

Figure 2-7:Tibialis Anterior (Copyright 2003-2004 University of Washington).

Peroneus brevis and peroneus longus, located on the lateral side of the leg, are the main evertors of the foot; in addition, they assist with plantar flexion of the ankle. The peroneus brevis has its origins on the inferior 2/3 of lateral fibular surface; also anterior and posterior intermuscular septa of leg, while the peroneus longus has its origins on the head of fibula, upper 1/2 - 2/3 of lateral fibular shaft surface; also anterior and posterior intermuscular septa of leg.

Figure 2-8: Peronius Brevis (Copyright 2003-2004 University of Washington).

Their tendons descend together on the lateral side of the ankle, passing behind and beneath the lateral malleolus. The tendons continue forward along the lateral surface of the calcaneal body: brevis passes above the peroneal tubercle, longus below. Peroneus brevis then inserts on the lateral surface of styloid process of 5th metatarsal base. Peroneus longus crosses the cuboid tuberosity, runs in a groove on the underside of the cuboid bone, and continues across the sole of the foot to insert on the plantar posterolateral aspect of medial cuneiform and lateral side of 1st metatarsal base.

Figure 2-9: Peronius Longus (Copyright 2003-2004 University of Washington).

Flexor hallucis longus, located deep inside the calf, is primarily a plantar flexor of the big toe; however, it also assists with plantar flexion of the ankle and inversion of the foot. It has its origins on the inferior 2/3 of posterior surface of fibula, lower part of interosseous membrane. Its tendon descends on the medial side of the ankle, alongside the tibialis posterior tendon. After passing beneath the medial malleolus, the tendon continues onto the sole of the foot, and inserts on the plantar surface of base of distal phalanx of great toe.

Figure 2-10: Flexor Hallucis Longus (Copyright 2003-2004 University of Washington).

Flexor digitorum longus, located deep inside the calf, is primarily a plantar flexor of the second through fifth toes; however, like flexor hallucis longus, it also assists with plantar flexion of the ankle and inversion of the foot. It has its origins on the posterior surface of tibia distal to popliteal line. Its tendon descends on the medial side of the ankle, alongside tibialis posterior and flexor hallucis longus. After passing beneath the medial malleolus, the tendon continues onto the sole of the foot, where it separates into four divisions. The four divisions after passing through medial intermuscular septum of plantar surface of foot; these slips then insert on plantar surface of bases of 2nd - 5th distal phalanges.

Figure 2-11: Flexor Digitorum Longus (Copyright 2003-2004 University of Washington).

Extensor hallucis longus, located in the front of the leg, is primarily a dorsiflexor of the big toe; however, it also assists with ankle dorsiflexion and foot inversion. It has its origins on the anterior surface of the fibula and the adjacent interosseous membrane. Its tendon descends over the front of the ankle, passes under the extensor retinaculum, and continues onto the dorsum of the foot, to insert on the base and dorsal center of distal phalanx of great toe.

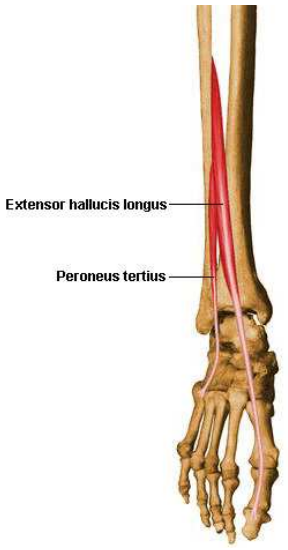

Figure 2-12: Extensor Hallucis Longus and Peroneus Tertius (Copyright 2003-2004 University of Washington).

Extensor digitorum longus, located in the front of the leg, is primarily a dorsiflexor of the second through fifth toes; however, it also assists with ankle dorsiflexion and foot eversion. It has its origins on the lateral condyle of fibula, upper 2/3 - 3/4 of medial fibular shaft surface, upper part of interosseous membrane, fascia cruris, and anterior intermuscular septum. It gives rise to five tendons, which descend together over the front of the ankle and pass under the extensor retinaculum. As they continue onto the dorsum of the foot, the tendons diverge. Four of them insert on the distal phalanges of the second through fifth toes. The fifth, called peroneus tertius, inserts on the fifth metatarsal. Peroneus tertius does not contribute to toe dorsiflexion; however, it helps dorsiflex the ankle and assists with foot eversion.

Except for the Achilles tendon, which descends vertically to insert on the calcaneus, all of the above tendons change their direction from vertical to horizontal as they cross the ankle. The lateral tendons: peroneus brevis and longus, change direction by passing under the lateral malleolus, which acts as a pulley. Peroneus longus then

changes direction a second time, with the cuboid bone as a pulley. Similarly, the medial tendons: tibialis posterior, flexor digitorum longus, and flexor hallucis longus, change direction as they pass under the medial malleolus.

Figure 2-13: Extensor Digitorum Longus (Copyright 2003-2004 University of Washington).

The anterior tendons: tibialis anterior, extensor digitorum longus, and extensor hallucis longus, change directions as they pass onto the dorsum of the foot, with the extensor retinaculum as the pulley. Each tendon, as it passes over its pulley, is enveloped by a tendon sheath lined with synovium. The synovial lining secretes a lubricating fluid that minimizes friction. Only the Achilles tendon has no pulley and no synovial sheath.

In addition to producing movements of the ankle, foot, and toes, the tendons of several extrinsic muscles help maintain the arches of the foot. The medial longitudinal arch is supported by tibialis posterior and anterior, as well as flexor hallucis longus and flexor digitorum longus. Of these, tibialis posterior is the most important. The lateral longitudinal arch is supported by peroneus brevis and longus, along with the lateral divisions of flexor digitorum longus. The transverse arch is supported by peroneus longus.

3 Image Base Analysis of Human Foot

The simple definition of research design is a specific plan for studying the research problem, providing the glue that holds the major parts of the research project: data acquisition (measures), simulation, and methods. It is the complete strategy of attack on the central research problem. It provides the overall structure for the procedures that the researcher follows, the data that the researcher collects, and the data analysis that the researcher conducts. In order to answer the main question concerning this study the data acquisition was divided in three stages:

1-Image Analysis (section 3.2),

2-Finite Element Analysis (section 3.3),

3-Pressure Measurements (section 4).

The main stages (steps) of the whole process, involved to answer the study questions, are depicted in Figure 3-1.

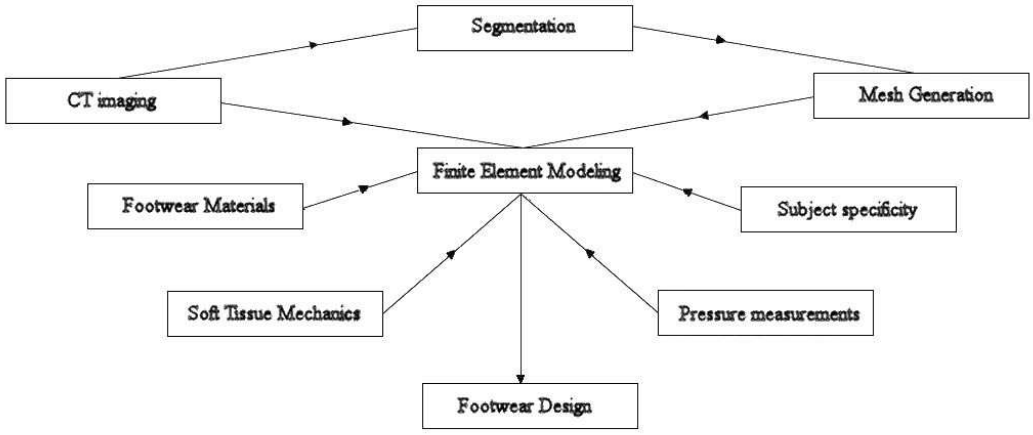

Figure 3-1: Methodology used to approach the problem.

3.1 Data Acquisition: Computed Tomography (CT) scans

The first step in the creation of a finite element model is to represent its geometry in the computer. Depending on the problem to be investigated, the numerical representation of the object under study can be achieved either two-dimensionally (2D) or three-dimensionally (3D) in several ways.

When objects to be modeled are based on so-called "primitive shapes" (i.e., circle, rectangle, sphere, tube, etc.), then the determination of linear measurements and their manipulation in commercially available computer-aided design (CAD) programs are readily accomplished. In cases of 2D anatomical shapes, their contours are converted into digital format after the tracing of histological sections or images of any kind (Korioth, 1997).

If the creation of a 3D anatomical structure is attempted, then more sophisticated techniques are required. Among these, the traditional way has been by means of recreation and digitization of planar outlines of the spatial anatomy. Once in digital format, the outlines or cross-sections are manipulated to form finite elements models, a process which often involves time-consuming efforts by the modeler.

In addition, this process is prone to errors due to shifts of the cross-sections, which often become more evident in the final models due to uneven surfaces. If left uncorrected, these geometric inaccuracies may induce faulty predictions; regardless of the degree of finite element mesh refinement.

However, there are more efficient methods available for the building of anatomically correct replicas. These include the application of specialized software for direct translation of the 3D information from imaging formats, e.g., computerized tomography (CT) (this technique was used in this study and it is briefly described in the following lines) or magnetic resonance imaging (MRI), into finite element meshes, including some material properties such as density values (Keyak et al., 1990; Cahoon and Hannam, 1994 *apud* Korioth et al. 1997). Small hard-tissue details in large systems such as the human foot can already be reliably reproduced in 3D by means of spiral CT and volumetric rendering of voxel sum images (Vannier et al., 1995 *apud* Korioth et al. 1997).

A computerized axial tomography scan is more commonly known by its abbreviated name, CAT scan or CT scan. It is an x-ray procedure which combines many x-ray images with the aid of a computer to generate cross-sectional views and, if needed, three-dimensional images of the internal organs and structures of the body.

A CAT scan is used to define normal and abnormal structures in the body and/or

assist in procedures by helping to accurately guide the placement of instruments or treatments. A large donut-shaped x-ray machine takes x-ray images at many different angles around the body. These images are processed by a computer to produce cross-sectional pictures of the body. In each of these pictures the body is seen as an x-ray "slice" of the body, which is recorded on a film. This recorded image is called a tomogram.

Technically, CT images are a pixel map of the linear X-ray attenuation coefficient of tissue. The pixel values are scaled so that the linear X-ray attenuation coefficient of air equals -1024 and that of water equals 0. This scale is called the Hounsfield scale after Godfrey Hounsfield, one of the pioneers in computerized tomography.

Using this scale, fat is around -110, muscle is around 40, trabecular bone is in the range of 100 to 300 and cortical bone extends above trabecular bone to about 2000. Just to exemplify, the Figure 3-2 shows some values of intensities in Hounsfield units for some biological tissues. Thus the various structures, composed of different tissues, inside the human body can be identified using image analysis, which is going to be explained in the section 3.2.

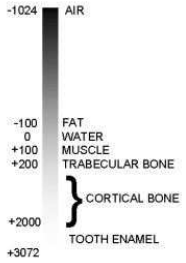

Figure 3-2: Some tissues intensity in Hounsfield units.

The pixel values are shown graphically by a set of gray levels that vary linearly from black to white as can be seen in the Figure 3-3. The mapping of pixel values into gray levels is specified by a level and a width. A gray scale is centered about its level.

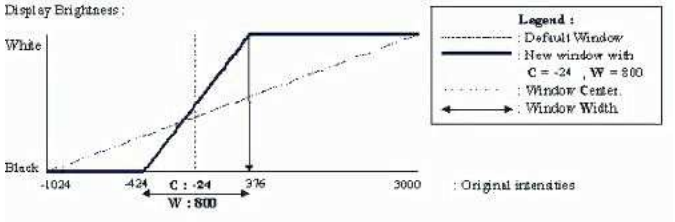

Figure 3-3: Pixels intensity scale.

Moreover, computer tomography is a non-destructive method used to scan complex geometries, including live bodies. It has several advantages, especially when

compared with other methods, such as the serial cuts method. Some advantages and disadvantages are summarized on the Table 3-1(Hart *et al.*, 1992):

	Advantages	Disadvantages
CT	Accuracy of cross-sectional geometry and achievement of bone density (HOUNSFIELD Unit)	Uncertainly regarding trabecular CT bone orientation
	Accuracy and speed of digitalization	Need to access to a CT scanner

Table 3-1: Advantages and disadvantages of the computer tomography technique.

Following an explanation about the CT technique, the natural step is to clarify the model's construction. The Finite Element model was constructed based on a right foot of a 50-year-old male subject, without any foot pathology. The CT scan images were acquired using a TOSHIBA/Aquilion scanner (Figure 3-4) with series of 277 scans taken at 1 mm interval in the transverse plane. The scanner resolution was 512 by 512 pixels and each pixel length 0.976 mm. This first step (CT scan) was performed by the Alive Human Body Team at RIKEN.

Figure 3-4: Computerized Tomography Scanner.

The next step is to perform segmentation. Thus: all the cross section foot images, acquired from the CT scan (2D DICOM format), were converted to bitmap format, and then transferred to a segmentation program called Mimics version 10.01 (Materialise Group 1996-2006).

Using this program, the segmentation of the different structures of the foot was performed, and the solids were generated. The solid, generated by this program, is an enclosed volume delimited by a 2D triangular mesh. This mesh was then exported to a meshing program (Mimics Remesh version 9.9) to increase the quality of triangles, as well to make the mesh more uniform. More details about mesh generation and quality check are going to be addressed in the section 3.3.2. From now, I shall dissertate about segmentation and some of its techniques (algorithms).

3.2 Volume Segmentation (image analysis)

Rapid advances in the field of medical imaging are revolutionizing medicine. Computed tomography (CT), magnetic resonance imaging (MRI), and other imaging modalities provide an effective means of non-invasively mapping the anatomy of a subject. This allows scientists and physicians to virtually interact with anatomical structures and learn potentially life saving information.

Today, the role of medical imaging is not limited to simple visualization and inspection of anatomic structures, but goes beyond that to patient diagnosis, advanced surgical planning and simulation, radiotherapy planning etc. Although modern volume visualization techniques provide extremely accurate and high quality 3D view of anatomical structures, their utilization for accurate and efficient analysis is still limited (Lakare, 2000).

One of the main reasons for this is the highly complex internal structure of animals and humans with vast number of anatomical organs bunched together, hindering the physicians view in more ways than one. Some visualization tricks like making an object transparent do not work in such cases.

To tackle this issue, the anatomical structure or the region of interest needs to be delineated and separated out so that it can be viewed individually. This technique is known as image segmentation in the world of medical imaging. In other words, segmentation is the partitioning of a digital image into multiple regions (sets of pixels), according to a given criterion such texture or intensity. These sets of pixels are denominated masks.

If the domain of the image is given by I, then the segmentation problem is to determine the sets or masks $S_k \subset \mathrm{I}$ whose union is the entire image I. Thus, the sets (masks) that make up a segmentation must satisfy

$$\mathrm{I} = \bigcup_{k=1}^{K} \mathrm{S}_k$$

Where for $S_k \cap S_j = 0$ for $k \neq j$, and each $\mathrm{S_k}$ is connected. Ideally, a segmentation method finds those sets that correspond to distinct anatomical structures or regions of interest in the image.

In order to make clear the idea of segmentation the best way is to provide an example. Considering the original mask (Figure 3-5 (top) which corresponds to a human lower leg), we want to obtain only the bony structures contained on it. First step is to

find one appropriate criteria to start the segmentation. In this example a single value of threshold was selected as criterion (Figure 3-2). After applying a segmentation technique (algorithm) the results, as a new mask (in red) can be seen in the Figure 3-5 (bottom). Notice that despite all bones were separated in a different mask, there still some extra pixels (structure surrounding the foot) that must be removed manually or via another segmentation algorithm.

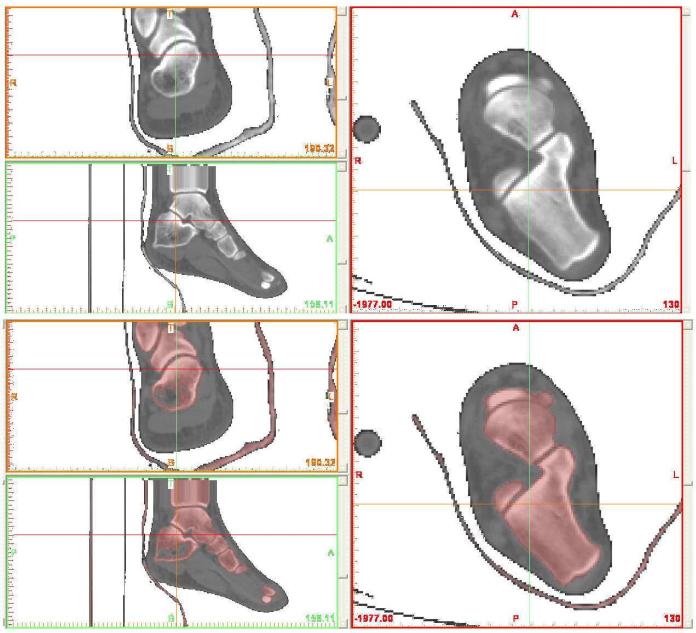

Figure 3-5: Example of segmentation aiming the foot bones: original mask (on the top) and after applying a segmentation process (on the bottom).

After this short depicted elucidation, let's go back to the analytical approach of this problem. Most of the image segmentation methods that I will describe can be posed as optimization problems where the desired segmentation minimizes some energy or cost function defined by the particular application. In probabilistic methods, this is equivalent to maximizing a likelihood or *a posteriori* probability. Given the image $\hat{x}$, we desire the segmentation

$$\hat{x} = \arg\min_{x} \varepsilon(x, y)$$

where ε, the energy function, depends on the observed image y and a

segmentation x. Defining an appropriate ε is a major difficulty in designing segmentation algorithms because of the wide variety of image properties that can be used, such as intensity, edges, and texture. In addition to information derived from the image, prior knowledge can also be incorporated to further improve performance. The advantage of posing a segmentation as an optimization problem is that it precisely defines what is desirable in the segmentation. It is clear that for different applications, different energy functions are necessary (Pham *et al.*, 1998).

Since segmentation of organs or region-of-interest from single image is of hardly any significance for volume rendering, we only concentrate on segmentation from 3D volumes (which are basically consecutive images stacked together). We thus refer to this technique as volume segmentation. Segmentation in medical imaging is generally considered a very difficult problem. This difficulty mainly arises due to the sheer size of the datasets coupled with the complexity and variability of the anatomic organs. The situation is worsened by the shortcomings of imaging modalities, such as sampling artifacts, noise, low contrast etc. which may cause the boundaries of anatomical structures to be indistinct and disconnected.

Thus the main challenge of segmentation algorithms is to accurately extract the boundary of the organ or region-of-interest and separate it out from the rest of the dataset. There are many approaches for segmentation proposed in literature. These vary widely depending on the specific application, imaging modality (CT, MRI, etc.), and other factors. For example, the segmentation of bone tissue has different issues than the segmentation of soft tissue. The same algorithm, which gives excellent results for one application, might not even work for another (Lakare, 2000).

General imaging artifacts such as noise, partial volume effects, and motion can also have significant consequences on the performance of segmentation algorithms. For example, a segmentation algorithm could be robust against noise, but at the same time, it might fail miserably in the presence of partial volume effects. Furthermore, each imaging modality has its own idiosyncrasies with which to contend (Pham *et al.*, 1998).

There is currently no single segmentation method that yields acceptable results for every medical image. Methods do exist that are more general and can be applied to a variety of data. This variability is what makes segmentation a very challenging problem. In fact, many important segmentation algorithms are too simple to solve this problem accurately: they compensate for this limitation with their predictability, generality, and efficiency. However, methods that are specialized to particular applications can often achieve better performance by taking into account prior knowledge.

Often a segmentation approach could consist of more than one segmentation algorithms applied one after the other. Selection of an appropriate algorithm or approach for segmentation can therefore be a difficult dilemma. In other words, it is important to understand that there is no universally applicable segmentation technique that will work for all images, and, no segmentation technique is perfect, as can be seen in the previous example (Figure 3-5).

Even tough there are various segmentation techniques that appeared in the literature so far, I choose a simple strategy to perform the foot's structure segmentation that is illustrate schematically in the Figure 3-6. The first algorithm used to start the segmentation was the thresholding approach. The second operation applied for the masks was then region-growing algorithm, and finally polylines curves. Between every operation, i.e., between every algorithm, reviewing every image was mandatory to check the integrity of the partitioned structure, and if needed, missing pixels or extra pixels were correct manually.

The choice, as well, a brief overview of each technique used on this work is explained on the following paragraphs. Moreover, I will try to discuss their merits and demerits.

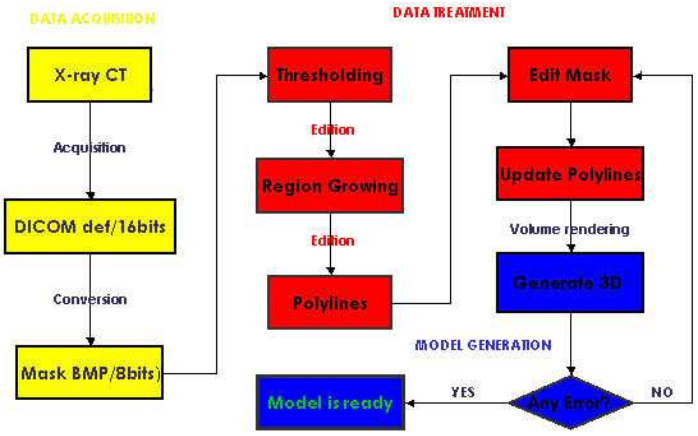

Figure 3-6: First stage of the research design: data acquisition, segmentation and volume rendering.

3.2.1 Thresholding Approach

Thresholding is probably the simplest of the segmentation techniques for scalar volumes (Weszka, 1978). In this technique a single value called threshold is used to create a binary partition of voxel intensities. All voxels with intensities greater than the threshold are grouped together into one class and those with intensities below the threshold are grouped together into another class. Use of a single threshold thus results in a binary-segmented volume.

The choice of the value is very important because this will define how the algorithm will separate different structures. Let's clarify through an example. Let's consider the structures depicted in the Figure 3-7 (ankle and subtalar joint): if the value is two high, the joints cannot be distinguish (left), i.e., tibia, talus and calcaneus are fused together as a single structure. Thus one requires manual edition to delimit it, or another segmentation algorithm. In the other hand, if the value is too low (right), the joints are promptly identified, but at cost of leaving big gaps inside the bones, which requires also manual edition or another segmentation technique.

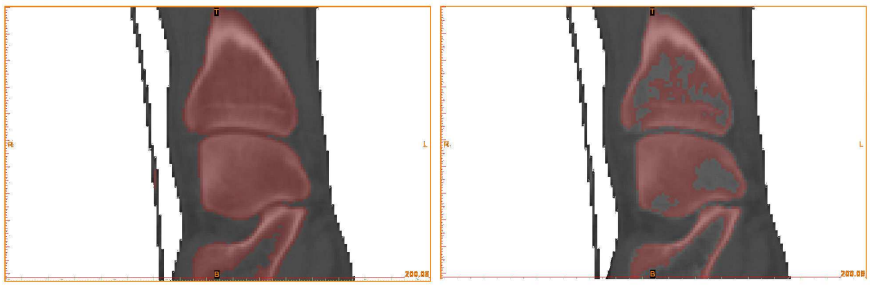

Figure 3-7: Example of thresholding technique with a high threshold value (left) and a low threshold value (right). The structures are the ankle and subtalar joints (top bone: tibia, center bone: talus, bottom bone: calcaneus).

Analytically, this simple concept can be expressed as follows: a parameter θ called the brightness threshold is chosen and applied to the image a [m,n]:

$$\begin{array}{lll} \text{If } a[m,n] \geq \theta & \text{then} & a[m,n]=\text{object}=1 \\ \text{Else} & & a[m,n]=\text{background}=0 \end{array}$$

This version of the algorithm assumes that we are interested in light objects on a dark background. For dark objects on a light background we would use:

If a[m,n]< θ then a[m,n]=object=1
Else a[m,n]=background=0

The output is the label "object" or "background" which, due to its dichotomous nature, can be represented as a Boolean variable "1" or "0". In principle, the test condition could be based upon some other property than simple brightness (for example, *If* (*Redness*{*a*[*m*,*n*]} >= θ_{red}), but the concept is clear.

This technique can be extended to using multiple thresholds, where a region is defined by two thresholds, a lower threshold and an upper threshold. Each voxel of the input volume then belongs to one of the regions based on its intensity. This technique is known as multithresholding (Sahoo *et al.*, 1988).

In Figure 3-8 we showed histogram of a volume. To apply thresholding, we take two thresholds T1 and T2 as shown. We then get three distinct regions as seen from the histogram. Although simple, this technique is very effective in getting segmentation done in volumes with a very good contrast between regions, i.e., different structures have contrasting intensities or other quantifiable features(Pham *et al.*, 1998). This is generally used as the first step towards segmentation of a volume.

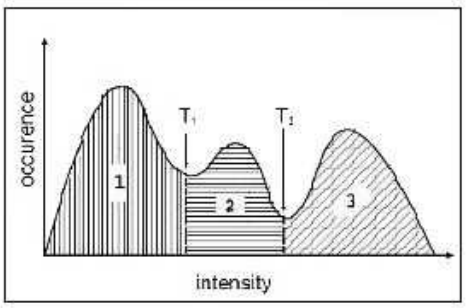

Figure 3-8: Histogram of a volume with two thresholds T1 and T2 dividing the histogram in three regions (Lakare, 2000).

The main drawback of this technique is that the results are too tightly coupled with the thresholds used. Any change in the threshold values can give a different segmented region. The thresholds are usually generated interactively by using visual feedback. Some automatic methods do exist with varying degree of success to automate the process of finding correct thresholds (Jiang. *et al.*, 1988). Another drawback which is a direct consequence of the previous one is that the technique is very sensitive to noise and intensity inhomogeneities (Pham *et al.*, 1998). Thus it cannot be easily applied to MRI and ultrasound volumes.

3.2.2 Region Growing

This is probably the simplest among the hybrid techniques. Region growing is a technique to extract a connected region from a 3D volume based on some pre-defined connecting criterion. These criteria can be as simple as the voxel intensity and/or edges in the image (Dzung, 1998).In the simplest form, region growing requires a seed point to start with, which can be choose manually. From the seed point, the algorithm grows till the connecting criterion, like the ones mentioned before, is satisfied. As with thresholding, region growing is simple, but not often used for segmentation by itself, i.e., it is not often used alone but within a set of image processing operations.

More often than not, region growing forms a part of a segmentation pipeline for a particular approach. It is often used as the primary method to understand a 3D data before more complex segmentation is applied to it. The primary disadvantage of this algorithm is that it requires seed points which generally means manual interaction. Thus for each region to be segmented, a seed point is needed. Region growing can also be sensitive to noise and partial volume effect causing the extracted region to have holes or disconnections (Pham *et al.*, 1998) (Figure 3-9). Conversely, partial volume effects can cause separate regions to become connected. To help alleviate these problems, a homotopic region growing algorithm has been proposed, that preserves the topology between an initial region and an extracted region (Mangin *et al.*, 1995). In another recent work, fuzzy analogies to region growing have also been developed (Udupa *et al.*, 1996).

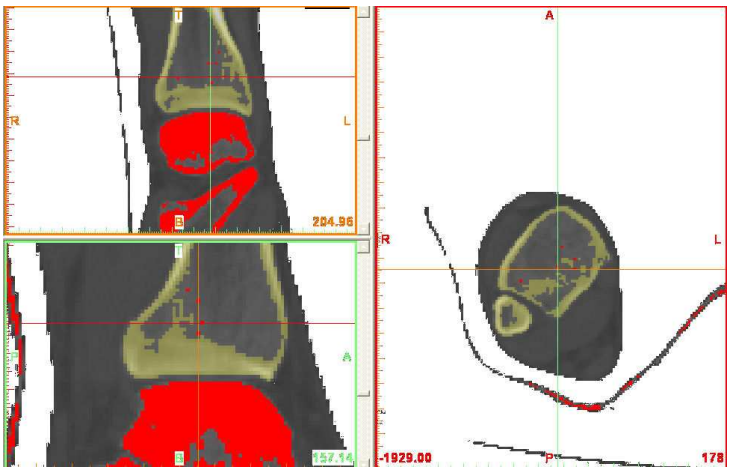

Figure 3-9: Example of region growing algorithm used to separate tibia bone (yellow mask) from the foot bones mask (red mask). Notice that still some extra pixels inside that mask, which requires manual edition or other image processing operation.

3.2.3 Calculation of Polylines

Polyline curves which are composed of line segments and arcs are widely used in engineering applications. These line segments and arcs are joined together with G^o continuity. The line segments and arcs are called as segments of a polyline curve. For each segment, we define a uniform structure SEG:

SEG={point； bulge}

Where the variable point denotes the starting point of this segment. The variable point of the next SEG can present the ending point of this segment. And the variable bulge describes whether this segment is an arc or not. If bulge=0, the segment denotes a line segment. Otherwise, it is an arc. For an arc, the value of bulge can be calculated by the expression $\tan(\theta/4)$ where θ is the central angle of the arc. And the sign of bulge is to determine how to select the arc segment.

For example, if bulge<0, we take the arc segment from the starting point to the ending point clockwise. Using the uniform structure, a polyline curve can be written as a sequence $\{s_1; s_2; \ldots; s_n\}$, where $s_i(i=1; \ldots; n)$ are the objects defined by SEG. If it is an open curve, the last SEG s_n does not represent a segment, but a point with the position stored in the variable point of s_n. The point is the ending point of s_{n-1}. Therefore, the polyline curve comprises n-1 segments. If the polyline curve is a closed curve, it is composed of n segments and s_n represents a segment from s_n point to s_1 point (Xu *et al.*, 2007). In this study this technique was used with two reasons: find gaps inside continuous structures (Figure 3-10) and pixels outside of the volume (Figure 3-10).

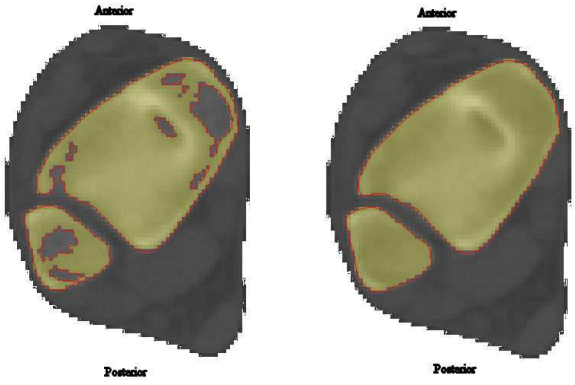

Figure 3-10: Polylines algorithm technique used to identify gaps, and missing pixels.

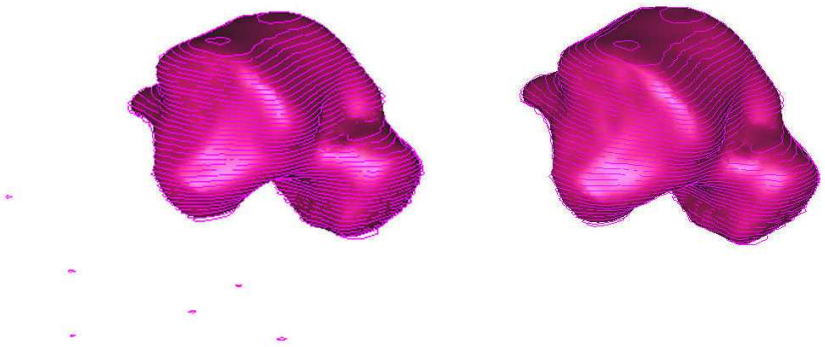

Figure 3-11: Polylines algorithm technique used to identify pixels outside of the volume (left). After manual edition or other segmentation algorithm the results can be seen at the right image. The bone used to exemplify the algorithm is the talus bone.

After these three processes, we started the volume rendering which is a technique used to display a 2D projection of a 3D discretely sampled data set. In our case, when referring to data set, we mean the group of 2D slice images acquired beforehand (section 3.1) and separated in masks (section 3.2), representing different structures. In our case, the different structures are, in fact, a 2D triangular mesh enclosing a volume. More details about mesh generation and edition is going to be given in section 3.3.2.

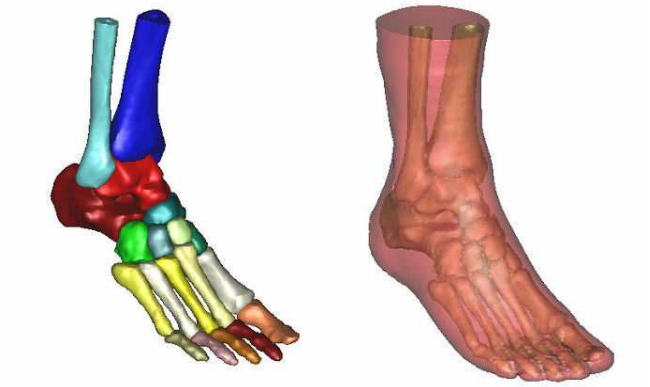

Figure 3-12: Final result of the segmentation operation: from 244 slices (with representation in 3 anatomical planes) 20 masks, corresponding to 19 bony structures and soft tissue, were separated (through 3 segmentation techniques). All soft tissues were embedded in one single volume. The approximate number of manual edition (reviews) was 43 920.

3.3 Finite Element Method: General Concepts

In his work entitled “Space Mapping: Models, Sensitivities, and Trust-Regions Methods” Vicente (2001) wrote the following clause: “When engineers face a mathematical problem that seems have no solution, it is quite common, instead of abandoning it, try to formulate an alternative approach which is determinable and can help understanding the original problem”.

In reality, because of the high complexity of the environment that surrounds us it is difficult to build models of it. However with some simplifications is perfectly reasonable think that one can obtain it. Among these simplifications, can be found the division of the system into its components or elements, whose behavior is readily understood.

Thus through the understanding of these elements, is relatively easy to rebuild the behavior of the system. Ergo, in many situations an adequate model is build using a finite number of elements of the original system. These kind of approaches are called discrete problems

To overcome the intractability of realistic types of continuum problems, various methods of discretization have from time to time been proposed both by engineers and mathematicians. All involve an approximation which, hopefully, approaches in the limit the true continuum solution as the number of discrete variables increases (Zienkiewicz *et al.*, 1967). Among these approximations is the Finite Element Method.

Finite element method (FEM) is a technique for obtaining a solution to a complex mechanical problem by dividing the problem domain into a collection of much smaller and simpler domains or “elements” of “finite” dimensions, when combined form the “mesh model of the investigated structure (Nath, 1974). The process of creating the mesh, elements, their respective nodes, and defining boundary conditions is referred to as “discretization” of the problem domain (Geng, 2001).

On this domain the field variables can be interpolated with the use of shape functions. Each element can adopt a specific geometric shape, i.e., triangle, square, tetrahedron, etc., with a specific internal strain function. Using these functions and the actual geometry of the element, one can write the equilibrium equations between the external forces acting on the element and the displacements occurring at its corner points or "nodes" (Korioth, 1997).

There will be one equation for each degree of freedom for each node of the element. These equations are most conveniently written in matrix form for use in a computer algorithm. From the stiffness matrices of the individual elements, the

so-called overall or global stiffness matrix [C] can be assembled for the entire discretized structure. The overall stiffness matrix relates overall forces on the structure to displacements at all the nodes:

$$\{F\} = [C]\{d\}$$

Where [C] denotes the overall stiffness matrix of the structure, {F} represents the overall force vector which lists the externally applied forces at all the nodes, and {d} symbolizes the displacements at all the nodes. The square and curved brackets denote rectangular matrices and vectors, respectively.

The global stiffness matrix is then solved for the unknown displacements, given the known forces and restraining conditions. This is done by ensuring that the equilibrium and compatibility conditions are satisfied at all nodes in the structure. Whereas the equilibrium conditions will be satisfied when all forces and moments about a given point equal zero, the compatibility conditions will be ensured if the displacements, i.e., nodal and elemental, within the deformed structure are continuous.

These latter conditions thus imply that even though the finite element model will yield an approximation of the correct answer, it would be possible to converge on this answer with a less-than-infinite number of nodes and elements. It is also important to note that equation presented above, can be solved only if a sufficient number of boundary conditions are introduced. From the displacements at the nodes, the strains in each element can then be calculated, and based on these as well as the material properties, the stresses can be derived.

Thus, when one is solving a problem, to arrange it properly, one needs to specify:

1. The geometry of the solid. This is done by generating a finite element mesh for the solid, i.e., to divide the continuum or solution region into elements. Although the number and the type of elements in a given problem are matters of engineering judgment, the analyst can rely on experience of others for guidelines. The mesh can usually be generated automatically from a CAD representation of the solid.

2. The properties of the material. This is done by specifying a constitutive law for the solid.

3. The nature of the loading applied to the solid. This is done by specifying the boundary conditions for the problem.

4. If your analysis involves contact between two or more solids, you will need to specify the surfaces that are likely to come into contact, and the properties, e.g.

friction coefficient, of the contact.

5. For a dynamic analysis, it is necessary to specify initial conditions for the problem. This is not necessary for a static analysis.

6. For problems involving additional fields, you may need to specify initial values for these field variables, e.g. you would need to specify the initial temperature distribution in a thermal analysis.

Originally introduced as a method for solving structural mechanics problems, finite element analysis was quickly recognized as a general procedure of numerical approximation to all physical problems that can be modeled by a differential equation description, and then, it has also been applied to the description of form changes in biological structures (Korioth *et al.*, 1997).

Moreover, such a numerical method for addressing mechanical problems is a powerful contemporary research tool providing precise insight into the complex mechanical behavior of natural and artificial structures affected by three-dimensional stress fields, which are still very difficult to assess otherwise.

Furthermore, over the past 20 years, the finite element method (FEM) has evolved into a well-established computational tool in biomechanics and has become the most extended and popular tool to analyze the mechanical behavior of musculo-skeletal system, often characterized by a complex material behavior and complicated geometry (Huiskes and Chao, 1981; King, 1984).

Moreover, once validated, a finite element model can be used as a tool for parametric investigation of stress distribution in biological structures (Bandak *et al.*, 2001), and that is the main reason this method was chosen to be used in this study.

3.3.1 Historical Highlights

Although the label *finite element method* first appeared in 1960, when it was used by Clough (Clough, 1960) in a paper on plane elasticity problems, the ideas of finite element analysis date back much further (Huebner *et al.*, 2001). In fact, the questions who originated the finite element method? and when did it begin? have three different answers depending on whether one asks an applied mathematician, a physicist, or an engineer. All of these specialists have some justification for claiming the finite element method as their own, because each developed the essential ideas independently at different times and for different reasons.

The applied mathematicians were concerned with boundary value problems of continuum mechanics; in particular, they wanted to find approximate upper and lower bounds for eigenvalues. The physicists were also interested in solving continuum problems, but they sought means to obtain piecewise approximate functions to represent their continuous functions. Faced with increasingly complex problems in aerospace structures, engineers were searching for a way in which to find the stiffness influence coefficients of shell-type structures reinforced by ribs and spars. The efforts of these three groups resulted in three sets of papers with distinctly different viewpoints (Huebner *et al.*, 2001).

The first efforts to use piecewise continuous functions defined over triangular domains appear in the applied mathematics literature with the work of Courant in 1943. Courant used an assemblage of triangular elements and the principle of minimum potential energy to study the St. Venant torsion problem (Courant, 1943). In 1959 Greenstadt, motivated by a discussion in the book by Morse and Feshback (Morse *et al.*, 1953), outlined a discretization approach involving “cells” instead of points; that is, he imagined the solution domain to be divided into a set of contiguous subdomains.

In his theory he describes a procedure for representing the unknown function by a series of functions, each associated with one cell. After assigning approximating functions and evaluating the appropriate variational principle to each cell, he uses continuity requirements to tie together the equations for all the cells. By this means he reduces a continuous problem to a discrete one. Greenstadt’s theory allows for irregularly shaped cell meshes and contains many of the essential and fundamental ideas that serve as the mathematical basis for the finite element method as we know it today.

As the popularity of the finite element method began to grow in the engineering and physics communities, more applied mathematicians became interested in giving the method for a firm mathematical foundation. As a result, a number of studies were aimed

at estimating discretization error, rates of convergence, and stability for different types of finite element approximations. These studies most often focused on the special case of linear elliptic boundary value problems. Since the late 1960s the mathematical literature on the finite element method has grown more than in any previous period (Huebner *et al.*, 2001).

While the mathematicians were developing and using finite element concepts, the physicists were also busy with similar ideas. The work of Prager and Synge (Prager *et al.*, 1947) leading to the development of the hypercircle method is a key example. As a concept in function space, the hypercircle method was originally developed in connection with classical elasticity theory to give its minimum principles a geometric interpretation. Outgrowths of the hypercircle method (such as the one suggested by Synge (Synge, 1952)) can be applied to the solution of continuum problems in much the same way as finite element techniques can be applied (Huebner *et al.*, 2001).

Physical intuition first brought finite element concepts to the engineering community. In the 1930s when a structural engineer encountered a truss problem such as the one shown in Figure 3-13a, he immediately knew how to solve for component stresses and deflections as well as the overall strength of the unit. First, he would recognize that the truss was simply an assembly of rods whose force–deflection characteristics he knew well. Then he would combine these individual characteristics according to the laws of equilibrium and solve the resulting system of equations for the unknown forces and deflections for the overall system (Huebner *et al.*, 2001).

This procedure worked well whenever the structure in question had a finite number of interconnection points, but then the following question arose: What can we do when we encounter an elastic continuum structure such as a plate that has an infinite number of interconnection points? For example, in Figure 3-13b, if a plate replaces the truss, the problem becomes considerably more difficult.

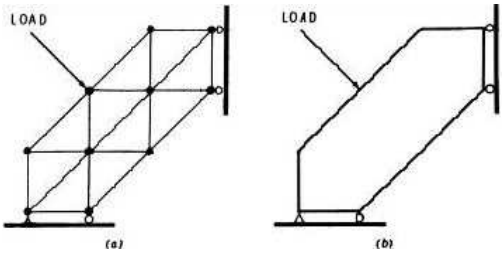

Figure 3-13: Example of (a) a truss and (b) a similarly shaped plate supporting the same load.

Intuitively, Hrenikoff reasoned that this difficulty could be overcome by assuming the continuum structure to be divided into elements or structural sections

(beams) interconnected at only a finite number of node points (Hrenikoff, 1941). Under this assumption the problem reduces to that of a conventional structure, which could be handled by the old methods. Attempts to apply Hrenikoff's "framework method" were successful, and thus the seed to finite element techniques began to germinate in the engineering community (Huebner *et al.*, 2001).

Shortly after Hrenikoff, McHenry (McHenry, 1943) and Newmark (Newmark, 1949) offered further development of these discretization ideas, while Kron (Kron, 1944; Kron, 1944) studied topological properties of discrete systems. There followed a ten-year spell of inactivity, which was broken in 1954 when Argyris and his collaborators (Argyris, 1954; Argyris, 1955; Argyris, 1957; Argyris, 1959; Argyris, *et al.*, 1960) began to publish a series of papers extensively covering linear structural analysis and efficient solution techniques well suited to automatic digital computation.

The actual solution of plane stress problems by means of triangular elements whose properties were determined from the equations of elasticity theory was first given in the now classical 1956 paper of Turner, Clough, Martin, and Topp (Turner *et al.*, 1956). These investigators were the first to introduce what is now known as the direct stiffness method for determining finite element properties. Their studies, along with the advent of the digital computer at that time, opened the way to the solution of complex plane elasticity problems.

After further treatment of the plane elasticity problem by Clough in 1960, engineers began to recognize the efficacy of the finite element method. In a 1980 paper Clough gives his personal account of the origins of the method, describing the sequence of events from the original efforts at Boeing that produced papers like "The Finite Element Method in Plane Stress Analysis," *Proceedings of 2nd ASCE Conference on Electronic Computation*, Pittsburgh, (1960) in which he introduced the label of *the finite element method*. In 1965 the finite element method received an even broader interpretation when Zienkiewicz and Cheung (Zienkiewicz *et al.*, 1965) reported that it is applicable to all field problems that can be cast into variational form.

During the late 1960s and early 1970s (while mathematicians were working on establishing errors, bounds, and convergence criteria for finite element approximations) engineers and other practitioners of the finite element method were also studying similar concepts for various problems in the area of solid mechanics. In the years since 1960 the finite element method has received widespread acceptance in engineering. Thousands of papers, hundreds of conferences, and many books appeared on the subject (Huebner *et al.*, 2001).

Hitherto, there are many publications and books about the Finite Element Method,

that their growing is considered exponential. Some of these are considered the classics and one can find the whole formulation about the method: Bathe (1996), Hughes (1987); Texas Series (1981), Zienkiewicz (1979) only to mention. In a not so recent paper (Noor, 1991), can be found a bibliography until 1991, listing nearly 400 finite element books. The bibliography also identifies over 200 international finite element symposia, conferences, and short courses that took place between 1964 and 1991.

What can be seen from the number of publications, and even a simple search on internet, is that the method is impressively growing worldwide, which shows a huge popularity and a promising future.

3.3.2 The Solid Geometry: the Finite Element Mesh

Before explaining about the specific mesh used for this study, I will dissertate briefly about this topic: finite element mesh. The choice of an appropriate element type will depend on the expected response of the model and thus the accomplishment of the objectives of the analysis.

Finite element analysis (FEA) offers a wide variety of different element types, which can be categorized by family, order, and topology. The element family refers to the characteristics of geometry and displacement that the element models. Among the most common families used for typical structural models are one-dimensional beam elements, 2D plane stress and plane strain elements, axisymmetric elements, and 3D shell and solid elements.

Beam elements are useful for modeling beam-like structures where length is much greater than other dimensions and the overall deflection and bending moments can be predicted. However, this type of model will not be able to predict the local stress concentrations at the point of application of a load or at joints.

Plane stress elements are appropriate for thin 2D structures, in which stresses out of the plane can be neglected. Plane strain elements simulate a special 3D stress state, occurring when out-of plane deformation is constrained (e.g., in relatively thick plates).

Axisymmetrical elements model 3D stress fields under 2D conditions, using well-defined characteristics of an axisymmetric geometry. Shell elements can be effectively used for 3D structures that are thin with respect to other dimensions, such as sheet metal parts where bending and in-plane forces are important. These elements, however, will not predict stresses that vary through the thickness of the shell due to local bending effects.

Ideally, all 3D conditions are modeled by means of solid elements. However, because the computational effort of most finite elements solvers is roughly proportional to the number of equations and the square of the bandwidth, the order of magnitude of such a solid model may impose practical limits on the choice of those elements.

Elements can also be categorized by order, which refers to the interpolation functions that approximate data in the domain of the element based on the number of nodes through which elements are interconnected. In the reviewed literature, both linear (first order) and parabolic (second order) elements are used, each of which has advantages and disadvantages for finite element analysis (FEA).

Linear elements have two nodes along each edge, parabolic have three. Higher-order elements are less stiff than lower-order elements (this is related to

bending), because additional nodes provide more degrees of freedom (DOF).

A DOF represents the liberty of translatory or rotational motion of a particular node in space. For example, shell elements have six DOF at each of their unrestrained nodes: three translations (x, y, and z) and three rotations (around the x, y, and z axes). In contrast, the unrestrained nodes in three-dimensional (solid) elements have only three translational DOF, and 2D elements have only two.

A higher number of DOF means more variables in the stiffness formulation, which is more computer-intensive. Higher-order elements offer more accurate results for an equal mesh grid, but a finer grid of lower-order elements can turn out to be more efficient with the same accuracy. For this reason, cubic order elements are rarely used in the reviewed FE studies.

Element topology refers to the general shape of the element (e.g., triangular or quadrilateral). The topology also depends on the family of the element (e.g., 2D or 3D). In general, quadrilateral elements may be considered more suitable than triangular in complex structural models, since the quadrilateral can match the true displacement function more accurately due to a higher number of DOF. Furthermore, the number of elements in meshes built from triangular elements tends to be larger. On the other hand, the simplicity of triangular elements makes them very attractive, e.g., for automatic mesh generation.

Triangular-shaped elements are easier to fit to geometrically complex structures. Combining different element topologies and element orders, such as triangular and parabolic, could increase the accuracy of a topologically lesser element. The shapes of the elements will affect the predictive accuracy of the model, since any deviation in shape from the "ideal" internal elemental strain function will contribute to mathematical inaccuracies.

Since finite element analysis offers an approximation to the exact solution, a numerical result closer to this true value will be achieved if the displacements in a finite element model become increasingly continuous. This convergence is usually accomplished by decreasing the element sizes (and consequently increasing the number of elements) and local refinements in a finite element mesh.

After this general information about the nature and importance of the finite element mesh, let’s resume the topic. Because of the geometry complexity, the element of choice was triangular. As was mentioned in section 3.2, after segmentation, the volume was defined by a 2D triangular mesh. This was quite useful; due to the fact that the preprocessor software (Hypermesh 8.0, Altair Engineering Inc., 1995-2006) used to create the solid mesh provides an automatic tetramesher that fills a volume enclosed by

a 2D triangular mesh. However before exporting this mesh to the preprocessor, the 2D triangular mesh was refined using a program called Mimics Remesh 9.9 (Materialise Group 1996-2006). This step aimed decrease the number of triangular elements that constitute the volume and make the mesh more uniform. Both have deep impact on the numerical solution.

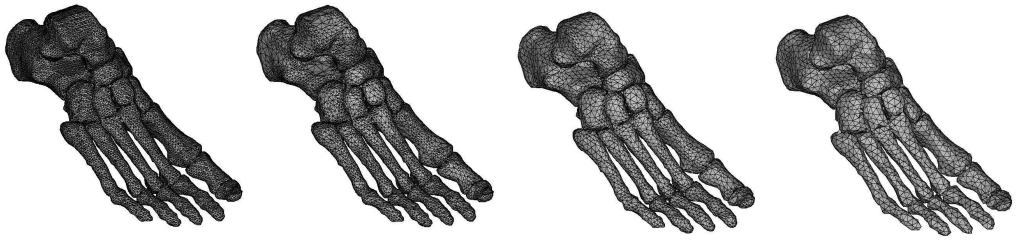

Figure 3-14: Example of the mesh reduction and smoothing for the foot bones. Starting from the left: 42 992 elements, 30026 elements, 13602 elements and 7672 elements.

Figure 3-15: Example of the mesh reduction and smoothing for the soft tissues. Starting from the left: 1200 004 elements, 24880 elements, and 20144 elements.

After importing these meshes to the pre processor, the first step was to increase the mesh quality, an important step to assure numerical stability. To make a good quality tetramesh, so we must ensure, for the 2D mesh, that: there are no duplicates, no elements fold on one another, elements do not overlap, the minimum triangle angle is not too low, and the difference in size between adjacent elements across a wall in minimal.

The next step was to generate a 3D mesh (tetrahedral elements) following quality criteria supplied by ABAQUS, which was the solver used to simulate that case. The

main concern was to avoid distorted elements which bring instability (convergence problems (section 3.5)) during numerical calculation. Based on that mesh, two different models (Figure 3-17) were built to simulate balanced standing while wearing two different kinds of insoles: flat and conform (Figure 3-16).

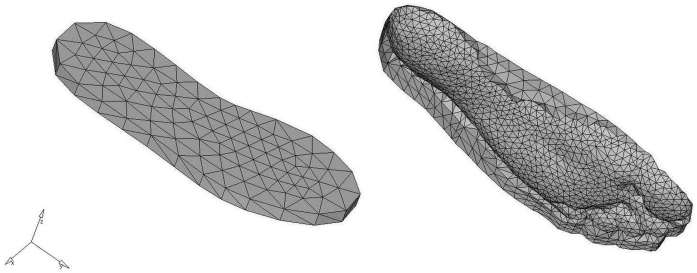

Figure 3-16: Insoles shapes used during simulation: flat (left) and conform (right).

The finite element models, as shown in Figure 3-17 consisted of 26 bony segments: talus, calcaneus, cuboid, navicular, 3 cuneiforms, 5 metatarsals, and 14 components of the phalanges all fused in one solid. It is expected that for this analysis (balanced standing position), joints, cartilages, ligaments and muscles do not play an important role in the plantar pressure, thus they will be neglect or considered encapsuled in a single volume.

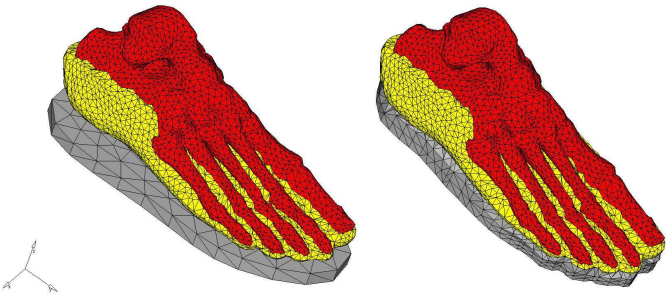

Figure 3-17: Detail of the models used to simulate standing position while using two kinds of insoles: flat (left) and conform (right).

The bony structures were merged with the encapsulated soft tissues. The bony and soft tissue structures were meshed with a total of 37093 tetrahedral elements (first order). Details about material properties for these structures will be explained in detail in the section 3.3.3.

The custom-molded insole was made from the unloaded shape of the subject's bare foot. The barefoot shape was obtained by manual edition of the shell mesh generate from the plantar region of the foot, and from it the solid models of the insole, using Hypermesh features. A 10-mm-thick insole was meshed into 3-D tetrahedral elements (first order) in a total of 496 and 4561, for flat and conform insole respectively. A

summary of the model properties can be found in the table 3-2.

Structure	**Element(first order)**	**Young Modulus E (MPa)**	**Poisson Ratio ν**
Bones	16991-Tetrahedral	7300	0.3
Soft Tissue	20102-Tetrahedral	1.15	0.45
Insole	4561-Tetrahedral(conform) 496-Tetrahedral(flat)	0.3(Soft) 1000(Hard)	0.4

Table 3-2: Details about the models used for simulation.

3.3.3 Material Properties

The assignment of proper material properties to a FE model is a necessary step to ensure predictive accuracy. Stress and strain in a structure are derived based on the material properties. These properties can be classified as isotropic, transversely isotropic, orthotropic, and an isotropic.

For an isotropic material, the properties are the same in all directions. Since the Young's modulus (or modulus of elasticity), the shear modulus (or modulus of rigidity), and the Poisson's ratio are interrelated in case of isotropy, only two out of the three variables need to be determined for the elastic behavior to be characterized completely (Gere and Timoshenko, 1990).

Hence, the relationships between stress and strain are fairly simple. Transversely isotropic materials behave similarly in every direction about a single axis of symmetry. In contrast, the mechanical properties of orthotropic materials have three orthogonal planes of mechanical symmetry. A material is anisotropic if its properties are different when measured in different directions.

A significant difficulty for anatomical models resides in selection of the biological material properties, which are most often dependent on the nature of the applied load, e.g., the loading rate (Gefen, 2000). In my model、three different materials were taken into account: bone, soft tissue, and insole, i.e., two biological materials and an artificial one. Let’s make some considerations about bone tissue.

From a mechanical point of view, bone is a composite material with several distinct solid and fluid phases. However, the mechanical properties of bone are primarily related to the presence of the mineral phase that permeates the organic matrix. The stress-strain law of cortical and trabecular bone is very sensitive to the porosity of bone and to the alignment of the microstructures.

Since the mineral content and the structures alignment are distributed in a very inhomogeneous way, bones have a complex inhomogeneous and anisotropic mechanical behavior. However, this viscoelastic behavior can be neglected when the applied loads are maintained below 1 Hz, as in most of the common activities such as walking, running, etc. Therefore, in most situations bone can be considered as an inhomogeneous and anisotropic elastic material (Terrier A., 1999).

The major difference between cortical and trabecular bone is the difference in relative densities, which has profound influence on the elastic modulus. Mechanical tests showed that the elastic modulus is related to the relative density by a power law function with an exponent ranging between two and three. Although these relationships were

initially derived from compression tests, tensile tests indicate that the elastic modulus of bone is approximately the same in compression and in tension. Elastic constants for cortical bone depend on its porosity and elastic constants of one trabecula depend on its degree of mineralization.

In general, cortical and trabecular bone structures are anisotropic. For cortical bone, this anisotropy is caused by the alignment of the osteons along the longitudinal axis of long bones. The longitudinal elastic modulus is about 50% greater than the transverse elastic modulus. The shear modulus is also different in the longitudinal or transverse direction.

For trabecular bone, the anisotropy is caused by the alignment pattern of the trabecular. Although cortical and trabecular bone are fully anisotropic, transverse isotropy is a good compromise between model complexity and validity. Indeed, for many bones, including long load bearing bones, there is clearly a privileged direction, where the stiffness value is about twice the value of the other two equivalent directions (Terrier A., 1999).

Huiskes and Chao (1983) have reported that in the case of quasi-static loading (and probably *in vivo* loading), both cortical and trabecular bones behave approximately in a linear elastic manner. In other work, Keaveny et al. (1994) have reported that trabecular bone is linearly elastic until yielding and has equal tensile and compressive moduli.

These elastic and yield properties are also characteristic of cortical bone. Although no Young's modulus data seem to be available specifically for the foot bones, values measured for various bones of arm and leg show little difference, so a value in this range can reasonably be chosen.

Thus, for the bones I will assume that this tissue is homogeneous, isotropic, and linear elastic material. For the foot bones, Young’s modulus is taken as 7300 MPa (Gefen, 2000) and the Poisson ratio as 0.3 (Nakamura *et al.*, 1981). These values were selected by weighing cortical and trabecular elasticity values and, consequently are considered to be suitable for the present analysis.

The two other materials, soft tissue and insole, I will assume that, they also are homogeneous, isotropic and linear elastic materials (Table 3-2). The elastic modulus of the soft tissues was obtained from the literature: the Young modulus and Poisson ratio were assigned to foot soft tissues as 1.15 MPa (Chen *et al.*, 2003) and 0.45 (Cheung *et al.*, 2005), respectively.

The insole material will be modeled with a Poisson ratio of 0.4 and a varied Young modulus of 0.3 (soft), and 1000MPa (hard) for simulation of open-cell

polyurethane foams, such as Professional Protective Technology's PPT material; and polypropylene materials, respectively.

Structure	**Element(first order)**	**Young Modulus E (MPa)**	**Poisson Ratio ν**
Bones	16991-Tetrahedral	7300	0.3
Soft Tissue	20102-Tetrahedral	1.15	0.45
Insole	4561-Tetrahedral(conform) 496-Tetrahedral(flat)	0.3(Soft) 1000(Hard)	0.4

Table 3-3: Details about the models used for simulation.

3.3.4 Boundary Conditions

The boundary conditions in FE models basically represent the loads imposed on the structures under study and their fixation counterparts, the restraints. In addition, they may involve interaction of groups of interconnected finite elements (constraints) or physically separate bodies (contact).

When performing a static analysis, it is very important to make sure that boundary conditions are applied properly. A finite element program can only solve a problem if a unique static equilibrium solution to the problem exists; otherwise, quantitative and qualitative errors in prediction may be introduced.

It is known that for linear Finite Element models, errors in magnitudes of the loads will not have a direct effect on the predictions, as opposed to small changes in load direction, which has already been proven to be an important and sensitive variable in finite element analysis (Anusavice and Hojjatie, 1988; Hojjatie and Anusavice, 1990). Difficulties arise if the user does not specify sufficient boundary constraints to prevent rigid body motion of a solid.

3.3.4.1 Constraints and Applied Load

In this case study, we considered a person with a body mass of 70kg. This person applies a vertical force of 350N on each foot during balanced standing. Force vectors corresponding to half of the body weight and the reaction of the Achilles' tendon were applied.

Moreover, the vertically upward force of the Achilles' tendon, with a magnitude of 175N, was represented by 10 equivalent force vectors at the posterior extreme of the calcaneus (Figure 3-18). This value of Achilles' tendon loading was based on the study of Simkin *apud* (Cheung *et al.*, 2005) who calculated that the Achilles' tendon force was approximately 50% of the force applied on the foot during balanced standing.

Although the resultant load is about a quarter (175 N) of the total load (700 N) during the studied position, i.e., balanced standing position (350 N by foot for a perfect balanced standing position), it is considered that this disposition of forces is not so appropriate.

However, this choice of forces was done because similar studies that use the same applied loads, e.g., Cheung and collaborators (2005). Thus, the simulation results obtained during this study can be compared directly with such study results. Consequently the model can be validated in two different fronts: comparing to another studies results and experimental results obtained during the present study.

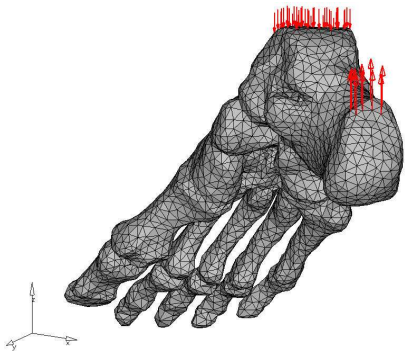

Figure 3-18: Applied loads: Talus (top-left) and Calcaneus (bottom-right).

A net normal vertical force of 350N was applied on 40 nodes on the talus' throclea for the tibia (Figure 3-18). Follow the same way, a net normal vertical forces of 175 N was applied on 10 nodes on the triceps surae insertion. The points of load application, i.e., the 50 nodes mentions above, were allowed to move in the vertical direction only.

Besides that, the bottom faces of each insole, used in simulation, were constrained, i.e., all nodes on the bottom were constrained (encastre) (Figure 3-19). For the flat insole, 94 nodes were constrained, in the other hand, on conform insole, 294 nodes were constrained.

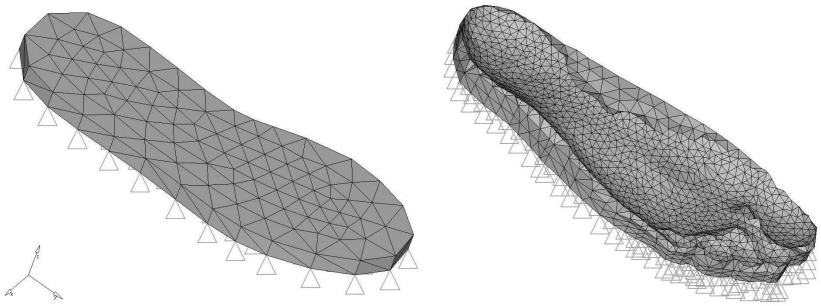

Figure 3-19: Constraints: flat (left, 94 nodes) and conform insole (right, 297 nodes).

3.3.4.2 Contacting Surfaces and Interfaces

In addition to being subject to forces or prescribed displacements, solid objects are often loaded by coming into contact with another solid. In our study, the region between the plantar region and the insoles were modeled as contact regions (Figure 3-20 and Figure 3-21).

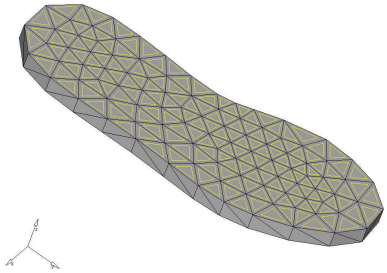

Figure 3-20: Example of contact region defined for the problem (marked in yellow).

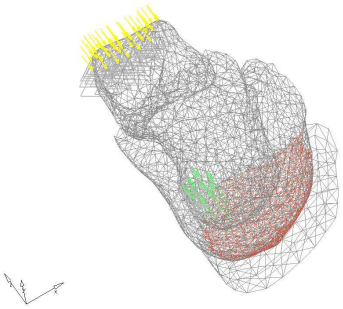

Figure 3-21: Another example of contact region, in this case: rear foot, defined for the problem (marked in red).

Modern finite element codes contain sophisticated capabilities for modeling contact. Unfortunately, contact can make a computation much more difficult, because the region where the two solids come into contact is generally not known *a priori*, and must be determined as part of the solution, which requires a lot of careful manual edition before running the solver.

The choice of the contact region for the plantar surface that was used during simulation was based on an experiment: a subject standing on a glass surface had his feet photographed (6 pictures) from below, and then a similar pattern was defined as contact region (Figure 3-22).

It was decided, after analyzing all pictures that the fourth pattern (from left to right) was going to be used as a reference for the contact region. The choice was made based on our understanding of what a healthy feet contact region should be.

Again is interesting to mention that, the initial contact region must be defined *a priori*, i.e., before simulation, due to the fact that the numerical solver asks it as a necessary requisite to solve the problem. Consequently, the experiment patterns were used as a basis to the initial contact surfaces.

Anyhow, the final contact area can be obtained after simulation, thus both contact areas (experimental and simulation) can be compared quantitatively, which is advantageous.

Figure 3-22: Contact region obtained from a short experiment.

Contact almost always makes the problem *nonlinear* – even if both contacting solids are linear elastic, as the ones considered in this study case. In addition, if there is friction between the contacting solids, the solution is history dependent. For this reason, many options are available in finite element packages to control the way contacting surfaces behave.

Whenever one models contact, one will need to

1. Specify pairs of surfaces that might come into contact. One of these must be designated as the *master surface* and the other must be designated as the *slave surface.* In our case study, the insole was considered master surface, and plantar region, slave surface. The choice was based on ABAQUS manual, which advices to choose the slave surface as the more refined surface or the surface on the more deformable body. For a sufficiently fine mesh, the results should not be affected by the choice of master and slave surface. However, it improves *convergence* (see section 3.5) if one chooses the more rigid of the two surfaces to be the master surface. When in doubt about each one is more rigid, just make a random choice. If there is convergence problems, a good strategy would be just switching them over.

2. Define the way the two surfaces interact, e.g. by specifying the coefficient of friction between them. The choice of the interaction between the two surfaces was based on a study by Cheung (2005), which sets contact with friction (coefficient of friction of 0.6).

This rather obscure finite element terminology refers to the way that contact constraints are actually applied during a computation. The geometry of the master surface will be interpolated as a smooth curve in some way (usually by interpolating between nodes). The slave surface is not interpolated. Instead, each individual node on the slave surface is constrained so as not to penetrate into the master surface. For example, the red nodes on the slave surface shown in the Figure 3-23 would be forced to remain outside the red boundary of the master surface.

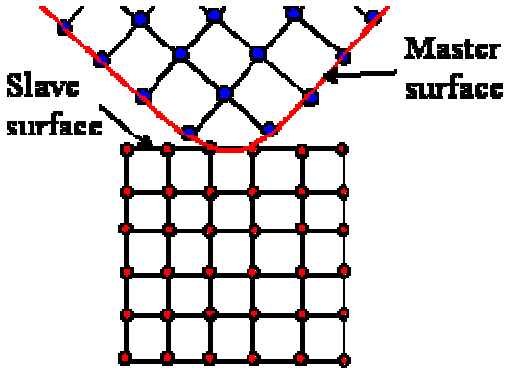

Figure 3-23: Example of contact problem (courtesy of Brown University).

Besides the interaction, the solver used to simulate this situation allows to define several parameters that control the behavior of two contacting surfaces. They are:

1. The contact formulation - `finite sliding' or `small sliding' – specifies the expected relative tangential displacement of the two surfaces. `Finite sliding' is the most general, but is computationally more demanding. `Small sliding' should be used if the relative tangential displacement is likely to be less than the distance between two adjacent nodes. The choice in our simulation was small sliding.

2. One can specify the relationship between the contact pressure and separation between the contacting surfaces. Alternatively, you can assume the contact is `hard' – this means the interface can't withstand any tension, and the two contacting surfaces cannot inter-penetrate, which was our choice.

3. One can specify the tangential behavior of the interface – for example by giving the friction coefficient, as mention above.

3.4 Non-linear Solution Procedures for Static Problems

If a problem involves contact, plastically deforming materials, or large geometry changes it is nonlinear. This means that the equations of static equilibrium for the finite element mesh have the general form

$$\mathbf{F}^{(b)}\left(\mathbf{u}^{(a)}\right)=0$$

Where **F()** denotes a set of *b=1,2…N* vector functions of the nodal displacements $\mathbf{u}(\mathbf{x}^a)$, *a=1,2…N*, and *N* is the number of nodes in the mesh.

The nonlinear equations are solved using the Newton-Raphson method, which works like this. One first guess the solution to the equations in the form: $\mathbf{u}^a=\mathbf{w}^{(a)}$. Obviously, **w** won't satisfy the equations, so one try to improve the solution by adding a small correction $d\mathbf{w}$. Ideally, the correction should be chosen so that

$$\mathbf{F^{(b)}}\left(\mathbf{w^{(a)}}+d\mathbf{w^a}\right)=0$$

However it's not possible to do this. So instead, take a Taylor expansion to get

$$\mathbf{F}^{(b)}\left(\mathbf{w}^{(a)}+d\mathbf{w}^a\right)\approx\mathbf{F}^{(b)}\left(\mathbf{w}^{(a)}\right)+\frac{d\mathbf{F}^{(b)}(\mathbf{u})}{d\mathbf{u}^{(a)}}d\mathbf{w}^{(a)}=0$$

The result is a system of linear equations of the form $\mathbf{F}^{(b)}+\mathbf{K}d\mathbf{w}^{(a)}=0$, where $\mathbf{K}=d\mathbf{F}^{(b)}/d\mathbf{u}^{(a)}$ is a constant matrix called the *stiffness matrix*. The equations can now be solved for $d\mathbf{w}$; the guess for **w** can be corrected, and the procedure applied over again. The iteration is repeated until $\left|\mathbf{F}^{(b)}\left(\mathbf{u}^{(a)}\right)\right|<\varepsilon$, where ε is a small tolerance.

In problems involving *hard contact*, an additional iterative method is used to decide which nodes on the slave surface contact the master surface. This is just a

brute-force method – it starts with some guess for contacting nodes; gets a solution, and checks it. If any nodes are found to penetrate the master surface, these are added to the list of nodes in contact. If any nodes are experiencing forces attracting them to the master surface, they are removed from the list of nodes in contact.

The problem with any iterative procedure is that it may not *converge* – that is, repeated corrections $d\mathbf{w}$ either take the solution further and further away from the solution, or else just spiral around the solution without every reaching it. The solution is (naturally) more likely to converge if the guess $\mathbf{w}^{(a)}$ is close to the correct solution. Consequently, it is best to apply the loads to a nonlinear solid gradually, so that at each load step the displacements are small. The solution to one load increment can then be used as the initial guess for the next.

3.5 Convergence

Convergence problems were a hard and very common issue during the development of this project. The strategy used to avoid this kind of problems was as follows:

1. Apply the load in smaller increments. ABAQUS does this automatically – but will stop the computation if the increment size falls below a minimum value. In this study we opt by 100 increments. The choice was based on pilot studies and comparison between the values found in our simulation and previous studies. One example with this kind of problem is presented in the Figure 3-24.

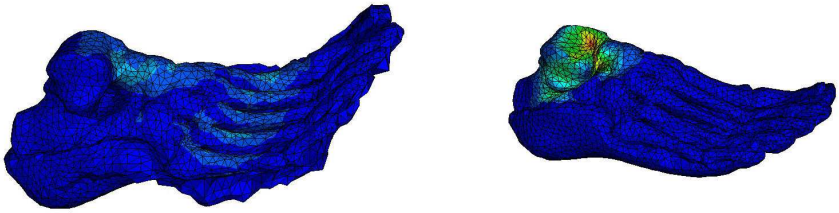

Figure 3-24: Example of convergence problem. The number of increments is small for two cases (7 increments). The left model was simulated without non linear geometry. In the other hand the right model considered it, however, as mentioned before, the number of increments was two small.

2. Convergence problems are sometimes caused by *ill conditioning* in the stiffness matrix. This means that the equations $\mathbf{F}^{(b)} + \mathbf{K}d\mathbf{w}^{(a)} = 0$ cannot be solved accurately. Ill conditioning can arise because of

(i) Severely distorted elements in the mesh;

(ii) Material behavior is incompressible, or nearly incompressible; and

(iii) The boundary conditions in the analysis do not properly constrain the solid (Figure 3-25).

One can fix severely distorted elements in the mesh by modifying it – some FEM codes contain capabilities to automatically remove element distortion during large deformation. That was not the case. However ABAQUS identifies distorted elements, which leave us with the task of editing the mesh again, using the preprocessor (Hypermesh 8.0, Altair Engineering Inc., 1995-2006) and solve such problem.

One can avoid problems with incompressibility by using reduced integration elements or hybrid elements. Problems with boundary conditions can usually be corrected by adding more constraints. There is one common problem where this is hard to do – if the motion of a body in your analysis is constrained only by contacts with other solids (e.g. a roller between two surfaces) the stiffness matrix is always

singular at the start of the analysis. ABAQUS allows you to introduce a fictitious viscous force between the contacting solids that will stabilize the analysis.

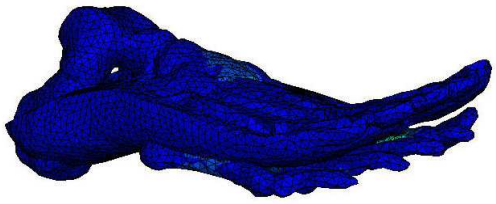

Figure 3-25: Example of convergence problem. Number of constraints and contact definition is not enough to avoid it.

3. Isolate the source of the problem. Convergence issues can often be traced to one or more of the following:

(i) Severe material nonlinearity;

(ii) Contact and

(iii) Geometric nonlinearity.

When facing convergence problems, we change our model to remove as many of these as possible. We tried different approaches; however the best options were to analyze the two contacting solids separately, without the contact; or simulate the model without nonlinear geometry. Once the source of the problems was traced, we were able to fix it by changing the material properties, contact properties or loading conditions.

4. Convergence problems are often caused by some kind of mechanical or material failure in the solid, which involve a sudden release of energy. In this case, the shape of the solid may suddenly jump from one static equilibrium configuration to another, quite different, equilibrium configuration. There is a special type of loading procedure (called the Riks method) that can be used to stabilize this kind of problem.

4 Experiment for Plantar Pressure Acquisition

The experiment was divided in two stages: a pilot study and a final experiment. The pilot study aimed the understanding of the variables involved in the manipulation of the apparatus, i.e., the acquisition system and its nuances. Moreover, the pilot study was important to understand how to use work with the data (processing, filtering, rectifying) and find meaningful insights from it. The data in question was the pressure distribution on the plantar region. The measurement system was the Tekscan F-scan. The system is a flexible, 0.15 mm thick plastic sole-shape having 960 resistive pressure sensors (cells), ranging from 6.89 kPa to 1250 kPa, maximum sampling rate of 165 Hz, and spatial resolution of four sensors/cm^2 (Figure 4-1 and Figure 4-2).

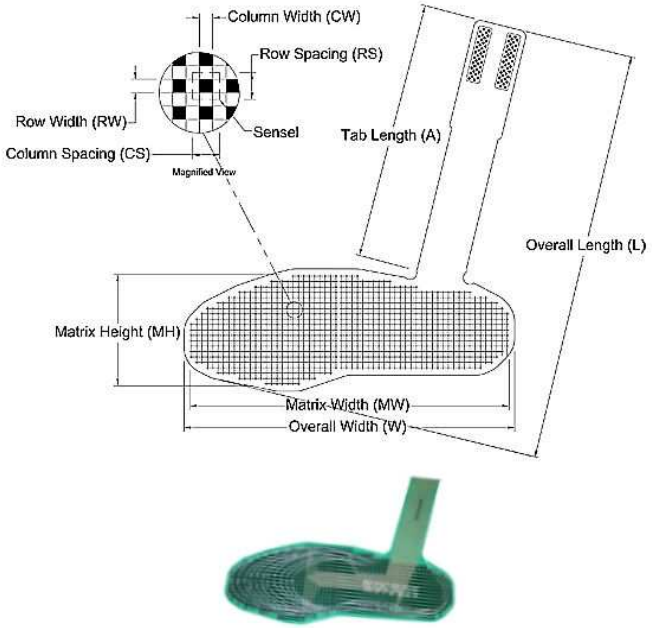

Figure 4-1: Sensors details (Tekscan F-scan Lite System, cell model: 3000).

Each cell acts as a force measuring device; the system software calculates the average pressure on each cell based on the measured vertical load and the cell area. Software correction is also necessary to achieve a linear relationship between output voltage and applied force. Signal processing units, attached distally at the lateral part of the lower leg, umbilical cables and dedicated interface boards are use to acquire and transfer data to an IBM compatible PC (Figure 4-3). F-Scan software allows measurement of vertical ground reaction force, pressure, peak pressure, contact area, and gait cycle timings (Woodburn *et al.*, 1996).

The resistance of pressure sensitive ink, contained between two polymer-film substrates, decreases as the pressure, applied normal to the substrate, increases. Ahroni et al. (1998) and Mueller and Strube (1996) *apud* (Verdejo *et al.*, 2004) reviewed studies on F-scan sensors; some researchers reported good reliability and reproducibility, while others reported a decrease of sensor output with time at fixed pressure. Woodburn and Helliwell (1996) (Woodburn *et al.*, 1996) concluded that they were not suitable for accurate, repeatable measurements. However, two factors contribute to the choice of use of these sensors: the number of the measurements was low (did not exceed ten), and peak pressure measurements observed in this study are similar to those reported previously, what indicate that the choice was reasonable.

Figure 4-2: Sensors before (right) and after (left) preparation (Tekscan F-scan Lite System, cell model: 3000, distributed in Japan by Nitta Corporation).

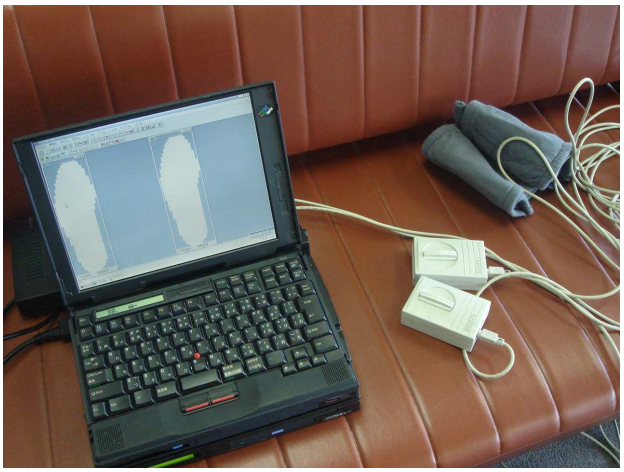

Figure 4-3: F-scan Lite system: computer, signal processing units and cables.

4.1 Pilot Experiment

The term 'pilot studies' refers to mini versions, i.e., small scale version of a full-scale study (also called 'feasibility' studies), as well as the specific pre-testing of a particular research instrument such as a questionnaire or interview schedule. In our case, the pilot study was used as a way to pre-test the research instrument was used to measure plantar pressure distribution (Tekscan F-scan Lite System). One of the advantages of conducting a pilot study is that it might give advance warning about where the main research project could fail, where research protocols may not be followed, or whether proposed methods or instruments are inappropriate or too complicated. In the words of De Vaus (1993) "Do not take the risk. Pilot test first."

These are important reasons for undertaking a pilot study, but there are additional reasons, for example convincing funding bodies that your research proposal for the main study is worth funding. Thus pilot studies are conducted for a range of different reasons as (Van Teijlingen *et al.*, 2001):

- Developing and testing adequacy of research instruments
- Assessing the feasibility of a (full-scale) study/survey
- Designing a research protocol
- Assessing whether the research protocol is realistic and workable
- Establishing whether the sampling frame and technique are effective
- Assessing the likely success of proposed recruitment approaches
- Identifying logistical problems which might occur using proposed methods
- Estimating variability in outcomes to help determining sample size
- Collecting preliminary data
- Determining what resources (finance, staff) are needed for a planned study
- Assessing the proposed data analysis techniques to uncover potential problems
- Developing a research question and research plan
- Training a researcher in as many elements of the research process as possible
- Convincing funding bodies that the research team is competent and knowledgeable

- Convincing funding bodies that the main study is feasible and worth funding
- Convincing other stakeholders that the main study is worth supporting

Thus aiming find the right research design, a pilot study was conducted. The process is explained in the next paragraphs. Two subjects, with athletic background, were chosen randomly. These two subjects gave their informed permission to participate in the experiment (their anthropometric data specified in the (Table 4-1)). The experiment was performed in Toshiba Hospital at Ooi Machi, Tokyo, Japan.

Subject	Age(years)	Weight(kg)	Height(m)
1	23	75	1.75
2	34	71	1.73

Table 4-1: Anthropometric data of the athletes used to measure plantar pressure.

The first part of the experiment consisted of preparing the sensors: gluing, cutting, and placing them in the shoes, as can be seen in the Figure 4-4.

Figure 4-4: Sensors assembling (starting from the top).

The second part of the experiment consisted of system calibration. The calibration of the F-Scan system uses total body mass applied directly over each sensor in a static manner. The procedure involves the patient standing on one foot, and then both, the calibration force being equivalent to the body mass. The settings used for calibration, as well the experiment, have the following characteristics:

Recording Parameter	Amount
Total time (s)	8
Sampling Rate (Hz)	50
Period (s)	0.02
Number of frames	400

Table 4-2: Experiment Settings.

After calibration, the signal processing units were placed in the distal lateral portion of the lower leg, as mentioned before, thus the mounting of the apparatus necessary to measure plantar pressure distribution was finished .The disposition of it can be seen in the Figure 4-5.

Figure 4-5: Signal processing units placed laterally at lower leg.

Participants wore tennis Adidas model adiZero, which are shoes targeting long distance runners with a neutral or minimal over-pronation, which were instrumented before hand (Figure 4-4). While wearing these shoes, three study cases were recorded: balance standing (Figure 4-6), walking and a similar movement as baseball fielders commonly do, i.e., side step, ball catch and ball throwing (Figure 4-7).

Figure 4-6: Balanced Standing.

Figure 4-7: Fielder movement recorded.

Because the first study case is a static position, it was recorded only two sets of data. For walking case, the subjects were asked to walk an approximate distance of 5 m. The total number of trials was five. To minimize possible errors, the first and last steps, at the beginning of the movement, were not considered to statistically calculate the peak pressure values. The third study case: fielder movement was recorded 11 times. The best movement was chosen based on video analysis criteria, i.e., the trial used to collect the plantar pressure data represents the most natural movement possible. Obviously, many of the trials failed because of the signal processing units and cables attached to the lower leg, which make the natural movement difficult.

It is important to mention that due to possible changes in foot loading resulting from fatigue, this experiment was design as a short experiment. The data obtained from two cases: walking and side catch with throwing, will be analyzed in a future work. However the values were compared to similar studies and were consistent, which

indicate a successful experiment.

Figure 4-8: More details about the signal processing units fixation method.

4.2 Final Experiment

The final experiment consisted of three case studies: balanced standing position, walking, and running. For the present work, walking and running data, discussion and conclusions will not be presented. The same subject used on the pilot study (subject 2, so refer to Table 4-2 for details), performed the activities described above. We will just mention the general procedures (methodology) used to acquire data for balanced standing position. Further details about the other movements are specified in section 9.1.

For balanced standing position, there are three cases: barefoot standing, insole standing (Figure 9-1), and shod standing. For all trials, the distance between the shoes was fixed based on the shoulders distance. To avoid possible errors from changes in the standing position, a tape was placed on the floor (Figure 4-10), thus the subject must place his foot (rearfoot region) on the border of it. Moreover, the signal processing units were fixed during the trials to avoid errors of measure.

Figure 4-9: Insole place during standing position.

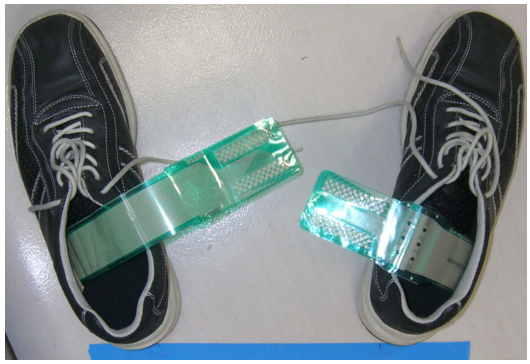

Figure 4-10: Detail of the reference line during standing position study case.

For two study cases (insole standing and shod standing) different sets of insoles

were used:

- Flat and Conform insoles,
- Three different thicknesses: 2mm, 4mm and 8mm, denoted as T1, T2 and T3, respectively.
- Two different materials: EVA and PE, denoted as M1 and M2, respectively.
- Four different hardness: 35, 45, 58 and 60 cc.

All trials were recorded during 10 seconds with a sampling rate of 50 Hz. Extra information about the experiment settings are in the Table 4-3.

Recording Parameter	Amount
Total time (s)	10
Sampling Rate (Hz)	50
Period (s)	0.02
Number of frames	500

Table 4-3: F-scan settings used during standing case.

Figure 4-11: Some of the insoles used during experiment. From left to right: flat insoles (4 pairs) and conform insoles (7 pairs).

5 Results and Discussion

Even though the predicted plantar pressure distribution pattern was, in general, comparable to the F-scan measurement (Figure 5-1), the predicted values of peak pressure were higher than the F-scan measurements (Table 5-1 and Table 5-2), which naturally indicate that the best way to use this data is in a qualitative analysis. These differences may be caused by different factors:

- Resolution differences between the F-scan measurement and the finite element analysis. Having a spatial resolution of about 4 sensors per cm^2, the F-scan sensors recorded an average pressure for an area of 25 mm^2. By contrast, the finite element analysis provided solutions of nodal contact pressure rather than an average pressure calculated from nodal force per element surface area (Cheung *et al.*, 2005).
- Absence of nonlinear materials on the model. The assumption that all materials are homogeneous, isotropic and linear elastic material may contribute to underestimate the real values for peak plantar pressure.
- Neglecting joints on the model may increase the total stiffness of the model, consequently increasing the peak plantar pressure, i.e., the omission of rigid body motion, as relative motion between bones, during standing position, might act as a factor to increase peak plantar pressure observed during simulation.
- Subject used during experiment and the subject used to acquire the foot image (CT scan) are not the same individual. Additionally, during computer tomography the subject's foot was not in balanced standing position, which means that foot geometry in both cases were not the same.

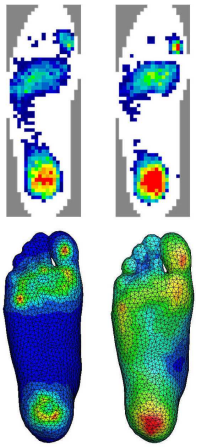

Figure 5-1: Plantar pressure patterns for F-scan measures (top) and simulation results (bottom) for flat (left) and conform insoles (right).

Besides, the wide range of variations in peak pressures, reported in various plantar pressure measurement studies might be due to the possible variations between measuring techniques, subjects, gait patterns, and orthoses. However, among these studies, there is consensus about how some of the footwear design variables affect plantar pressure distribution. Moreover, the finite element results obtained on this study showed similar trends of pressure distributions of the high plantar pressure regions and the pressure values were within the range of previously reported pressure values.

Thus start with the analysis of the results for the footwear design variables involved in this study, beginning with conformity

Support	Region	Peak Plantar Pressure (kPa)			
		Present Study		Cheung(2005)	
		Experiment	Simulation	Experiment	Simulation
Soft	Phalanges	41.3	200	-	-
	Forefoot	38.6	196	70	162
	Midfoot	31.6	78	-	-
	Rearfoot	126.7	233	130	214
Hard	Phalanges	75.6	234	-	-
	Forefoot	49.0	231	90	194
	Midfoot	10.3	53	-	-
	Rearfoot	132.7	274	140	266

Table 5-1: Simulation results for standing position (Flat Insole). A similar case that was measured during experiment and a previous work were placed for comparison.

Support	Region	Peak Plantar Pressure (kPa)		
		Present Study		Cheung(2005)
		Experiment	Simulation	Simulation
Soft	Phalanges	28.3	133	-
	Forefoot	38.6	116	126
	Midfoot	27.3	84	50
	Rearfoot	120.2	183	182
Hard	Phalanges	62.6	181	-
	Forefoot	47.9	163	146
	Midfoot	27.7	91	77
	Rearfoot	135	200	201

Table 5-2: Simulation results for standing position (Conform insole). A similar case that was measured during experiment and a previous work were placed for comparison.

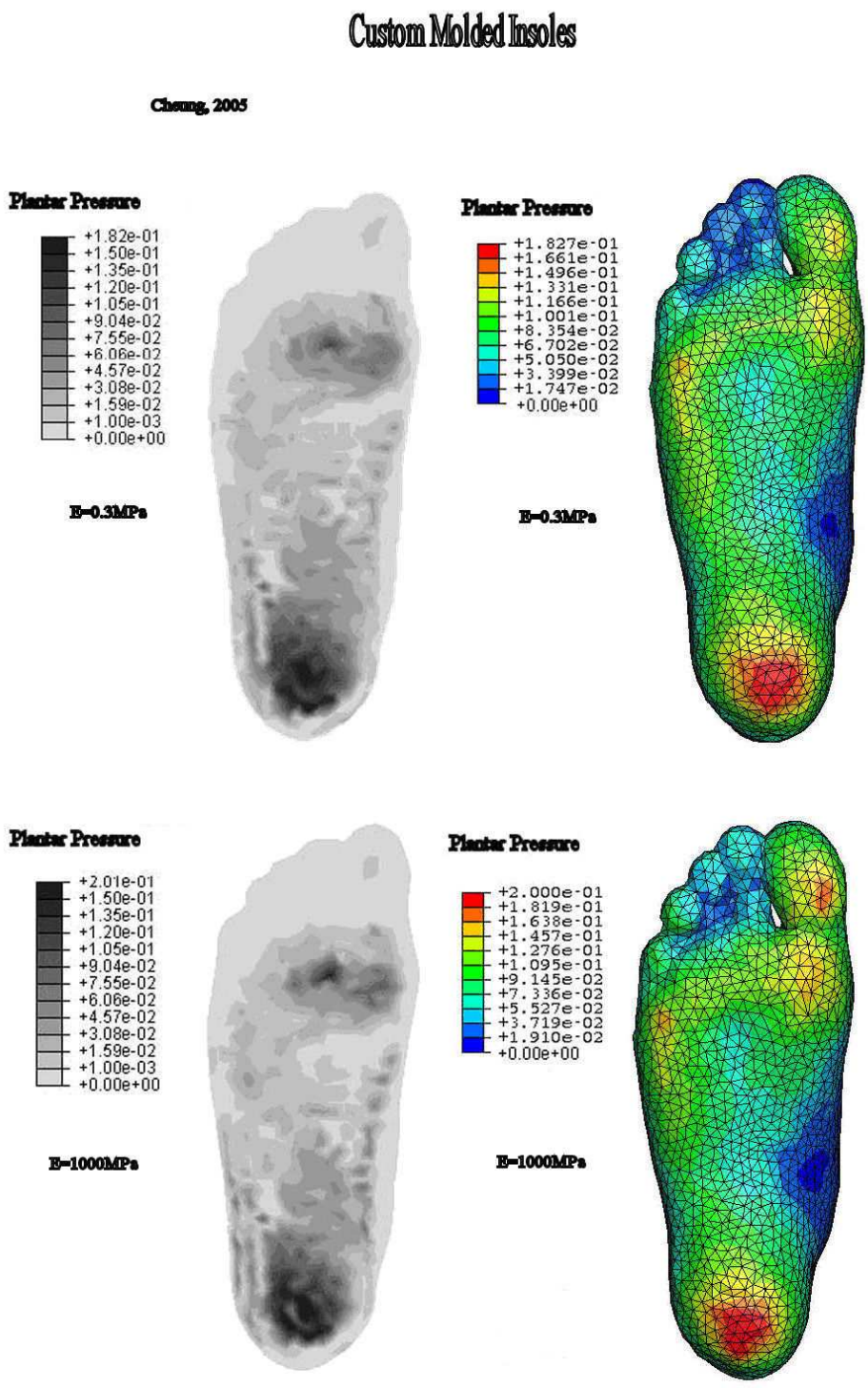

Figure 5-2: Comparison with Cheung's simulation for conform insoles.

5.1 Conformity

The first footwear design variable tested (conformity) proved to have a great influence on the plantar pressure distribution and peak pressure values, and no region was independent on that variable. There are at least two possible theories that may account for the reduction in pressure by conforming insoles. The first one is that the load is clearly distributed over a larger area, and this may be the principal mechanism for pressure reduction.

This hypothesis is supported by measurements made by Goske et al. (2006), which show that contact areas increase in the insole condition, i.e., conforming insoles have a bigger contact area which could, consequently, decrease plantar pressure. The data obtained on this study showed the same trend. However the behavior was opposite for one of the foot regions: midfoot (increase of peak plantar pressure).

Thus the best way to analyze the effect of the variables studied here is separating the plantar region in four, which is in agreement with anatomy: phalanges, forefoot, midfoot, rearfoot (Refer to section 2 for details). After this short explanation let us return to the effect of conformity on plantar pressure distribution. Thus the first region to be analyzed is rear foot region.

For this region the biggest amount of reduction, while supported by a soft material, was about 41% (simulation result) and 63% (experimental result) when compared with barefoot condition (Table 5-3). Some other researchers, such as Lobmann et al. (2001) and Bus et al. (2004), reported reductions up to 23% by simply using insoles that conform to the heel. They found absolute reductions in heel peak pressures (when compared to barefoot) were up to 60% when using an insole that conformed to the heel.

The results for this region are also supported by a previous finite element analysis on single total contact insoles presented by Cheng and collaborators (2003).

Region	Peak Pressure (kPa)			
	Present Study		Goske(2006)	
	Experiment	Simulation	Experiment	Simulation
Phalanges	114.1	236.7	-	-
Forefoot	263.0	277.8	-	-
Midfoot	12	72	-	-
Rearfoot	354.1	311.7	332±5	343

Table 5-3: Simulation results for standing barefoot.

The decreases between flat and conforming insole for the rearfoot region were 27% and 21.5% (simulation results), for hard material (E=1000 MPa) and soft material (E=0.3MPa) (Figure 5-3) respectively. From the experimental data (Figure 5-4), comparing two different conditions (see Table 5-4 for details), the reduction ranges from 0.2% to 9.4%, corroborating with the theory that cupping the heel is a main factor on plantar pressure decrease.

Probably the main reason for the small decrease observed, specially when compared to simulation results, is that for the experiment, conform insoles were in fact half conformed to the heel, a shape that is not so effective in plantar pressure reduction, as observed by Goske *et al.* (2006).

Material	Thickness[mm]	Peak Pressure [kPa]		%
		Flat	Conform	
1	2	130.9	130.6	0.2
1	4	101.2	99.0	2.2
2	4	132.7	120.2	9.4

Table 5-4: Experimental results for rearfoot region.

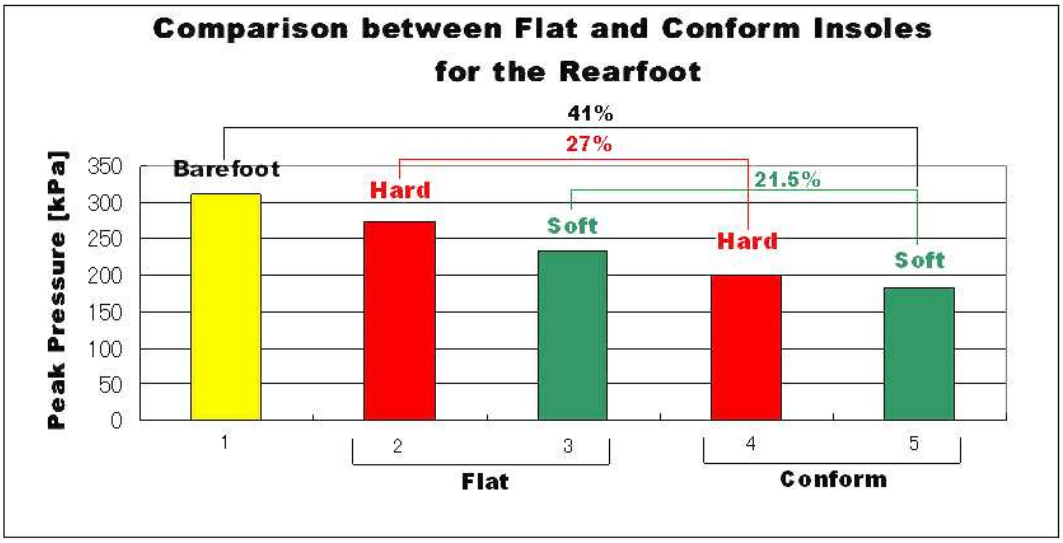

Figure 5-3: Data obtained from the simulation: barefoot (1), flat insoles (2, 3) and conforming insoles (4, 5) for rigid (E=1000 MPa, red color) and soft material (E=0.3MPa, green color).

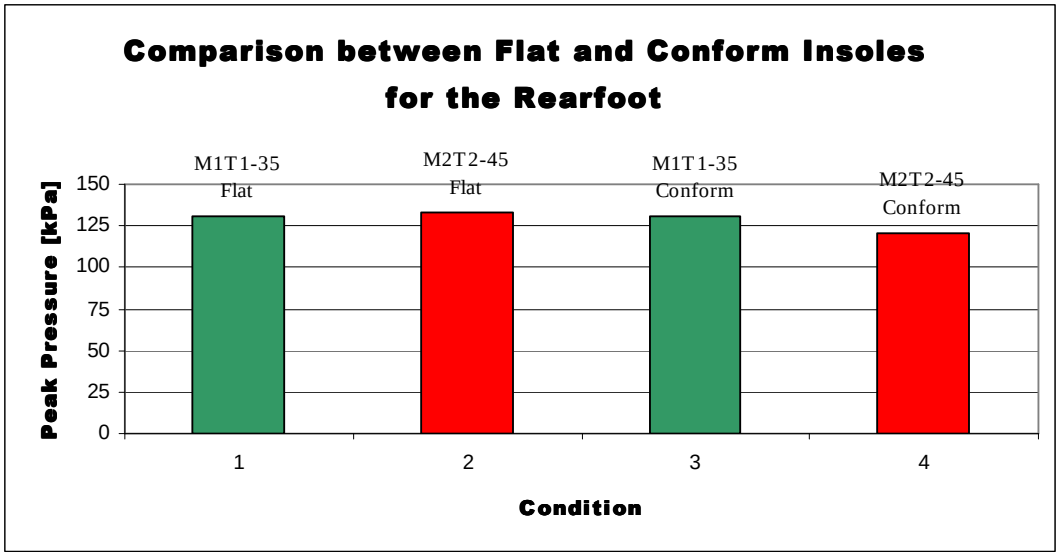

Figure 5-4: Data obtained from the experiment: 2 mm (T1) flat insole of EVA (1), 4mm (T2) flat insole of PE(2), 2mm (T1) conforming insole of EVA (3), and 4 mm (T2) conforming insole of PE(4).

The second hypothesis about cupping the heel says that it is possible that a conforming heel pad exploits the incompressibility of the soft tissue and restricts outward displacement of the soft tissue, thereby maintaining a thicker layer of biological ‘‘cushioning’’ under the calcaneus. This hypothesis is supported by measurement of soft tissue thickness made by Goske et al. (2006) which indicated that with the flat insoles, maximal soft tissue compression was between 34% and 37% of its original thickness while for the conforming insoles, this value ranged from 22% to 29%.

For two more regions the same behavior (peak pressure decrease) was observed: forefoot and phalanges. The amount of the decrease was 29.5% and 40.7%, for hard material (E=1000 MPa) and soft material (E=0.3MPa), respectively, on the forefoot region (simulation results (Figure 5-5)). The experimental data (see for Table 5-5 and Figure 5-6 for reference) showed reduction ranging from 31.4 % to 11.6%, for hard and soft material, respectively.

Material	Thickness[mm]	Peak Pressure [kPa]		%
		Flat	Conform	
1	2	62.7	55.4	11.6
2	2	55.5	38.1	31.4
2	4	49.0	38.4	21.6

Table 5-5: Experimental results for forefoot region.

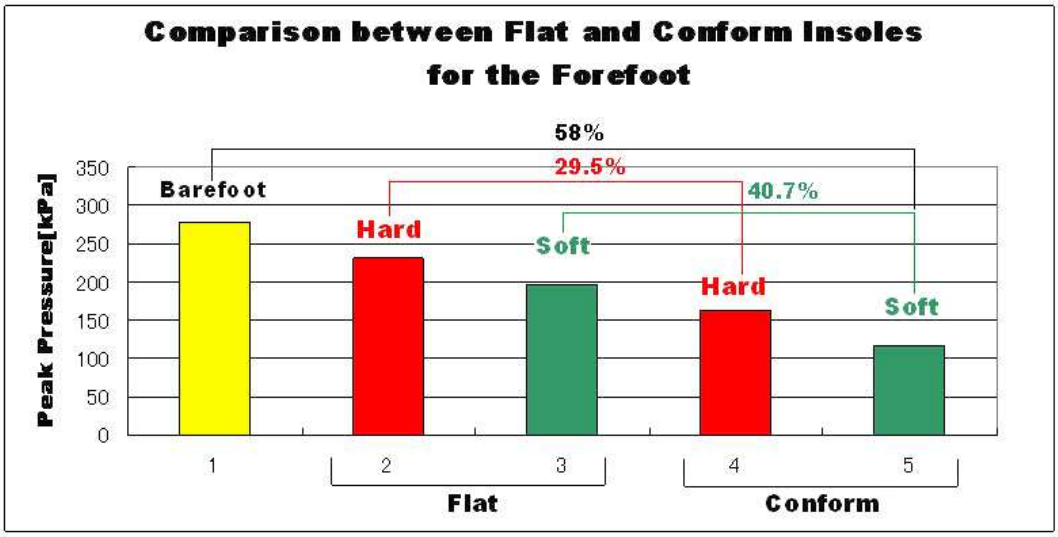

Figure 5-5: Data obtained from the simulation: flat insoles (2, 3) and conforming insoles (4, 5) for hard (E=1000 MPa, red color) and soft material (E=0.3MPa, green color).

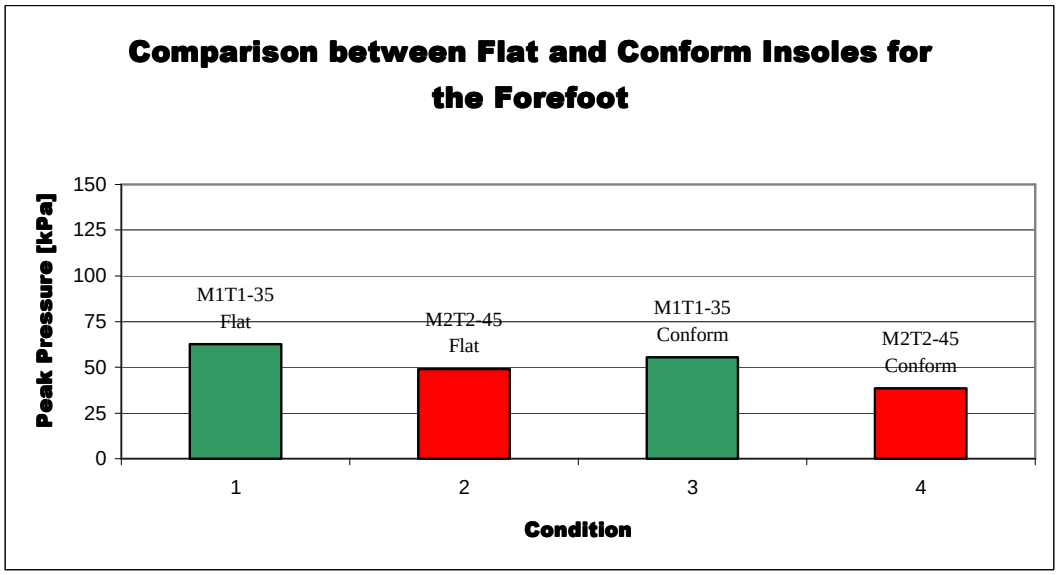

Figure 5-6: Data obtained from the experiment: 2 mm (T1) flat insole of EVA (1), 4mm (T2) flat insole of PE(2), 2mm (T1) conforming insole of EVA (3), and 4 mm (T2) conforming insole of PE(4).

The second region mentioned above (phalanges) showed reductions of 22.6% and 33.5%, for hard material (E=1000 MPa) and soft material (E=0.3MPa), respectively (simulation results (Figure 5-7)). The experimental data (see Table 5-6 and Figure 5-8 for details) showed reduction of 62.6% to 43.7%, for hard and soft material, respectively.

Material	Thickness[mm]	Peak Pressure [kPa]		%
		Flat	Conform	
1	2	64.3	36.2	43.7
2	2	60.4	50.7	16.1
2	4	75.6	28.3	62.6

Table 5-6: Experimental results for phalanges region.

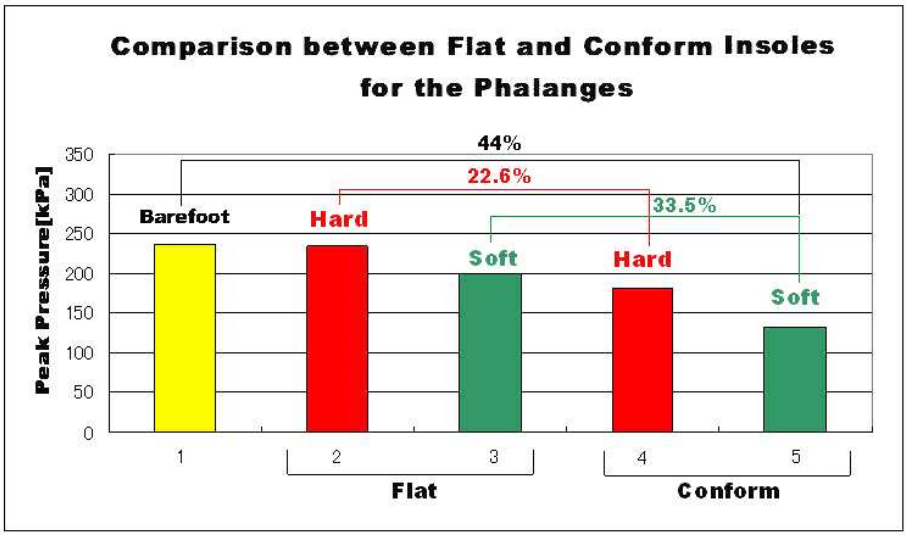

Figure 5-7: Data obtained from the simulation: barefoot (1), flat insoles (2, 3) and conforming insoles (4, 5) for hard (E=1000 MPa, red color) and soft material (E=0.3MPa, green color).

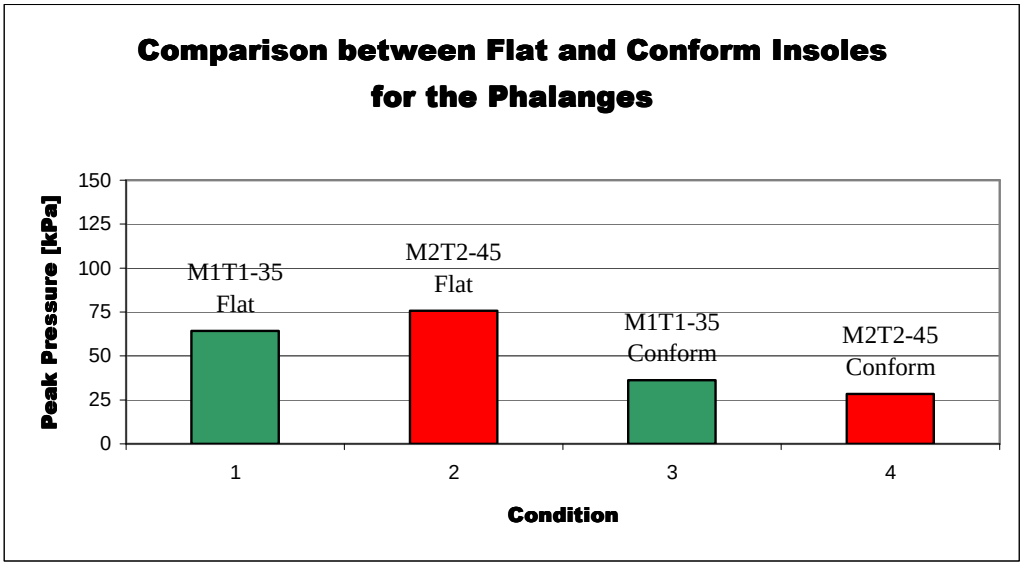

Figure 5-8: Data obtained from the experiment: 2 mm (T1) flat insole of EVA (1), 4mm (T2) flat insole of PE(2), 2mm (T1) conforming insole of EVA (3), and 4 mm (T2) conforming insole of PE(4).

On the other hand, midfoot region presented an opposite behavior: an increase in plantar pressure. The amount of this increase was 71.1% and 7.8%, for hard material (E=1000 MPa) and soft material (E=0.3MPa), respectively. The experimental data (see Table 5-7 for details) showed increase ranging from 38.3% to 23.0%, for hard and soft material, respectively. This increase in peak pressure was expected, because midfoot region is fully supported while wearing conform insoles. Both, experimental and simulation results are depicted in Figure 5-9**.**

Material	Thickness[mm]	Peak Pressure [kPa]		%
		Flat	Conform	
1	2	28.2	39.0	38.3
2	2	20.7	22.8	10.1
2	2	22.2	27.3	23.0

Table 5-7: Experimental results for midfoot region.

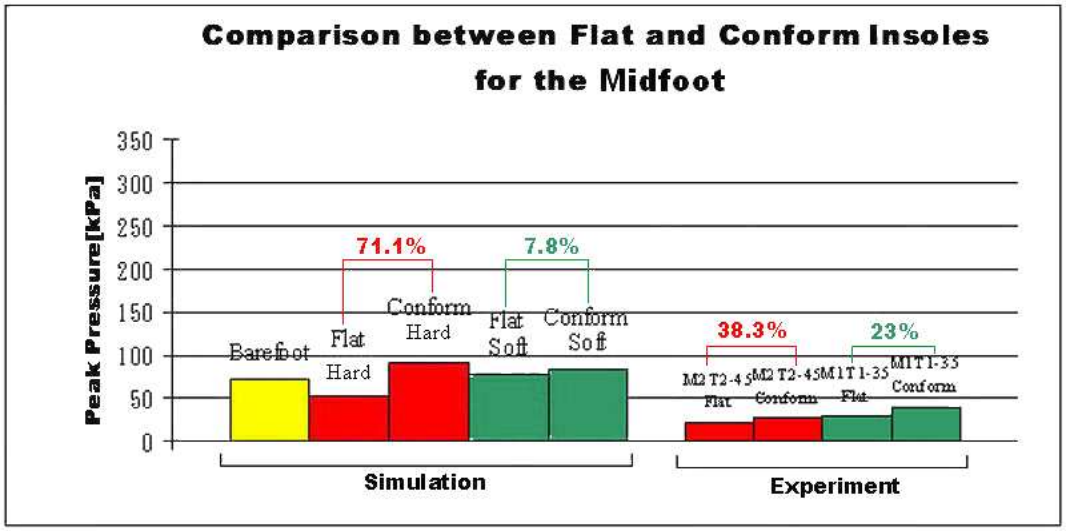

Figure 5-9: Data obtained from the simulation: flat insoles (2, 3) and conforming insoles (4, 5) for hard (E=1000 MPa, red color) and soft material (E=0.3MPa, green color). Data obtained from the experiment: 2 mm (T1) flat insole of EVA (1), 4mm (T2) flat insole of PE (2), 2mm (T1) conforming insole of EVA (3), and 4 mm (T2) conforming insole of PE(4).

A summary of both, experimental and simulation results are presented on the Figure 5-10 and 5-11. From these two images is easy to see the effect of geometry on peak plantar pressure, i.e., changing geometry from flat to conform was observed a decrease in peak plantar pressure.

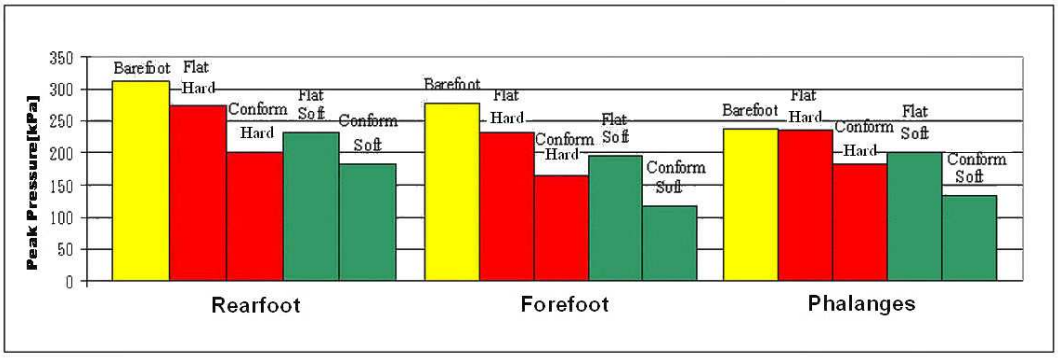

Figure 5-10: Summary of simulation results for conformity.

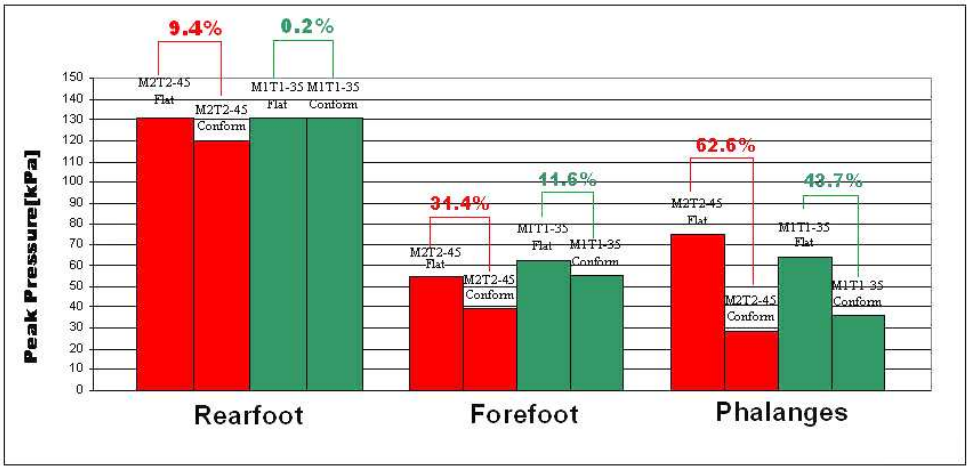

Figure 5-11: Summary of experimental results for conformity.

5.2 Material

The second footwear design variable analyzed was the material itself. Similarly to the first variable studied, simulation and experimental results showed a trend that softer materials can reduce plantar pressure. This point is going to be explored more, in the next paragraphs.

It is interesting to mention that the peak plantar pressure decrease is calculated comparing soft and hard material, while keeping the same geometry (flat or conform insole). From the simulation, the data showed a decrease in peak plantar pressure of: 14.5%, 15.4%, -46.4% (anomalous result) and 15.1%, for phalange, forefoot, midfoot and rearfoot, respectively, for a flat insole (Table 5-8). For a conform insole the extent of the decrease was 26.5%, 28.8%, 7.7% and 8.7% for phalange, forefoot, midfoot and rearfoot region, respectively (Table 5-8). Refer to Figure 5-12, 5-13 and 5-14 to have a better understanding about the effect of this variable.

Region	Decrease in Peak Plantar Pressure%	
	Flat insole	**Conform Insole**
Phalanges	14.5	26.5
Fore foot	15.4	28.8
Mid foot	-46.4	7.7
Rear foot	15.1	8.7

Table 5-8: Simulation results: decrease between rigid and soft material for two conditions: flat and conform insoles (separated by region). Negative value stands for an increase in peak plantar pressure. Comparison keeping geometry fixed.

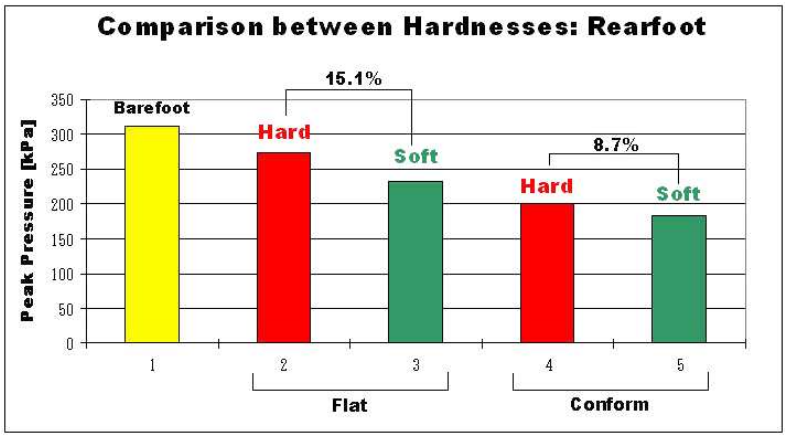

Figure 5-12: Simulation results for Rearfoot (hardness).

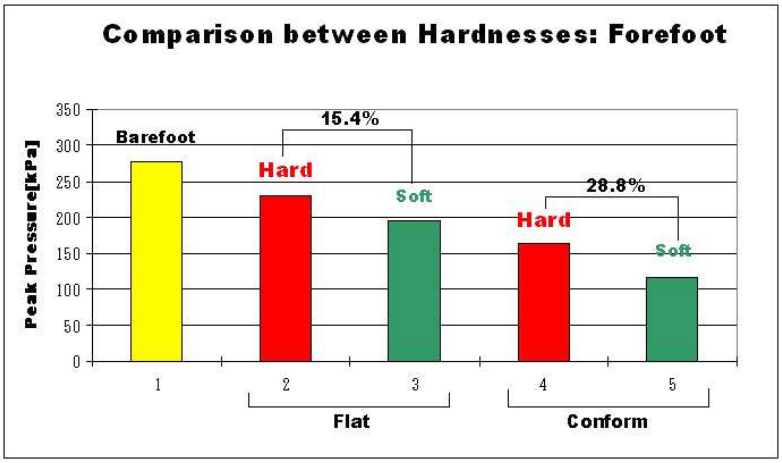

Figure 5-13: Simulation results for Forefoot (hardness).

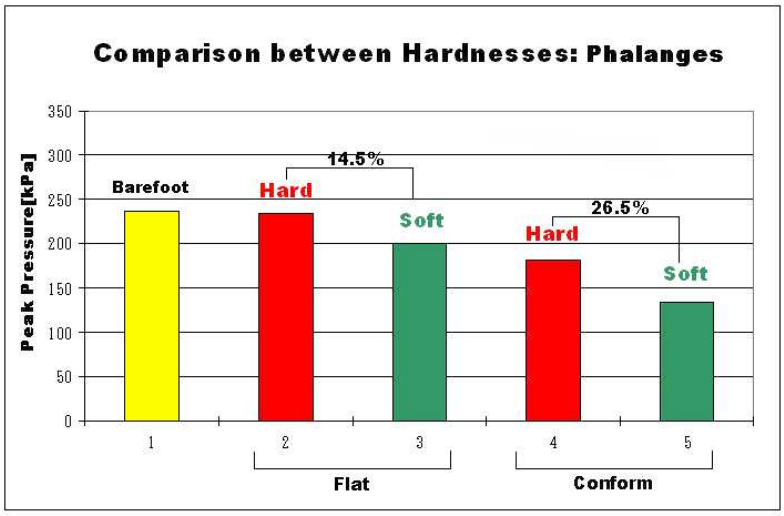

Figure 5-14: Simulation results for Phalanges (hardness).

Experimental data presented decrease of an extent of 7.8%, 19.9%, 7.1% and 4.5% for phalange, forefoot, midfoot and rearfoot region, respectively, for a flat insole (Table 5-9 and Figure 5-16). For a conform insole this order was 26.4%, 11.2%, 21.2% and 9.9% for phalange, forefoot, midfoot and rearfoot, respectively (Table 5-9 and Figure 5-17).

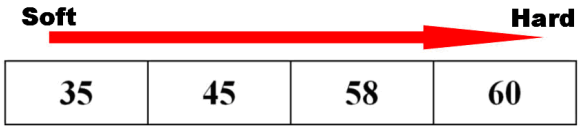

Figure 5-15: Hardness scale for the insoles used for the experiment.

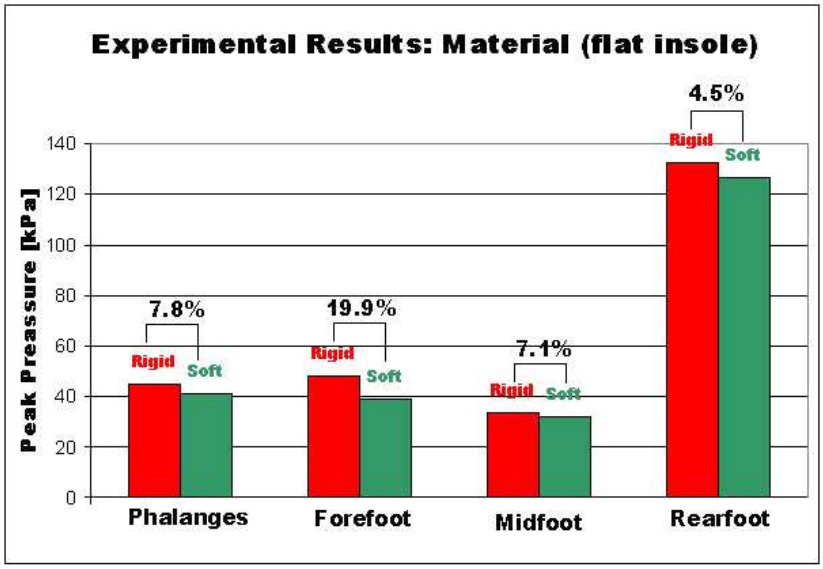

Figure 5-16: Experimental results for flat insole (hardness).

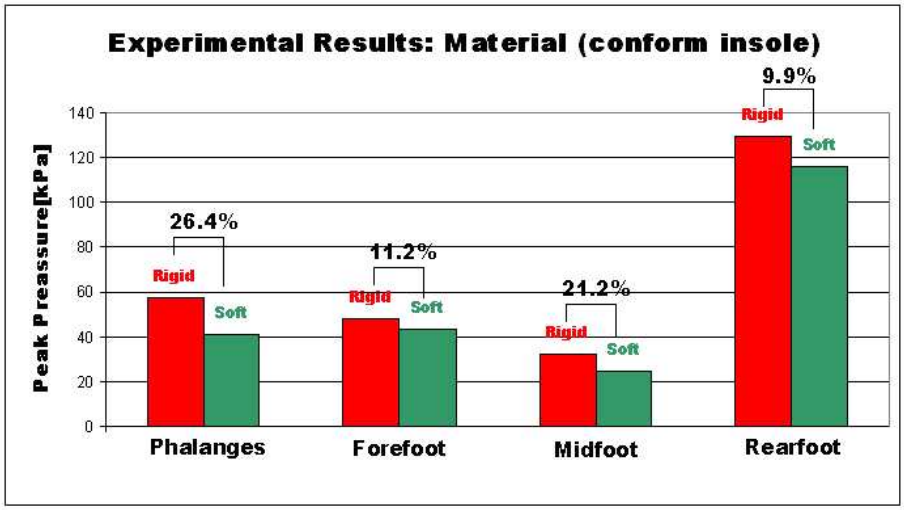

Figure 5-17: Experimental results for conform insole (hardness).

Just to compare, in 2005 Cheung and colleagues found that custom-molded, soft insole reduced the peak plantar pressure by 40.7% and 31.6% at the metatarsal (forefoot) and heel region, respectively, compared with those under a flat, hard insole. Comparing these two conditions in our case study we have 33.2% and 43.2%.

Aerts and De Clercq (1993) reported a decrease in heel pad compression when using a hard midsole (EVA 65) compared to a softer one (EVA 40) which is opposite to our findings. The two studies are not directly comparable because Aerts and De Clercq (1993) did comparisons at the same input energy level whereas we used the same force levels.

Geometry	Material	Thickness [mm]	Region	Peak Pressure[kPa]				%
				Hardness				
				35	45	58	60	
Flat	2	4	Phalanges	41.3	44.8	-	-	7.8
			Forefoot	38.6	48.2	-	-	19.9
			Midfoot	31.6	34.0	-	-	7.1
			Rearfoot	126.7	132.7	-	-	4.5
Conform	1	4	Phalanges	-	43.5	45.6	-	4.6
			Forefoot	-	50.0	47.0	-	-6.4
			Midfoot	-	31.0	30.4	-	-2.0
			Rearfoot	-	99.0	122.5	-	19.2
	2	2	Phalanges	50.7	-	-	63.3	19.9
			Forefoot	38.1	-	-	49.1	22.4
			Midfoot	22.8	-	-	33.1	31.1
			Rearfoot	119.7	-	-	137.1	12.7
	2	4	Phalanges	28.3	-	-	62.6	54.8
			Forefoot	39.5	-	-	47.9	17.5
			Midfoot	22.1	-	-	33.7	34.4
			Rearfoot	130.6	-	-	127.8	-2.2

Table 5-9: Experimental results: comparison among different materials. The results are presented in a crescent scale of hardness (see Figure 5-15). Negative values represent increase in peak plantar pressure.

6 Conclusion

A geometric, detailed 3-D finite element model of the human foot, based on CT scan, was developed to estimate the peak plantar pressure. As consequence, the internal stress and strain in the bony and soft tissue structures under loading and supporting conditions, simulating balanced standing position, can be estimated also.

Thus, despite the fact that the main goal of this study is to estimate peak plantar pressure, other interesting studies involving the structures mentioned above can be conducted. Moreover, the capabilities of this model, makes it a valuable tool to study the complex biomechanical behavior of the foot-footwear interaction, thus this is certainly a prerequisite to further enhance the design of proper footwear.

Nevertheless, the best way to start the rationale of this study, is by delimiting its scope, i.e., qualifying it. In other words, is necessary to present its limitations. To simplify the analysis in this study, we assigned homogeneous and linearly elastic material properties to the model. The use of linear elasticity for the material used during the simulation may be have under or overestimated the real values for peak plantar pressure. Consequently, this approach is improbably the real situation, thus the inclusion of nonlinear properties seems like a promising and natural path for a future work.

In the current finite element model, joints of the foot were not considered. As a consequence, ligaments and cartilage, structures with major role in joint stability and constraint, were not considered either. Therefore, this assumption potentially overestimates stiffness, and consequently overestimates peak plantar pressure. The model also did not account for the surface interactions between bony, ligamentous and muscles structures. This kind of structural simplification would have influence on peak plantar pressure, however for the condition studied (balanced standing position), its effects are expected to be minimal.

Only the Achilles’tendon loading was considered, whereas other intrinsic and extrinsic muscle forces were not simulated. Consequently, the exclusion of muscles prevents accurate force application, which leads to erroneous stress and strain distributions. Again here we have to say, that the inclusion of accurate muscle loadings is a promising topic for a future study.

After this brief, but important, study qualification, let us go into the results, keeping in mind that the goal of this study is to estimate the effect of two footwear design variables on peak plantar pressure: conformity and material. The finite element analysis and experimental data indicated that conformity is an important factor in peak plantar pressure reduction.

Data indicates that the geometry (conformity) of the insole has an important role on peak plantar pressure decrease. This phenomenon can be seen in all areas of the foot with an exception to midfoot region. For phalanges, forefoot and rear foot simply changing the geometry of the insole from flat to conform produces reductions, supported by enough body of evidence (experimental and simulation data), allowing us to answer the first question (Does conformity have an effect on peak plantar pressure value?)without any doubt.

Thus, the first design variable (conformity) DOES have an effect on peak plantar pressure. Moreover, all plantar region of the foot experience this effect. However, the nature of this effect depends on the region, which is going to be stated below. Based on experimental and simulation data, we claim that conformity is an important peak plantar pressure decrease factor for three of the foot's region: rearfoot, phalanges and forefoot. The remainder region, midfoot presents opposite behavior: peak plantar pressure increase. The explanation for these effects was discussed in the section 5.

The second question of this study (Does material have effect on peak plantar pressure's value?) has a similar answer: the second variable DOES have effect on peak plantar pressure also. Repeating what was observed to the first variable, all region of the foot showed some influence from it. Opposite to conformity, this effect seems not to have any relation with the region observed, i.e., it seems more like a global behavior, where all regions present a decrease of peak plantar pressure inversely proportional to hardness. Our claim for this variable is that the values of peak plantar pressure are directly proportional to insole material hardness, with enough body of evidence (experimental and simulation data) to corroborate with this theory.

Finally it can be said, supported by finite element prediction and experimental data, that both a softer material and a conform insole have a role in the reduction of peak plantar pressure. These insoles aided in assimilating the plantar pressure in a more uniform manner than a hard, flat insole. Thus, it can be claimed that, regarding footwear design, conform insoles made of soft material must be always thought as important, especially when a footwear aids people with foot disorder.

Summarizing, finite element prediction and experimental data indicate that an appropriate insole can reduce high plantar pressure. Consequently, many people with foot disorders would be benefited. Furthermore, this kind of design would be a good strategy to be adopted in order to prevent many diseases associate with transient forces experienced by the foot during daily activities.

7 Future Work

7.1 Nonlinear Material Properties

A number of assumptions were made in the current finite element analysis. The material properties for the foot bone, soft tissue, and insole were assumed to be homogeneous, linear, and elastic solids. Thus, the finite element model that has been developed can be refined to simulate the actual situations more realistically by incorporating nonlinear material properties for the ligamentous and soft tissue. For example: some of the simulations can use hyperelastic properties for the soft tissue and insole.

Hyperelastic materials are described in terms of a "strain energy potential", U(ε), which defines the strain energy stored in the material per unit of reference volume (volume in the initial configuration) as a function of strain at that point in the material. As an alternative approach to simulate the soft tissue, it can be modeled as a single incompressible layer with the strain energy function (U) represented by a first-order Ogden form (Twizell *et al.*, 1986) as

$$U = \frac{2\mu}{\alpha^2}\left(\lambda_1^{\alpha} + \lambda_2^{\alpha} + \lambda_3^{\alpha} - 3\right)$$

Where $\lambda_{1\text{-}3}$ are the deviatoric principal stretches and μ and α are the material properties representing the hyperelastic behavior of the heel. Under uniaxial compression,

$$\lambda_1 = \lambda$$

$$\lambda_2 = \lambda_3 = \lambda^{-1/2}$$

$$\lambda = 1 + \varepsilon$$

Where ε is the compressive strain. The compressive stress (σ) is calculated from strain energy function, U, as

$$\sigma = \frac{2\mu}{\alpha}\left(\lambda^{\alpha-1} - \lambda^{-(\alpha/2)-1}\right)$$

Heel-specific material properties (μ and α) were iteratively calculated by Erdermir *et al* (Erdemir *et al.*, 2006), by an inverse finite element analysis of the indentation procedure, which minimized the error between the model-predicted and actual in vivo heel-specific experimental force-displacement curves. In other words, these coefficients were adapted from in vivo testing. The values of these parameters for the soft tissue were calculated as μ=14.3 kPa and α=7.3.

Lemmon (1997) modeled the material of the soft tissue considering it a general hyperelastic material and employing a second-order polynomial strain energy to represent it. The values obtained during a experiment were: C_{10}= 85550 N m^{-2}, C01= -58400 N m^{-2}, C20=38920 N m^{-2}, C11= -23100 N m^{-2}, C02= 8484 N m^{-2}, D1= 0.4370E-05 m^2N^{-1}, D2= 0.6811E-06 m^2N^{-1}.

Different materials can be used to simulate the insole. However in order to find application to this kind of simulation, it is interesting the possibility of analyzing commercial materials. The main characteristic of these materials, regards their mechanical properties: viscoelastic. Manufacturers have been using a wide range of viscoelastic materials, both in the construction of footwear and as insoles. Thus the importance of modeling these kind of mechanical behavior while simulating footwear biomechanics.

Those which have been used clinically fall into seven groups:

(1) Polyurethane elastomers (e.g.Cambion, Sorbothane, Viscolas);

(2) Polyurethane foams (e.g. Cleron, Poron, PPT);

(3) Polyethylene foams (e.g. Evazote, Frelon, Pelite, Plastazote);

(4) Polyvinyl chloride foams (e.g. Implus);

(5) Ethylene vinyl acetate (EVA);

(6) Synthetic rubber foams (e.g. Neoprene, Noene, Spenco, Ucolite, Zdel), and

(7) Silicone rubber.

The main viscoelastic materials used for footwear and insoles were reviewed by Rome (*apud* Whittle, 1999). Thus, a good start point for approaching these materials could be a hyperfoam strain energy function as the one showed below

$$U = \sum_{i=1}^{2} \frac{2\mu_i}{\alpha_i^2}\left[\lambda_1^{\alpha_i} + \lambda_2^{\alpha_i} + \lambda_3^{\alpha_i} - 3 + \frac{1}{\beta_i}\left(J_{el}^{-\alpha_i\beta_i} - 1\right)\right] \tag{4.1}$$

Where

$$\beta_i = \frac{\nu_i}{1-2\nu_i} \tag{4.2}$$

Where $\lambda_{1\text{-}3}$ are the deviatoric principal stretches and μ, α and ν (the effective Poisson's ratio) are the material properties representing the behavior of the insole.

The values used for the insole materials were obtained by fitting stress-strain data under compression by several researchers as Lemmon (1997), Edermir (2004), and Goske (2006). It is just a matter of implementing these material properties in the model.

7.2 Refining the Model: Muscles Loadings, Joints, and Ligaments

For the case studied, balanced standing, the model built was enough to bring meaningful insight on the questions raised. However if other activities are going to be considered, some other points should be put into account. The first point is the inclusion of the loading-bearing characteristics of the foot under different activities. Therefore, other loading conditions should be considered besides the conditions considered in the current study.

In order to do that, it is necessary to incorporate detailed muscular loading and joint interaction. The first change is not exceedingly time consuming, because is just a matter of defining vectors for all forces acting during specific movements. That is solved by a careful literature review about muscle insertions, muscles forces and during which movement they are activated. The first part of this task was done and can be seen in the section 2. Choosing an activity by increasing degree of complexity and frequency, a natural choice would be gait. For walking, the other two steps: muscles forces and activation time are well known (Figure 7-1, and Table 7-1).

Due to the spatial anatomic complexity of the extrinsic and intrinsic muscles, as well as various joint surfaces, the foot's force system can be defined as being non-coplanar and non-concurrent-that is a system in which the force vectors neither lie in the same plane nor intersect at a unique location. Theoretically, this force system can be reduced to an equivalent force-couple system at a unique location, consisting of a force resultant equal to the sum of the forces of the system, and of a couple vector of the moment equal to the moment resultant of the system (Geffen, 2000).

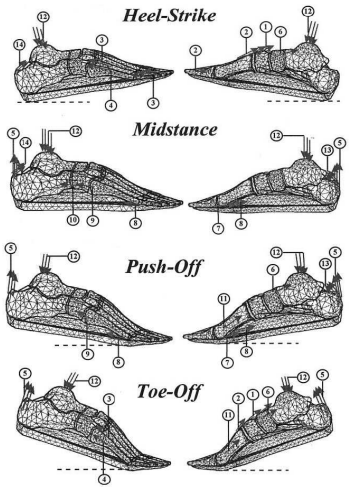

Figure 7-1: Muscle forces that act on the foot model during four characteristic subphases of walking (Geffen, 2000).

Muscles/Loads/Reactions	Gait Subphases Forces [N]			
	Heel-strike	Midstance	Push-off	Toe-off
1-Tibialis Anterior	535	-	-	267
2-Extensor Hallucis Longus	424	-	-	212
3-Extensor Digitorum Longus	372	-	-	186
4-Peroneus Tertius	17	-	-	9
5-Triceps Surae	-	550	1100	300
6-Tibialis Posterior	94	110	258	222
7-Flexor Hallucis Longus	-	923	322	-
8-Flexor Digitorum Longus	-	16	4	-
9-Peroneus Longus	-	1164	1206	-
10-Peroneus Brevis	-	66	-	-
11-Abductor Hallucis	-	-	55	27
12-Ankle Joint Load	1350	2100	3000	300
13-Reaction at the medial pulley	-	645	865	-
14-Reaction at the lateral pulley	716	256	-	-

Table 7-1: The active muscles and structural loads acting on the model during walking (Gefen, 2000).

Thus, the problem of appropriate loading for different activities may be solved relatively easily. However, when it comes to joints, we have a challenging issue. Trying to model joint brings immediately many issues: model joint space (which involves modeling cartilage and ligaments), and rigid body motion combined with deformation.

To solve the first issue: modeling joint space, geometry manipulation is strictly necessary, i.e. , the use of a advanced CAD software to generate perfect solids for all bones is an important, in the other hand, time demanding part of a future study. Moreover, modeling the contact between bony structures and soft tissue must go through the same path: geometry manipulation. It is interesting keep in mind that these issues will cause an increase in the total computational time required to find a solution, which is an arduous issue by itself.

At least but not last, in this study, insoles were modeled as isolated components, ignoring other features of footwear, such midsoles and sidewalls. These components must be taken into account, because they alter pressure distribution (see Table 7-2 and Table 7-3). Thus future work should concentrate to identify how these structures affect this distribution as a whole, providing insight into the basics of shoe construction.

Material	Thickness[mm]	Hardness	Region	Insole	Shod
				Peak Pressure [kPa]	Peak Pressure [kPa]
M1	2	35	phalanges	64.3	22.3
			forefoot	62.7	21.2
			midfoot	28.2	12.0
			rearfoot	111.3	81.1
M2	2	35	phalanges	60.4	32.0
			forefoot	55.5	36.0
			midfoot	20.7	17.6
			rearfoot	110.4	82.4

Table 7-2: Experimental results for flat insole: comparison among balanced standing position on insole and while wearing shoes (same insole).

Material	Thickness[mm]	Hardness	Region	Insole	Shod
				Peak Pressure[kPa]	Peak Pressure[kPa]
M1	2	45	phalanges	36.2	29.7
			forefoot	55.4	27.8
			midfoot	39.0	45.9
			rearfoot	147.5	81.4
M1	2	58	phalanges	39.6	23.4
			forefoot	61.3	31.6
			midfoot	27.0	54.9
			rearfoot	127.3	62.6
M1	4	45	phalanges	50.0	32.3
			forefoot	54.9	32.3
			midfoot	31.0	57.4
			rearfoot	103.9	86.2
M1	4	58	phalanges	45.6	30.2
			forefoot	45.6	35.3
			midfoot	30.4	62.6
			rearfoot	122.5	102.3
M2	2	35	phalanges	94.1	31.1
			forefoot	38.1	30.2
			midfoot	22.8	46.3
			rearfoot	127.8	71.0

M2	2	60	phalanges	45.7	22.3
			forefoot	54.4	20.7
			midfoot	19.6	54.9
			rearfoot	137.1	57.1
M2	4	35	phalanges	69.8	10.2
			forefoot	39.5	20.1
			midfoot	22.1	52.2
			rearfoot	135.0	68.0
M2	4	60	phalanges	62.6	17.4
			forefoot	47.9	22.8
			midfoot	27.7	44.6
			rearfoot	120.2	65.3

Table 7-3: Experimental results for conform insoles: comparison among balanced standing position on insole and while wearing shoes (same insole).

7.3 Thickness

Thickness presents itself as another design variable to be studied. As well conformity and material, thickness is expected to have effect on peak plantar pressure. In fact, insole thickness has previously been identified as an important variable in designing footwear to reduce peak plantar pressure (Lemmon et al., 1997).

A possible theory accounts that as the foot moves towards the ground; it has to be brought to a halt in a finite distance. The shorter the distance, the less time it has to decelerate and the higher the force which is needed to provide the necessary deceleration. When attempting to reduce the magnitude of the heelstrike transient using viscoelastic insoles, the thickness of the insole is a major factor determining its efficacy (Whittle, 1999).

Our experimental data (Table 7-2) showed an interesting trend: it seems that the nature of the thickness effect (increase or decrease) on peak plantar pressure depends on geometry (flat or conform insole) and region. For example, increasing the insole thickness was observed on phalanges, and forefoot, a decrease in peak plantar pressure. Flat insoles have reduction amount of 32.6% and 26.8%, respectively.

For a different geometry, conform insoles presented reduction extent of 9% and 9.4%, respectively. The other two regions midfoot and rearfoot, for conform geometry also presented the same behavior: decrease of peak plantar pressure (6.8 and 9% respectively). In the other hand, for midfoot and rearfoot, it was observed an increase of peak plantar pressure for flat insole (60.2% and 10.6%).

Some other researchers like Goske and collaborators (2005) point out that increasing the insole thickness of the full-conforming insole from 6.3 to 12.7mm resulted in additional peak pressure reductions up to 12.1% (280–246 kPa). However they conclude that these reductions did not seem to be dependent on the conformity of the insole, which is not so clear in our data.

Thus everything that we can claim here is that thickness has effect on peak plantar pressure, however to make the argument more solid, and prepare a good claim, the experiment data should be compared to simulation data. Furthermore, Simulation data would make us able to compare thickness, material and conformity and find possible correlations between them.

Geometry	Material	Hardness	Region	Peak Pressure[kPa]	
				T1(2mm)	T2(4mm)
Flat	1	35	Phalanges	64.3	43.5
			Forefoot	62.7	41.3
			Midfoot	28.2	18.0
			Rearfoot	111.3	125.7
	2	35	Phalanges	60.4	41.3
			Forefoot	55.5	38.6
			Midfoot	20.7	31.6
			Rearfoot	110.4	126.7
	2	45	Phalanges	75.6	50.0
			Forefoot	49.0	41.3
			Midfoot	10.3	27.2
			Rearfoot	132.7	138.2
Conform	1	45	Phalanges	36.2	43.5
			Forefoot	55.4	50.5
			Midfoot	39.0	31.0
			Rearfoot	147.5	99.0
	1	58	Phalanges	39.6	45.6
			Forefoot	61.3	45.6
			Midfoot	27.0	30.4
			Rearfoot	127.3	122.5
	2	35	Phalanges	94.1	69.8
			Forefoot	38.1	39.5
			Midfoot	22.8	22.1
			Rearfoot	119.7	135.0
	2	60	Phalanges	45.7	25.0
			Forefoot	54.4	50.6
			Midfoot	33.1	27.7
			Rearfoot	137.1	120.2

Table 7-4: Experimental results: comparison among different thicknesses. The values highlighted (in red) correspond to insoles with thicknesses of 4 mm (T1) and 8 mm (T2), respectively.

8 References

[1]Abboud, R.J. (2002). "Relevant Foot Biomechanics." Current Orthopaedics **16**: 15.

[2]Argyris, J.H and Kelsey, S. (1960). "Energy Theorems and Structural Analysis." Butterworth - London.

[3]Argyris, J.H. (1954). "Energy Theorems and Structural Analysis." Aircraft Engineering **26**: 347-356,383-387,394.

[4]Argyris, J.H. (1955). "Energy Theorems and Structural Analysis." Aircraft Engineering **27**: 42-58,80-94,125-134,145-158.

[5]Argyris, J.H. (1957). "The Matrix Theory of Statics." Ingenieur Archiv **25**: 174-192.

[6]Argyris, J.H. (1959). "The Analysis of Fuselages of Arbitrary Cross-Section and Taper."AircraftEngineering 31:62-74,101-112,133-143,169-180,192-203,244-256,272-283.

[7]Bandak F.A., Tannous R.E and Toridis T. (2001). "On the development of an osseo-ligamentous finite element model of the human ankle joint." International Journal of Solids and Structures **38**: 1681-1697.

[8]Bergmann G., Kniggendorf H., Graichen F. and A., and Rohlmann (1995)." Influence of shoes and heel strike on the loading of the hip joint." Journal of Biomechanics **28**: 817-827.

[9]Bobbert M.F., Schamhardt H.C. and and Nigg, B.M. (1991). "Calculation of vertical ground reaction force estimates during running from positional data." Journal of Biomechanics **24**: 1095-1105.

[10]Burdett, R.G. (1982). "Forces predicted at the ankle joint during running ".

[11]Cavanagh P.R. (1980). "The running shoe book." Mountain View, CA. Anderson World, Inc.

[12]Cavanagh P.R. and Lafortune M.A. (1980). "Ground reaction forces in distance running." Journal of Biomechanics **13**: 397-406.

[13]Chen, W.C., Ju C.W. and Tang F.T. (2003). "Effects of total contact insoles on the plantar stress redistribution: a finite element analysis." Clinical Biomechanics **18**: S17-S24.

[14]Cheung, J.T.M. and Zhang M. (2005). "A 3-Dimensional Finite Element Model of the Human Foot and Ankle for Insole Design." Archives of Physical Medicine and Rehabilitation **86**: 353-358.

[15]Chi, Kai-Jung and Schmitt, Daniel (2005). "Mechanical energy and effective foot mass during impact loading of walking and running." Journal of Biomechanics **38**: 1387–1395.

[16]Clarke T.E., Frederick E.C. and C.L., Hamill (1983). "The effects of shoe design parameters on rearfoot control in running." Medicine Science Sports Exercise **5**: 376-381.

[17]Clement D.B., Taunton J.E., Smart G.W. and McNicol, K.L. (1981). "A survey of overuse running injuries." The Physician and Sports Medicine **9**: 47-58.

[18]Clough, R.W. (1960). "The Finite Element Method in Plane Stress Analysis." Proc. 2º A. S. C. E. Conference in Electronic Computation.

[19]Cook S.D., Brinker M.R. and P., Mahlon (1990). "Running shoes: their relation to running injuries." Sports Medicine **10**: 1-8.

[20]Courant, R. (1943). "Variational Methods for the Solutions of Problems of Equilibrium and Vibration." Bulletin of the American Mathematics Society **49**: 1-23.

[21]David Lemmon, T. Shiang, Azfar Hashmi, Jan S. Ulbrecht and Peter R. Cavanagh (1997). "The effect of insoles in therapeutic footwear-a finite element approach." Journal of Biomechanics **30**(6): 6.

[22]De Wit B., De Clercq D. and M., Lenoir (1995). "The effect of varying midsole

hardness on impact forces and foot motion during foot contact in running." Journal of Applied Biomechanics **11**: 395-406.

[23]Denoth J. (1986). "Load on the locomotor system and modelling. In B.M. Nigg, (Ed.), Biomechanics of running shoes." Human Kinetics Publ., Champaign, IL, USA: 63-116.

[24]Dzung L. Pham, Chenyang Xu, Jerry L. Prince (1998). "A survey of current methods in medical image segmentation." Annual Review of Biomedical Engineering: 27.

[25]Eichner E.R. (1989). "Does running cause osteoarthritis?" The Physician and Sports Medicine **17**: 147-154.

[26]Erdemir, A., Viveiros, M. L., Ulbrechtc, J.S. and Cavanagh, P.R. (2006). "An inverse finite-element model of heel-pad indentation." Journal of Biomechanics **39**.

[27]Felippa, C. A. (2001). "A Historical Outline of Matrix Structural Analysis: a Play in Three Acts." Computers and Structures **79**: 1313-1324.

[28]Frederick E.C. and J.L., Hagy (1986). "Factors affecting peak vertical ground reaction forces in running." Journal Sports Biomechanics **2**: 41-49.

[29]Fung, Y. C. (1994). "A First Course in Continuum Mechanics" Prentice Hall, Englewood Cliffs, NJ.

[30]Gefen, A. (2000). "Biomechanical analysis of the three-dimensional foot structure during gait: a basic tool for clinical applications." Journal of Biomechanics Engineering **122**: 630-639.

[31]Goske S., Erdemir A., Petre M., Budhabhatti S. and P.R., and Cavanagh (2006). "Reduction of plantar heel pressures: Insole design using finite element analysis." Journal of Biomechanics **39**: 2363-2370.

[32]Hamill J., Bates B.T., Knutzen K.M. and J.A., Sawhill (1983). "Variations in ground reaction force parameters at different running speeds." Human Movement Science **2**:

47-56.

[33]Hamill J., Freedson P.S., Boda W. and Reichsman, F. (1988). "Effects of shoe type on cardiorespiratory responses and rearfoot motion during treadmill running." Medicine Science Sports Exercise **20** 515-521.

[34]Hart Richard T., Hennebel Vincent V. , Nisra Thongpreda, Buskirk, William C. Van and Anderson, and Ronald C. (1992). "Modeling the biomechanics of the mandible: a three-dimensional finite element study." Journal of Biomechanics **25**: 26.

[35]Hrenikoff, A. (1941). "Solution of Problems in Elasticity by Framework Method." Journal of Applied Mechanics **8**: 169-175.

[36]Huebner, K.H., Dewhirst, D.L., Smith, D.E. and Byrom, T.G. (2001). "The Finite Element Method for Engineers." J.Wiley & Sons,New York.

[37]Jacob S., Patil K. M., Braak L. H. and A., Huson (1996). "Stresses in a 3-D Two Arch Model of a Normal Human Foot." Mech. Res. Commun. **23**: 387–393.

[38]James S., Bates B. and L., Osternig (1978). "Injuries in runners." The American Journal of Sports Medicine **6**: 40-50.

[39]Jiang T., Merickel M. B. and Parrish E. A. (1988). "Automated Threshold Detection Using a Pyramid Data Structure." In 9th International Conference on Pattern Recognition: 689-692.

[40]Konradsen L., Berg-Hansen E.M. and L., Söndergaard (1990). "Long distance running and osteoarthritis." The American Journal of Sports Medicine **18**: 379-381.

[41]Korioth T.W.P. and Versluis A. (1997). "Modeling the mechanical behavior of the jaws and their related structures by finite element (FE) analysis." Crit Rev Oral Biol Med **8**(1): 15.

[42]Krissoff W.B. and W.D., Ferris (1979). "Runner's injuries." The Physician and Sports Medicine **7**: 55-64.

[43]Kron, G. (1944). "Equivalent Circuits of the Elastic Field." Journal of Applied Mechanics **66**: A149-A161.

[44]Kron, G. (1944). "Tensorial Analysis and Equivalent Circuits of Elastic Structures." J.Franklin Inst. **238**: 400–442.

[45]Lafortune M.A. (1991). "Three-dimensional acceleration of the tibia during walking and running." Journal of Biomechanics **24**: 877-886.

[46]Lafortune M.A. and E.M., Hennig (1991). "Contribution of angular motion and gravity to tibial acceleration." Med. Sci. Sports Exercise **23**: 360-363.

[47]Lakare, Sarang (2000). "3D segmentation techniques for medical volumes." 23.

[48]Lane N.E., Bloch D.A., Jones H.H., Marshall W.H., Wood P.D. and J.F., Fries (1986). "Long distance running, bone density and osteoarthritis." JAMA **255**: 1147-1151.

[49]Light L.H., MacLellan G.E. and L., Klenerman (1979). "Skeletal transients on heel strike in normal walking with different footwear." Journal of Biomechanics **13**: 477-488.

[50]Mündermann A., Nigg B.M., Humble N. and D.J., Stefanyshyn (2004). "Consistent immediate effects of foot orthoses on comfort and lower extremity kinematics, kinetics and muscle activity." Journal of Applied Biomechanics **20**: 71-84.

[51]Mangin J.F., Frouin V., Bloch I., Regis J. and Lopez-Krahe, J. (1995). "From 3D magnetic resonance images to structural representations of the cortex topography using topology preserving deformations." Journal of Mathematical Imaging and Vision **5**.

[52]McClay I. and K., Manal (1997). "Coupling parameters in runners with normal and excessive pronation." Journal of Applied Biomechanics **13**: 109-124.

[53]McHenry, D. (1943). "A Lattice Analogy for the Solution of Plane Stress Problems." Journal of Institute Civil Engineering **21**(59-82).

[54]Milani T.L., Schnabel G. and E.M., Hennig (1995). "Rearfoot motion and pressure distribution patterns during running in shoes with varus and valgus wedges." Journal of Applied Biomechanics **11**: 177-187.

[55]Morse, P.M. and Feshback, H. (1953). "Methods of Theoretical Physics." McGraw-Hill, New York: Section 9.4.

[56]Nakamura, S., Crowninshield, R. D. and Cooper, R. R. (1981). "An Analysis of Soft Tissue Loading in the Foot: A Preliminary Report." Bull. Prosthet.Res. **18**: 27–34.

[57]Nath, B (1974). "(1974). Fundamentals of finite elements for engineers." University of London.

[58]Nawoczenski D.A., Cook T.M. and C.L., Saltzman (1995). "The effect of foot orthotics on threedimensional kinematics of the leg and rearfoot during running." Journal of Orthopaedic Sports Physical Therapy **21**: 317-327.

[59]Newmark, N. M. (1949). "Numerical Methods of Analysis in Engineering." L. E. Grinter (ed.), Macmillan, New York, 1949.

[60]Nigg B.M. (1997). "Impact forces in running." Current Opinion in Orthopedics **8**: 43-47.

[61]Nigg B.M. (2001). "The role of impact forces and foot pronation - a new paradigm. ." Clin. Journal Sports Medicine **11**: 2-9.

[62]Nigg B.M., Cole G.K. and G.P., Brüggemann (1995). "Impact forces during heel-toe running." Journal Applied Biomechanics **11**: 407-432.

[63]Nigg B.M., Eberle G., Frei D., Segesser B. and B., Weber (1977). "Bewegungsanalyse für Schuhkorrekturen (Movement analysis for shoe corrections)." Medita **9a**: 160-163.

[64]Nigg B.M. and M., Morlock (1987). "The influence of lateral heel flare of running shoes on pronation and impact forces." Med. Sci. Sports Exercise **19**: 294-302.

[65]Nigg M. B. and Herzog W. (1994). Biomechanics of the Musculo-skeletal System, Chichester:John Wiley.

[66]Noor, A. (1991). "Bibliography of Books and Monographs on Finite Element Technology." Appl. Mech. Rev. **44**(6): 307-317.

[67]Nurse M.A. and Nigg, B.M. (1999). "Quantifying a relationship between tactile and vibration sensitivity of the human foot with plantar pressure distributions during gait." Clinical Biomechanics **14**: 667-672.

[68]Pham D. L., Xu C. and Prince J. L. (1998). "A survey of current methods in medical image segmentation." Annual Review of Biomedical Engineering: 27.

[69]Prager, W. and Synge, J.L. (1947). "Approximation in Elasticity Based on the Concept of Function Space." Q. Appl. Math. **5**: 241-269

[70]Radin E.L. and I.L., Paul (1971). "Response of joints to impact loading." Arthritis and Rheumatism **14**: 356-362.

[71]Radin E.L., Orr R.B., Kelman J.L., Paul I.L. and R.M., Rose (1982). "Effects of prolonged walking on concrete on the knees of sheep." Journal Biomechanics **15**: 487-492.

[72]Reinschmidt C., van den Bogert A.J., Murphy N., Lundberg A. and B.M., Nigg (1997). "Tibiocalcaneal motion during running - measured with external and bone markers." Clinical Biomechanics **12**: 8-16.

[73]Robbins S. and Waked E. (1997). "Balance and Vertical Impact in Sports: Role of Shoe Sole Materials." Archives in Physical Medicine and Rehabilitation **78**: 463-467.

[74]Robbins S.E. and Gouw G.J. (1990). "Athletic footwear and chronic overloading." Sports Medicine **9**: 76-85.

[75]Sahoo P. K., Soltani S. and C., Wong A. K. (1988). "A Survey of Thresholding Techniques." Computer Vision, Graphics, and Image Processing **41**.

[76]Schwellnus M.P., Jordaan G. and T.D., Noakes (1990). "Prevention of common overuse injuries by the use of shock absorbing insoles." The American Journal of Sports Medicine **18**: 636-640.

[77]Scott S.H. and D.A., Winter (1990). "Internal forces at chronic running injury sites." Med. Sci. Sports Exercise **32**: 357-369.

[78]Stacoff A., Nigg B.M., Reinschmidt C., van den Bogert A.J. and A., Lundberg (2000). "Tibiocalcaneal kinematics of barefoot versus shod running." Journal of Biomechanics **33**: 1387-1396.

[79]Stefanyshyn D.J. and B.M., Nigg (1997). "Mechanical energy contribution of the metatarsalphalangeal joint to running and sprinting." Journal of Biomechanics **30**: 1081-1085.

[80]Synge, J.L. (1952). "Triangulation in the Hypercircle Method for Plane Problems." Proc.R. Irish Acad.. **54A21**.

[81]Terrier A. (1999). "Adaptation of bone to mechanical stress : theoretical model,experimental identification and orthopedic applications." Physics Department Swiss Federal Institute of Technology.

[82]Turner, M.J. , Clough, R.W., Martin, H.C. and Topp, L.C. (1956). "Stiffness and Deflection Analysis of Complex Structures." Journal of Aeronatical Sciences **23**(9): 805-823,854.

[83]Twizell, E.H. and Ogden, R.H. (1986). "Non-linear optimization of the material constants in Ogden's stress-deformation function for incompressible isotropic elastomers." Journal of the Australian Mathematical Society **Series B 24**: 424–444.

[84]Udupa J. K. and Samarasekera S. (1996). "Fuzzy connectedness and object definition: Theory, algorithms and applications in image segmentation." Graphical Models and Image Processing **58**(3): 246–261.

[85]Van Teijlingen, E.R. and Hundley, V. (2001). "The importance of pilot studies." Department of Sociology, University of Surrey,Guildford GU2 5XH, United Kingdom.

[86]Verdejo, R. and Milss, N.J. (2004). "Heel−shoe interactions and the durability of EVA foam running-shoe midsoles." Journal of Biomechanics **37**: 1379-1386.

[87]Wakeling J.M. and B.M., Nigg (2001). "Modification of soft tissue vibrations in the leg by muscular activity." Journal of Applied Physiology **90**: 412-420.

[88]Wakeling J.M. and B.M., Nigg (2001). "Soft-tissue vibrations in the quadriceps measured with skinmounted transducers." Journal of Biomechanics **34**: 539-543.

[89]Wakeling J.M., Pascual S.A, Nigg B.M. and V., Von Tscharner (2001). "Surface EMG shows distinct populations of muscle activity when measured during sustained sub-maximal exercise " European Journal of Applied Physiology **86**: 40-47.

[90]Walter S.D., Hart L.E., Sutton J.R., McIntosh J.M. and M., Gauld (1988). "Training habits and injury experience in distance runners, age and sex related factors." The Physician and Sportsmedicine **16**: 101-111.

[91]Weszka, J. S. (1978). "A Survey of Thresholding Techniques." Computer Graphics, and Image Processing **7**: 259-265.

[92]Whittle, M. W. (1999). "Generation and attenuation of transient impulsive forces beneath the foot: a review." Gait and Posture **10**: 264–275.

[93]Williams K. (1985). "The relationship between mechanical and physiological energy estimates." Med. Sci. Sports Exercise **17**: 317-325.

[94]Woodburn, J. and Helliwell, P. S. (1996). "Observations on F-scan in-shoe pressure measuring system." Clinical Biomechanics **11**(5): 301-304.

[95]Xu-Zheng Liu, Jun-Hai Yong and Guo-Qin Zheng, Jia-Guang Sun (2007). "An offset algorithm for polyline curves." Computer in Industry **58**.

[96]Zienkiewicz, O.C. and Cheung, Y.K. (1965). "Finite Elements in the Solution of Field Problems." Engineer **220**: 507-510.

[97]Zienkiewicz O.C. and Taylor R.L. (1967). "The Finite Element Method."

Butterworth - Heinemann.

9 Appendices

9.1 Methodology used for walking and running cases

The choice of the velocity for the aerobic exercises performed during the experiment is a very important point. The velocity was calculated based on the subject's target heart rate (HR), which currently is considered the most appropriate way to calculate exercise intensity for aerobic activities. In general, professionals advice to keep a velocity that enable a value of heart rate between 60% and 75% of the maximum. A simple experiment was design to calculate the target heart rate, and consequently, the walking velocity. The subject was asked to walk a course of 200 meters in three different ways: slowly, fast, and as fast as he could do it. For the last 10 meters the time was recorded, and consequently the velocity was calculated. Just after the ending of the 10m, the heart rate was measured during one (1) minute, by the subject himself. The target heart rate is calculated in the following way:

$$HR = (220 - age) \bullet (0.6 \sim 0.75)$$

The values for all variables are found in the Table 9-1 below.

Time[s]	Velocity[m/s]	Heart Rate	Target Heart Rate (75% and 60%)
9.04	1.11	80	140.25
6.16	1.62	109	112.2
4.98	2.01	126	

Table 9-1: Data from the aerobic experiment

Based on this data one can calculate the regression line for the subject, i.e., the relation between his heart rate and walking speed. The Figure 9-1 depicts this relation. It is important to mention, that for that interval, and activity, this relation is expected to be linear. From this experiment we can obtain values for the whole range, it is just a matter of using the function calculated (depicted in Figure 9-1). However, for experimental reasons, it is better to fix a value. For this experiment we are going to use 30% of the maximal heart rate as a basis to calculate the velocity.

In other words, for the second study case (walking) the velocity is kept constant at 1.11 m/s (4 km/h). For the third case study (running) the velocity is kept constant at 2.78m/s (10 km/h). In order to keep the velocity constant, a treadmill was used (Figure 9-2).

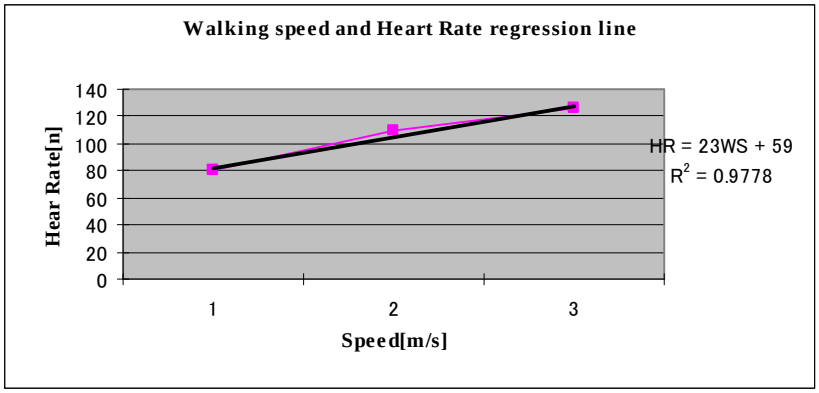

Figure 9-1: Regression line for aerobic activities.

Figure 9-2: Treadmill used during experiment.

For both, walking and running, the subject started the movement and after ten (10) seconds the trials were recorded during the subsequent ten (10) seconds. The settings for the F-scan system can be seen in the Table 9-2.

Recording Parameter	Amount
Total time (s)	10
Sampling Rate (Hz)	50
Period (s)	0.02
Number of frames	500

Table 9-2: Final Experiment Settings.

Acta est fabula.